Nucleoredoxin – a redox modulator of calcium calmodulin kinase 2a promoting the exploratory behavior in mice

Dissertation
zur Erlangung des Doktorgrades
der Naturwissenschaften

vorgelegt beim Fachbereich Pharmazie
der Johann-Wolfgang-Goethe-Universität
in Frankfurt am Main

von
Bao Ngoc Tran
aus Halle/Saale (Sachsen-Anhalt)

Frankfurt (2022)
(D 30)

vom Fachbereich Pharmazie der

Johann Wolfgang Goethe – Universität als Dissertation angenommen.

Dekan:	Prof. Dr. Clemens Glaubitz
Gutachter:	Prof. Dr. Dr. Achim Schmidtko
	Prof. Dr. Irmgard Tegeder

Datum der Disputation: 14. November 2022

1. Abstract

Redox homeostasis must be kept in balance for an intact redox signaling, which is necessary to control neuronal pathways such as growth cone pathfinding, synaptic plasticity and transmission (Oswald, Garnham, Sweeney, & Landgraf, 2018). Nucleoredoxin (NXN) is an oxidoreductase and thioredoxin-like protein holding two conserved cysteine residues in its structure (Funato & Miki, 2007), which are essential for its redox-regulating functionality. The function of NXN in neurons is still less well studied. But the expression of NXN in neurons, which was confirmed through analyzing adult NXN-LacZ reporter mice, suggested a dominant functional role in neuronal pathways. Initial experiments revealed calcium-calmodulin-dependent kinase 2 a (Camk2a) as a potential interaction partner through a Yeast-2-Hybrid screen (not shown) which is the major protein to induce synaptic plasticity during neuronal activity. Therefore, neuronal expression of NXN and the potential interaction with Camk2a prompted us to investigate deeper into the neuronal pathway. The goal of this work was to confirm the interaction of Camk2a and NXN with further experiments and to characterize behavior of mice carrying a neuronal NXN deletion.

To achieve a pan-neuronal depletion of NXN expression in our mouse model, we used the Cre/loxP system with a NestinCre driver. We did not achieve the expected complete deletion of NXN due to unknown compensatory mechanisms. Nevertheless, the partial deletion of NXN in our transgenic mouse model prevented embryonic lethality as occurring in complete NXN knockout mice (Funato et al., 2010). The interaction of Camk2a and NXN was confirmed through proximity ligation assay (PLA) and immunofluorescence staining of primary cortical neurons. Investigations of the functional interaction revealed a lower redox-sensitivity of Camk2a activity in NXN-deficient brain samples. Additionally, the respiratory activity was significantly reduced in mitochondria of NXN deficient mouse brain pointing to possible dysfunctional mitochondria which is also observed in various neurodegenerative diseases, e.g.: Alzheimer, Parkinson, and Huntington disease (Norat et al., 2020). Unexpectedly, behavioral studies revealed only a subtle effect of the pan-neuronal NXN-deficiency. Significant differences between genotypes were found at the reduction of exploratory behavior and a reduced motivation for the voluntary wheel running in NesNXN$^{-/-}$ mice, which is normally seen as a joyful and

rewarding activity. The observed behavior of NesNXN$^{-/-}$ mice potentially results from interaction mechanisms of NXN with Camk2a, as well as decreased oxidation of Camk2a and further unidentified target proteins of NXN.

Conclusively, function of NXN was revealed as a non-essential redox modulator of Camk2a in neurons. The behavioral phenotype of NesNXN$^{-/-}$ mice is probably compensated through unknown mechanisms. Redox signaling of Camk2a in neurons is regulated through various components such as TXN or GSH, which can backup each other (Branco et al., 2017; Ren et al., 2017). NXN is an additional but not essential regulator.

2. Table of Content

1. Abstract ..... - 3 -

2. Table of Content ..... - 5 -

3. Introduction ..... - 8 -

3.1 Redoxhomeostasis ..... - 8 -

3.1.1 Brain energy metabolism ..... - 8 -

3.1.2 Redox system in the central nervous system ..... - 12 -

3.2 Calcium/Calmodulin-dependent protein kinase 2 ..... - 16 -

3.2.1 Synaptic plasticity at dendritic spines ..... - 16 -

3.2.2 Characteristics of Camk2 ..... - 16 -

3.2.3 Role of Camk2 in the long term potention (LTP) ..... - 17 -

3.2.4 Long term depression (LTD) ..... - 19 -

3.2.5 Redoxregulation of LTP and LTD ..... - 20 -

3.3 Nucleoredoxin (NXN) ..... - 21 -

3.3.1 Characterisitcs of NXN ..... - 21 -

3.3.2 Clinical impact of NXN deficiency ..... - 21 -

3.3.3 Mechanisms of NXN ..... - 22 -

4. Materials And Methods ..... - 26 -

4.1 Mice ..... - 26 -

4.1.1 Generation conditioned NXN deficiency in neurons of mice ..... - 26 -

4.1.2 Genotyping ..... - 27 -

4.2 Immunhistochemical analysis ..... - 28 -

4.2.1 LacZ histochemistry (conducted by Lucie Valek) ..... - 28 -

4.2.2 Perfusion and Immunofluorescence of brain tissue ..... - 29 -

4.2.3 Immunofluorescence of primary neuronal culture ..... - 30 -

4.2.4 In-situ proximity ligation assay of primary cortical neurons ..... - 31 -

4.3 Cell culture ..... - 32 -

4.3.1 Primary culture of cortical and hippocampal neurons ..... - 32 -

4.4 Assays ..... - 33 -

4.4.1 Immunoprecipitation and Camk2 activity assay ..... - 33 -

4.4.2 Isolation of mitochondria from brain tissue ..... - 35 -

4.4.3 Seahorse analysis of oxygen consumption in isolated mitochondria ..... - 36 -

4.5 RNA analysis ..... - 38 -

4.6 Behavioral experiments ..... - 39 -

4.6.1 Phenomaster ..... - 39 -

4.6.2 Open field test ..... - 40 -

4.6.3 Elevated Plus Maze ..... - 40 -

4.6.4 Sociability and social memory test ..... - 40 -

4.6.5 IntelliCage ..... - 41 -

4.7 Statistical analysis ..... - 44 -

5. Results ..... - 47 -

5.1 NXN expression pattern in murine brain ..... - 47 -

5.2 NXN interacts with Camk2a sustaining its activity ..... - 49 -

5.3 NXN in neuronal fibers sustains neuronal respiratory activity ..... - 53 -

5.4 NesNXN$^{-/-}$ mice show reduced exploratory behavior and low interest in the reward ..... - 55 -

5.5 Learning and memory in NesNXN$^{-/-}$ mice ..... - 60 -

5.6 Lower interests in novel environments and low voluntary wheel running ..... - 63 -

6. Discussion ..... - 66 -

6.1 Expression pattern of NXN in the nervous system ..... - 66 -

6.2 NXN as a modulator of the redox-sensitive Camk2a ..... - 67 -

6.3 Neuronal deficiency of NXN reduces exploratory behavior ..... - 69 -

7. Zusammenfassung ..... - 73 -

8. References ..... - 78 -

9. Appendix ..... - 95 -

9.1 List of abbreviations ..... - 95 -

9.2 List of tables ..... - 98 -

9.3 List of figures ..... - 99 -

9.4 Curriculum Vitae ..... - 101 -

9.5 Acknowledgement ..... - 103 -

9.6 Declaration ..... - 104 -

3. Introduction

3.1 Redoxhomeostasis

Reactive species can be differentiated in reactive oxygen species (ROS), reactive nitric species (RNS) and reactive sulfur species (RSS) depending on their reactive atom. ROS can be distinguished between free radical and non-radical ROS. The greatest differences between both groups are the reactivity and specificity. They generated by incomplete reduction of oxygen molecules (Ray, Huang, & Tsuji, 2012). Major sources of endogenous ROS are oxidative metabolism in mitochondria through electron transport chain (ETC) and transmembrane NADPH oxidases (NOX). Hydrogen peroxide (H_2O_2) is a non-radical ROS, which acts as a signaling modulator for cell proliferation, differentiation, and migration at oxidative stress in a concentration dependent manner (Sies & Jones, 2020). But ROS levels can exceed the physiological concentration range due to uncontrollable ROS production during diseases or exogenous factors such as drugs, toxic agents, or physical stressors. Consequently, maladaptive cascades will cause cellular dysfunction if redox homeostasis cannot recover from oxidative stress through the antioxidative system (Eisner, Picard, & Hajnoczky, 2018). In summary, unbalanced ROS homeostasis result in pathological events causing myriad diseases.

3.1.1 Brain energy metabolism

ROS is generated at mitochondrial respiration during glucose metabolism to provide the brain with energy at various neuronal activities such as action potential generation, signal transmission and plasticity. Energy storage capacity in the brain is relatively limited regarding the high energy consumption (Peters et al., 2004). Therefore, a continuous energy supply is crucial for the functionality and survival of cells especially neurons and glia cells (Hyder, Rothman, & Bennett, 2013). The energy demand of neurons is relatively high compared to other cells in the body which explains the high sensitivity regarding the shortages of glucose and oxygen (Dienel, 2019).

3.1.1.1 Glucose oxidation

At healthy conditions, terminal oxidation of glucose remains as the most predominant catabolic pathway for ATP generation in the brain which requires a

sufficient oxygen level (Shannon et al., 2016). Glucose is phosphorylated after entering neurons and glia cells through glucose transporter (GLUT) to be generated into glucose-6-phosphate (glucose-6-P) in the cytosol. Glucose-6-P is the initial state of glucose for further reactions during glycolysis, and tricarboxylic acid cycle (TCA cycle) for direct ATP production or can also be converted to glycogen as an energy depot. Reduced nicotinamide adenine dinucleotide (NADH) and reduced flavin adenine dinucleotide (FADH2) accumulate as by-products during the TCA cycle which induces the mitochondrial ETC at the inner membrane. ETC generates a proton-gradient through its complexes which are tightly coupled with the TCA cycle. The proton-gradient is used by ATP-synthases to produce adenosine 5′-triphosphate (ATP) through oxidative phosphorylation (OXPHOS) under oxygen consumption. Free radicals, prevalently as superoxide anion radicals ($O2^{-\bullet}$), are generated by electron escape in ETC which can be converted to H_2O_2 with superoxide dismutase (SOD) (Sies & Jones, 2020).

3.1.1.2 Lactate shuttle from astrocytes to neurons

Astrocytes and neurons are working tightly together regarding metabolic mechanisms but also signal transmission and redox homeostasis. Astrocytes are the main reservoirs of glucose which are kept as glycogen. Besides supplying energy to neurons by providing lactate (Fig 3.1), astrocytes are also involved in signal transmission through the glutamate-glutamine cycle (Fig 3.2).

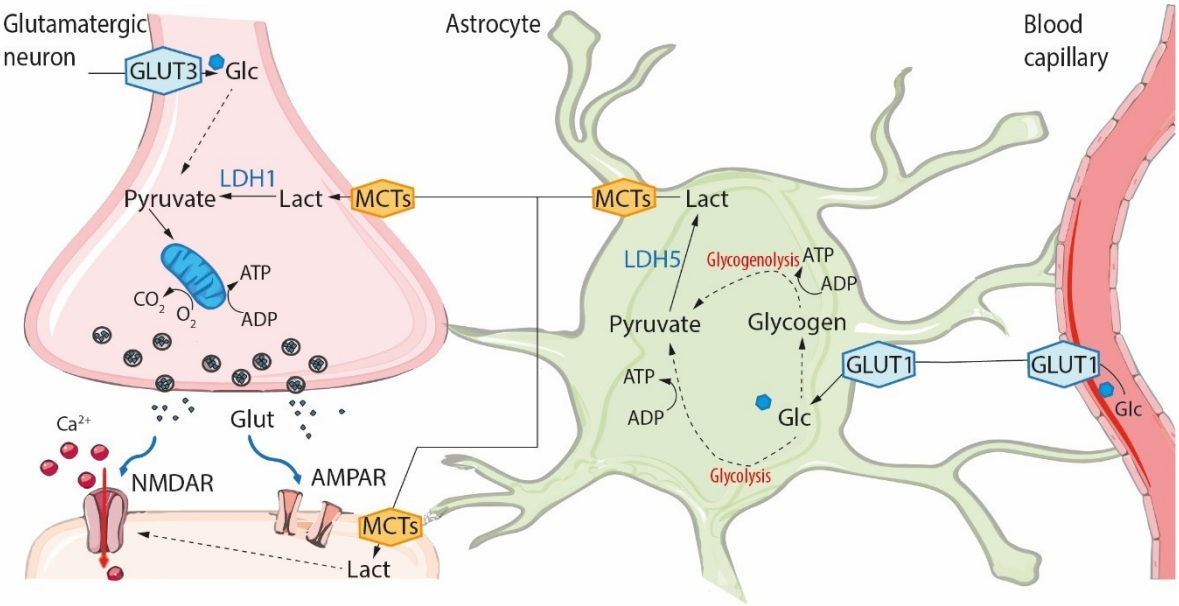

Fig 3.1 Lactate shuttle from astrocytes to neurons. Glucose molecules from blood capillaries can enter the central nervous system through glucose transporters GLUT1 which are expressed in endothelial cells of capillaries and astrocytes. In astrocytes glucose is either metabolized to lactate through aerobic glycolysis or

transformed to glycogen as an energy storage. Pyruvate received from glycolysis or glycogenolysis is converted to lactate with LDH 5 which is predominantly expressed in astrocytes. Lactate is transported to the neurons through MCTs where it is converted to pyruvate for ATP generation through the mitochondrial TCA cycle followed by OXPHOS. Glucose can also directly pass the neuronal membrane through glucose transporters GLUT3 where it can be metabolized completely through glycolysis and subsequent OXPHOS. Glc (glucose), Lact (lactate), GLUT1/3 (glucose transporters), MCTs (monocarboxylate transporters), LDH1/5 (lactate dehydrogenase), Glut (glutamate), vGlut (vesicular glutamate transporter).

Recent studies revealed the importance of lactate as an alternative source of energy (Rabinowitz & Enerback, 2020). Lactate generated from glycogen or glucose is not only a supportive energy source of energy but also plays a role as a signaling molecule (Magistretti & Allaman, 2018). Studies have shown that lactate interacts in mechanisms of neuroprotection and neuroplasticity (Margineanu, Mahmood, Fiumelli, & Magistretti, 2018). During the conversion of lactate to pyruvate through LDH1, NADH is generated as a by-product (Fig.3.1) which can stimulate N-methyl-D-aspartate receptor (NMDAR) for plasticity associated mechanisms (J. Yang et al., 2014). Experiments in rat hippocampus revealed that lactate converted from astrocytic glycogen is involved in processes of long-term memory and long-term potentiation (LTP) maintenance for synapse stability (Suzuki et al., 2011). However, glycogen storages cannot substitute glucose completely to stabilize neuronal functionalities (Shannon et al., 2016). Glycogen is rather supplementary energy source to satisfy high energy demand during neuronal activities. Even other alternative substrates such as ketone bodies, which are recruited during fasting states, are not sufficient to match the cerebral energy demand. Consequently, glucose remains as the major energy provider and is obligatory (Roberts, 2007) for the brain.

3.1.1.3 Glutamate–glutamine cycle

Glucose is also needed for neuronal synthesis of glutamate which cannot pass the blood brain barrier and must be produced directly in the brain (Fig. 3.2). Thereby, glucose is metabolized to accumulate the TCA cycle intermediate, 2-oxoglutarate, which is the precursor for glutamate (Maus & Peters, 2017). Additionally, excitatory amino acid transporters (EAATs) are responsible for the reuptake of synaptic glutamate to prevent an exhaustion of glutamate storages and to protect neurons from excitotoxicity.

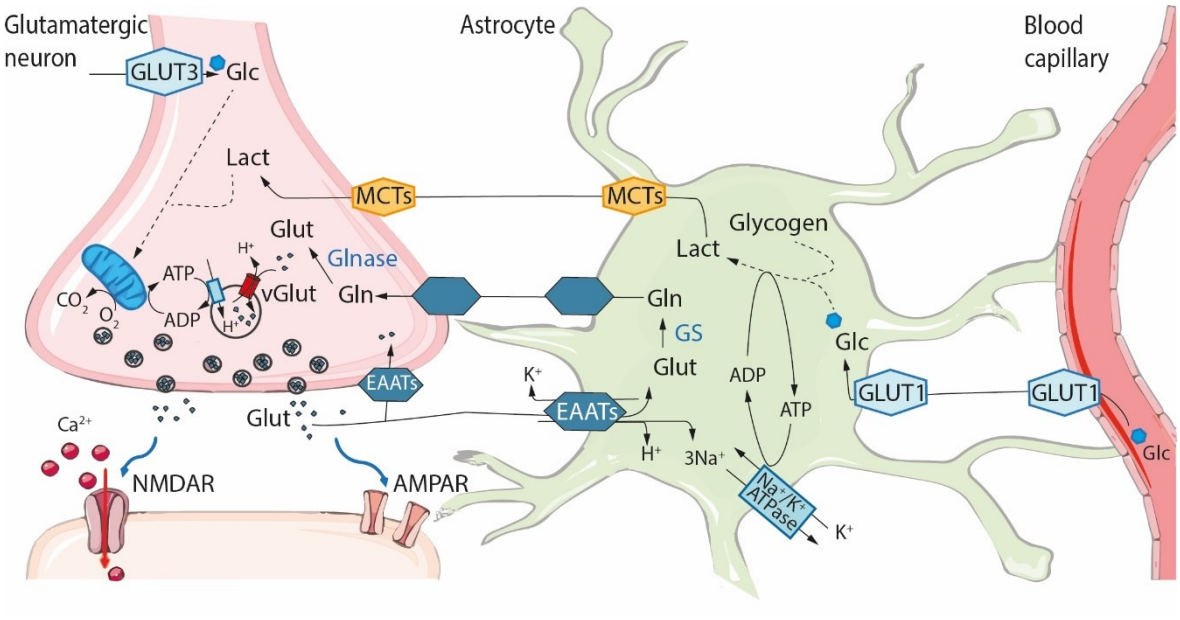

Fig 3.2 Glutamate-glutamine cycle between astrocytes and neurons. Glutamate can be transported from the synaptic cleft into astrocytes through EAATs which act as a symport for sodium ions (Na+) and antiport for potassium ions (K+) (Fahlke, Kortzak, & Machtens, 2016). Na^+/K^+ ATPase keeps the ion gradient for further EAATs transport activities (Magi, Piccirillo, & Amoroso, 2019). Na+ is evacuated from the astrocytes by Na+/K+ ATPase by consuming ATP which is provided by the generation of lactate. GS converts glutamate to glutamine in the astrocytes which can then shuttle to neurons through transporters. In neurons glutamate is regenerated from glutamine by the activation of GS and then stored in vesicles. Alternatively, glutamate can also be retaken into the neuron through EAATs expressed at the presynapse and subsequently transported into the vesicles. At the membrane of glutamate vesicles are vGlut and vesicular ATPase which pumps protons (H^+) into the vesicles under ATP consumption. The generated proton gradient is essential for vGlut which transports glutamate into the vesicle by exchanging H^+. EAATs (excitatory amino acid transporters), Glc (glucose), Lact (lactate), GLUT1/3 (glucose transporters), MCTs (monocarboxylate transporters), LDH1/5 (lactate dehydrogenase), Glut (glutamate), Gln (glutamine), GS (glutamine synthase), Glnase (glutaminase), vGlut (vesicular glutamate transporter).

Intracellular glutamate is transformed to glutamine which can shuttle to the neurons to regenerate glutamate by the activity of glutaminase (Belanger, Allaman, & Magistretti, 2011). Glutamate can then be stored in vesicles or metabolized to glutathione for antioxidative mechanisms.

3.1.2 Redox system in the central nervous system

ROS levels are kept in balance through ROS scavengers which can be roughly divided between enzymatic and chemical antioxidants (Lee, Cha, & Lee, 2020). High energy consumption is causing accumulations of ROS, especially in the brain and other organs with high oxidative activities such as liver, kidney and heart (Dienel, 2019). Especially high metabolic activities in the brain need antioxidant systems with enough capacity to keep ROS levels in balance and to prevent pathologic events caused by oxidative stress. There are enzymatic and non-enzymatic antioxidants (Tab. 3.1).

Enzymatic antioxidants	**Superoxide dismutase**	
	Catalase	
	Glutathione peroxide	
	Peroxiredoxin/Thioredoxin	
Non-enzymatic antioxidants	Transcription factor Nrf2	
	Antioxidant vitamins	Carotenoids (provitamin A), ascorbate (vitamin C), tocopherol (vitamin E)
	Antioxidant enzyme cofactors	Trace elements (selenium, copper, zinc), ubiquinone (coenzyme Q10)

Tab. 3.1 Simplified overview of antioxidants in the brain (Lee et al., 2020).

3.1.2.1 Enzymatic antioxidants

Free-radical ROS such as $O2^{-\bullet}$ is generated by the transition of one single electron to oxygen mostly during mitochondrial ETC at complex I and III (Kudin, Malinska, & Kunz, 2008). Reactive $O2^{-\bullet}$ can be transformed to H_2O_2 by SOD for further signaling function. To keep the ROS levels at physiological levels, peroxides including H_2O_2 are degraded into the corresponding alcohol or water. This reaction is generally catalyzed in the brain by catalases (CAT), thioredoxin (TXN) and glutathione peroxidase (GPX).

3.1.2.1.1 Disulfide reduction systems

Systems of thioredoxin/peroxiredoxin (TXN/PRDX) and glutathione/glutathione peroxidase (GSH/GPX) are disulfide reduction systems with major involvements in general redox signaling (Drechsel & Patel, 2010; Holmgren, 2000). Studies revealed interactions between TXN/PRDX and GSH/GPX systems (Fig. 3.3) while eliminating ROS in parallel with overlapping functions (Lu, Chew, & Holmgren, 2007).

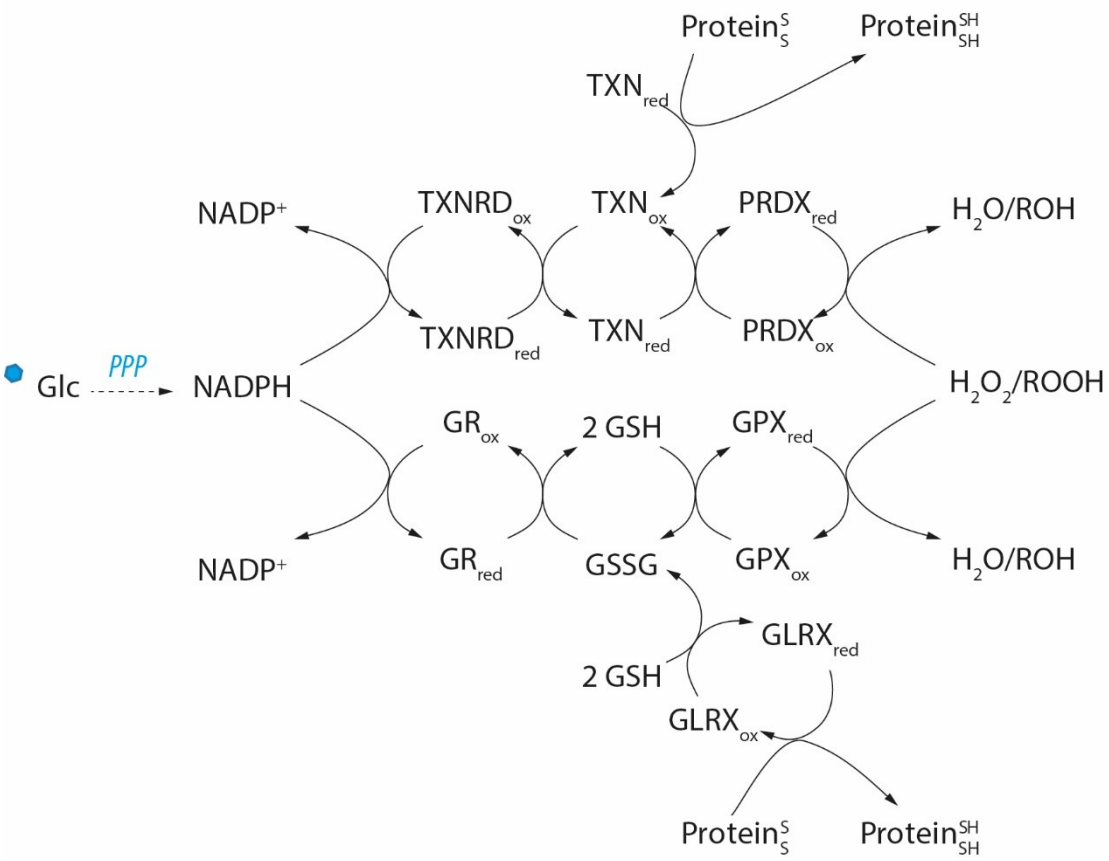

Fig 3.3 Connection between the cellular disulfide reductase systems of thioredoxin and glutathione (Aoyama & Nakaki, 2015). Reduction of hydrogen peroxide can be catalyzed by either PRDX or GPX. Both scavenging reactions are initially provided by NADPH as the electron donor which is produced during PPP. NADPH is needed to recover the reductases, TXNRD and GR, which are oxidized during oxido-reduction reactions. TXNRD reduces oxidated TXN which can subsequently reduce disulfide bonds of PRDX for further reduction of peroxides. In analogy to the TXN system, GR reduces disulfide bonds of GSSG to receive 2 GSH molecules. GSH can recover GPX as an electron donor to reduce peroxides. Additionally, GSH and TXN also reduce disulfide bonds of proteins. Glc (glucose), PPP (pentose phosphate pathway), GPX (glutathione peroxidase), GSH (reduced glutathione), GSSG (oxidized glutathione), GLRX (glutaredoxin), PRDX (peroxiredoxin), TXN (thioredoxin), TXNRD (thioredoxin reductase).

Glutathione (GSH) can reduce oxidated TXN to recover the redox activity of TXN (Du, Zhang, Zhang, Lu, & Holmgren, 2013). Elevated levels of oxidated glutathione mostly indicate mitochondrial dysfunction and has been defined as a biomarker for oxidative stress (Mischley et al., 2016; Rose et al., 2012; Rossi, Dalle-Donne, Milzani, & Giustarini, 2006). The thiol-based antioxidant cycles of TXN and glutathione, both share NADPH as their electron source. Reduced nicotinamide adenine dinucleotide phosphate (NADPH) is recruited from the pentose phosphate pathway (PPP) during glucose metabolism to support antioxidants, such as TXN (Magistretti & Allaman, 2018). GLRX induces deglutathionylation of proteins (Aoyama & Nakaki, 2015). Peroxides and H_2O_2 degradations are crucial because high levels of H_2O_2 in eukaryotes can cause hyperoxidation of PRDX cysteine residues which leads to inactivation of PRDX (Bolduc et al., 2018). Toxic

concentration of H_2O_2 induces irreversible oxidation of thiol-groups resulting in functional impairment of proteins (Finelli, 2020).

3.1.2.1.2 Posttranslational function of the disulfide reduction mechanisms

Both disulfide reduction mechanisms act as a backup for each other in case one of them is impaired (Branco et al., 2017; Ren et al., 2017). The role of H_2O_2 in redox signaling generally relies on oxidating cysteine thiol groups of proteins to a reversible state through S- glutathionylation, S- nitrosylation (SNO) or S-sulfenylation (D'Autreaux & Toledano, 2007; Kramer, Duan, Qian, & Marcinek, 2015). Those reversible posttranslational modifications are directly involved in cellular signaling, gene expression and apoptosis by modulating protein activity, stability and folding (Brandes, Schmitt, & Jakob, 2009; Janssen-Heininger et al., 2008; Kramer et al., 2015). The antioxidant system is necessary to prevent further oxidation of sulfenic acid sites (-SOH) which would lead to an irreversible impairment of protein function (Finelli, 2020). Glutathione (GSH) is the most abundant small antioxidant in the brain (Rice & Russo-Menna, 1998). Glutathione acts as a cofactor for GPX to degrade peroxides and for glutaredoxin (GLRX) to reduce disulfide bonds of proteins (Winterbourn & Metodiewa, 1999). In contrast, TXN can directly reduce disulfides of cysteine residues (Fig 3.3).

3.1.2.1.3 *Neuroprotective role of GSH*

GSH have been found in astrocytes at the highest amount followed by neurons (X. Sun et al., 2006). GSH can shuttle from astrocytes to neurons giving the astrocytes the important role in the redox homeostasis and neuroprotective mechanisms (Dwivedi, Megha, Mishra, & Mandal, 2020; Hirrlinger, Schulz, & Dringen, 2002). Additionally, early experiments showed elevated GSH levels in astrocytes rather than in neurons as a defensive response against excessive nitric oxide (NO) levels which verifies the neuroprotective function of astrocytes (Gegg et al., 2003). GSH can pass the blood brain barrier and reach astrocytes through transporters which are Na^+ dependent (Kannan, Chakrabarti, Tang, Kim, & Kaplowitz, 2000).

3.1.2.2 Non-enzymatic *a*ntioxidants *in the brain*

Nuclear factor erythroid 2–related factor 2 (NRF2) is a transcription factor which enhances the gene expression of antioxidant components such as GPX and glutathione S transferase (Singh & Devasahayam, 2020). Aside from the reductase system in the central nervous system (CNS), there is the selenium transporting

plasma protein, Selenoprotein P, which can pass the blood brain barrier (BBB) to supplement the redox system (Steinbrenner & Sies, 2013). Selenium was reported to enhance the expression of oxidoreductases from the selenoprotein family which include the GPX and TXNRD, in astrocytes to protect neurons from oxidative stress (Benhar, 2018). Supplementation of selenium in the central nervous system contributes to the upregulation of antioxidants which protects from inflammatory processes like in multiple sclerosis (Toledo et al., 2020). The field of antioxidant therapeutics remains less well studied so far. Studies recommend a combination of pharmaceutical drug therapy and dietary strategy, which is adjusted for each patient as an adjuvant intervention, to target pathological mechanism of neurodegeneration and the ageing effect of oxidative stress simultaneously (Winiarska-Mieczan et al., 2020)

3.2 Calcium/Calmodulin-dependent protein kinase 2

3.2.1 Synaptic plasticity at dendritic spines

Structural neuronal plasticity is describes the formation and stabilization of neuronal connections on the one side and the degradation of neuronal junctions on the other side depending on the neuronal activity (Citri & Malenka, 2008). Changes of neuronal junctions can occur within milliseconds which is termed as short term synaptic plasticity but also after hours and days known as the long term synaptic plasticity (Zucker & Regehr, 2002). Neuronal plasticity is essential to format neuronal circuits which consequently are important for emotions, behavior, information processing, learning and memory processes of each individuum (Abraham, Jones, & Glanzman, 2019; Citri & Malenka, 2008). The major part in the cortex are excitatory neurons that connect to the dendritic spines of other excitatory neurons (Keller, 2002). Dendritic spines (Fig. 3.4A) are protrusions of dendrites predominantly found at excitatory neurons and at a small subset of inhibitory neurons (Keck et al., 2011). Dendritic spines are highly dynamic structures (Frank et al., 2018). They can differ in their shapes and size. Mushroom shaped dendritic spines have the longest lifetime and appear at strong neuronal connections. While thin long spines, filopodia, are mostly found at developing neurons. Spines with their largest volume at the head regions do not reach larger sizes than 1 µm (Pchitskaya & Bezprozvanny, 2020). Additionally, their density at the postsynaptic site can vary depending on the neuronal activities. Thereby more axons can connect to the dendrites at the same space through the spine (Wefelmeyer, Puhl, & Burrone, 2016). The key regulator of neuronal plasticity is Calcium-calmodulin-dependent protein kinase 2 (Camk2) (Nicole & Pacary, 2020; G. Zalcman, N. Federman, & A. Romano, 2018).

3.2.2 Characteristics of Camk2

Calcium-calmodulin-dependent protein kinase 2 (Camk2) is a ubiquitous serine/threonine protein kinase, an abundant protein in the brain (Colbran, 1993; Erondu & Kennedy, 1985; Nicole & Pacary, 2020). Camk2 is described as the central protein in the postsynaptic density where it controls long term potentiation (LTP) at glutamatergic synapses (Lisman, Schulman, & Cline, 2002). There are four isoforms of Camk2 which are all expressed in the brain. CaMK2b and CaMK2d are prevalently expressed in the cerebellum, while Camk2a and b is mostly found at the

neocortex and hippocampus with a ratio of 3:1 (a: b) (Bayer, Löhler, Schulman, & Harbers, 1999; Coultrap & Bayer, 2012; Erondu & Kennedy, 1985). Camk2γ and Camk2d are also located in the periphery including the heart (Tobimatsu & Fujisawa, 1989). The isoform Camk2a was in focus of the most studies in the field of LTP and neuroplasticity (Nicole & Pacary, 2020; G. Zalcman et al., 2018). Several studies show that the number and volume of dendritic spines changes are induced by LTP (Engert & Bonhoeffer, 1999; Hill & Zito, 2013; Kulik, Watson, Cao, Kuwajima, & Harris, 2019; M. Matsuzaki, N. Honkura, G. C. Ellis-Davies, & H. Kasai, 2004).

3.2.3 Role of Camk2 in the long term potention (LTP)

The LTP is generally initiated by the NMDAR at glutamatergic neurons which allows an influx of calcium (Ca^{2+}). But NMDAR are only open for Ca^{2+} when several cofactors act together with glutamate binding (Fig. 3.4B). Ionotropic glutamate receptors encompass AMPAR and NMDAR. They are ion channels which open for cations when activated with glutamate. For instance, the AMPAR and kainate receptors, which are permeable for Na^{+}, can cause a depolarization of the postsynaptic membrane. The depolarization is subsequently essential to eliminate the magnesium blockades in the channel pore of NMDAR. Glutamate is then enabled to activate NMDAR when also glycine binds as a coactivator to NMDAR. Activation of NMDAR leads to a strong influx of cations with highest permeability to Ca^{2+} generating Ca^{2+} spikes (Fig. 3.4B). Ca^{2+} builds a complex with calmodulin (CaM) which binds to Camk2, an essential protein for creation of LTP (Lisman et al., 2002; G. Zalcman et al., 2018). Camk2 can translocate to accumulate at neighboring synapses with the higher Ca^{2+} concentration as a support of spine remodeling (Lemieux et al., 2012; Merrill, Chen, Strack, & Hell, 2005). Activation of Camk2 leads to the translocation of AMPAR on the membrane leading to a higher density at the postsynaptic site (Opazo & Choquet, 2011). Additionally, Camk2 phosphorylates AMPAR which enhances the conductance of these ion channels (Poncer, Esteban, & Malinow, 2002). Camk2 is important for reorganizing the actin-cytoskeleton during structural plasticity in spines (Okamoto, Bosch, & Hayashi, 2009). The activation of cofilin through phosphorylation of upstream protein by Camk2a promotes the depolymerization of F-actin which results in spine enlargements (Poncer et al., 2002).

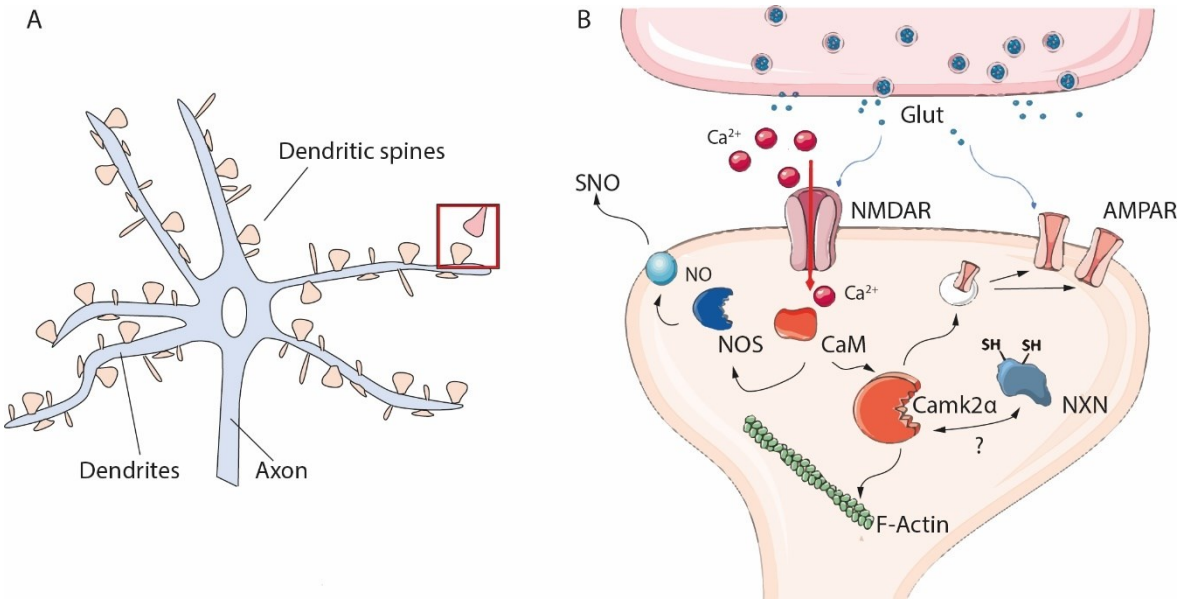

Fig 3.4 Mechanisms of synaptic plasticity at dendritic spines through long term potentiation (LTP). Dendritic spines are protrusions of dendrites predominantly from excitatory neurons. Their shape depends on their state of maturation. Numbers and shapes of dendritic spines vary fast during plasticity events. Red rectangle marks the synaptic connection between a presynapse and postsynapse. (B) Stabilization or formation of synaptic connectivity at glutamatergic neurons is controlled by LTP. Excreted glutamate activates NMDAR. The Mg2+ blockade will only dissociate with cofactors glycine and depolarization of the postsynaptic membrane generated by AMPAR activation which allows a strong calcium influx into the postsynapse. Ca2+ builds a complex with calmodulin which activates Camk2α, the key enzyme for LTP generation. Thus enhances the translocation of the glutamatergic receptors, AMPAR, which leads to a higher excitability of the neuron. Camk2α also stabilizes the synapse through f-actin which builds scaffolds with actin cytoskeletal mesh. Calmodulin activates NOS which subsequently generates NO diffusing into the synaptic cleft for SNO-ing. The post-translational modification, SNO-ing, is responsible for various modulations of protein function and stability. NO can also diffuse to the presynapse activating soluble guanylyl cyclase (cGMP) which enhances cGMP-dependent protein kinase (PKG) responsible for further release of glutamate. Glut (glutamate), NMDAR (N-methyl-D-aspartate receptor), AMPAR (AMPA receptor), CaM (calmodulin), Camk2α (calcium calmodulin kinase 2α), NXN (nucleoredoxin), NOS (nitric oxide synthase), SNO (s-nitrosylation)

3.2.3.1 Involvements of neuronal nitric oxide synthase in LTP

The neuronal nitric oxide synthase (nNOS) is activated through LTP which leads to a release of NO which causes a higher release of postsynaptic neurotransmitters like glutamate (Huang, 1997). SNO-ing of cysteine residues containing proteins with NO which is produced by nitric oxide synthase (NOS) contributes to posttranslational modification of proteins (Tegeder, Scheving, Wittig, & Geisslinger, 2011). S-nitrosylation does not occur directly between NO and thiol groups but instead needs a prior one-electron oxidation to create a transition stage of NO such as NO radicals or an oxidation to N_2O_3 (dinitrogen trioxide) (Smith & Marletta, 2012; Sun, Steenbergen, & Murphy, 2006). One-electron oxidation is dependent from oxygen, transition metals or other electron sinks (Smith & Marletta, 2012).There are three isotypes of NOS (inducible NOS, endothelial NOS, neuronal NOS), which are expressed in different tissues and thereby regulate distinct signaling cascades (Gould, Doulias, Tenopoulou, Raju, & Ischiropoulos, 2013). Neuronal NOS is

expressed at the postsynaptic site of glutamatergic neurons (Garthwaite, 2008) and γ-aminobutyric acid (GABA) mediated interneurons (Tricoire & Vitalis, 2012).

3.2.3.2 Autophosphorylation of Camk2

The Ca^{2+}/CaM-complex binding on Camk2 results into the relieve of the autoinhibition and consequently leads to the autophosphorylation at the threonine 286 site (T286) of Camk2a (Okamoto et al., 2009). This autophosphorylation enables autonomous kinase activities which are Ca^{2+} independent. Autonomous activity, which remains even after intracellular Ca^{2+} level reach the baseline level again, has been believed to be responsible for biochemical memory (Lisman et al., 2002). The autonomous activity of Camk2a is needed for induction of LTP and LTD during neuronal plasticity (Chang, Nakahata, Hayano, & Yasuda, 2019; Coultrap et al., 2014). Although, the activity driven by autophosphorylation is still not completely active and can be enhanced to a 5-fold activity by Ca^{2+}/CaM-complex (Barcomb et al., 2014; Coultrap & Bayer, 2012). Autophosphorylation of Camk2a at T286 also increases its affinity to CaM, which is termed as CaM trapping (Meyer, Hanson, Stryer, & Schulman, 1992). The most prevalent isoforms in the brain, Camk2a and b, differ in their balance of active and inhibitory autophosphorylation (M. Bhattacharyya et al., 2020). In-vitro experiments also revealed that the ratio of Camk2a and b shifts towards Camk2a levels with elevated neuronal activity while a shift towards Camk2b is observed at decreased neuronal activity (Thiagarajan, Piedras-Renteria, & Tsien, 2002). The oxidation at the autoinhibitory site of Camk2 develops an autonomous activity like the autophosphorylation at T286 (Erickson, He, Grumbach, & Anderson, 2011; Zhang, Connelly, Levitan, Sun, & Wang, 2021). Ischemia studies have shown an aggregation of Camk2 through oxidation which partially impairs its activity. The activity deficit of accumulated Camk2 was first balanced out by the autophosphorylation. But as ROS level increased too high, Camk2 aggregated and lost its activity completely (Shetty, Huang, & Huang, 2008).

3.2.4 Long term depression (LTD)

Long term depression (LTD) is as essential as LTP to support remodeling of neuronal circuits during processes of fear memory, spatial reversal learning and social recognition (Collingridge, Peineau, Howland, & Wang, 2010; Shen, Zhu, Panja, Gu, & Li, 2020). Excessive neuronal connections are eliminated through spine shrinkage or extinction also called as pruning (Zhou, Homma, & Poo, 2004).

LTD can be regulated by NMDAR and metabotropic glutamate receptors (mGlut) simultaneously through different cascades (Oliet, Malenka, & Nicoll, 1997). NMDAR and mGlut have bidirectional functions activating LTP or LTD for synapse plasticity (Huganir & Nicoll, 2013; H. Wang et al., 2016). NMDAR initiates LTD instead of LTP if depolarization at the postsynapse is weak due to low Ca^{2+} influx caused by low synapse activity (Luscher & Malenka, 2012). AMPAR, which are usually necessary to activate NMDAR during LTP, are internalized during LTD mechanisms (S. Bhattacharyya, Biou, Xu, Schluter, & Malenka, 2009). The mGlut dependent LTD occurs through activation of the phospholipase C (PLC) pathway which increases Ca^{2+} release from intracellular stores and initiates protein kinase C (PKC) for AMPAR endocytosis (Kang & Kaang, 2016; Kim, Park, Lee, & Ho, 2019).

3.2.5 Redoxregulation of LTP and LTD

ROS has a physiological role as a signaling molecule regulating LTP and LTD during neuroplasticity (Beckhauser, Francis-Oliveira, & De Pasquale, 2016). NMDAR stimulation induces NOX in hippocampal neurons representing the major source for $O2^{-\bullet}$ (Brennan et al., 2009), which can be converted to H_2O_2. Thereby, lower concentrations of H_2O_2 (1 µM) lead to LTP activation but excessive high concentrations (20–100 µM) shifts the mechanisms towards LTD creation (Kamsler & Segal, 2004). A lack of H_2O_2 leads to an impaired spatial memory due to insufficient growth of a neuronal network and distracted neuronal regeneration (Oswald et al., 2018). If H_2O_2 concentrations exceed physiological ranges, neurodegenerative processes and growth cone collapses will be accelerated leading to pathophysiological symptoms (Wilson, Munoz-Palma, & Gonzalez-Billault, 2018). The major Ca^{2+} source in neurons is the intake through NMDAR. An excessive intracellular Ca^{2+} level through NMDAR was reported to be excitotoxic because subsequent Ca^{2+} overload in mitochondria enhances oxidative metabolisms in mitochondria provoking ROS generation from ETC and OXPHOS (Duan, Gross, & Sheu, 2007; Mammucari et al., 2018). Toxic ROS concentrations cause mitochondrial damages by causing impaired ATP production and decreased glucose conversion in the PPP to generate NADPH. Thus subsequently impairs the redox scavenging capacity of GSH leading to oxidative stress in the neuron (R. R. Robinson, Dietz, Maroof, Asmis, & Forsthuber, 2019).

3.3 Nucleoredoxin (NXN)

3.3.1 Characterisitcs of NXN

Early studies described nucleoredoxin (NXN) as a nuclear oxidoreductase due to its predominant localization in the nucleus of cells transfected with expression vector of NXN (Kurooka et al., 1997). Later studies found NXN mainly in the cytosol which suggested a translocation of NXN between nucleus and cytosol. The gene encoding NXN is conserved in mammalian organisms especially between homo sapiens and mus musculus. NXN was identified in different species (Funato & Miki, 2007). NXN is seen as a member of the thioredoxin-like proteins holding two thiol-groups in his structure which are essential for the redox-regulating functionality. 3 D structures of NXN is still unknown. The N-terminus of this protein contains cysteine residues which are suggested to be essential for redox regulating functionality of NXN, similar to the catalytic center of thioredoxins (Funato & Miki, 2007). Further, the C-terminus is constructed similar to the b' domain of protein disulfide protein isomerase (PDI) which is not essential for catalytic effects but contributes to its ability for specific substrate recognition (Klappa, Ruddock, Darby, & Freedman, 1998).

3.3.2 Clinical impact of NXN deficiency

The clinical relevance of functional deficiency of NXN in humans is reported with the Robinow syndrome. Most patients with Robinow syndrome show abnormalities in skeletal development causing shortened upper limbs and shortened stature (Funato et al., 2010; J. J. White et al., 2018). Noticeable are typical dysmorphic face characteristics and hypoplastic genital development. The mortality of this syndrome is low but elevated by cardiac impairment (Roifman, Brunner, Lohr, Mazzeu, & Chitayat, 2019). Pathogenic changes in DVL-1, DVL-3, WNT-5A and ROR2 were found in patients with Robinow syndrome but variants in the gene of NXN were also identified. NXN-related Robinow syndrome also named as recessive Robinow syndrome-2 (RRS2) are passed down from parent to child through autosomal recessive inheritance, while RS related to changes in genes of DVL-1, DVL-3, WNT-5A were reported as autosomal dominant. Pathogenic mutations found in RRS2 patients were identified as nonsense mutation and base pairs deletions in the NXN gene. Investigations about variants of affected genes including Ras-related C3 botulinum toxin substrate 3 (RAC3), led to conclusions that Robinow syndrome is

caused by anomalies in the WNT/PCP pathway (J. J. White et al., 2018). The identified variations in genes encoding proteins relevant for the WNT pathway, including NXN, underline their importance for embryonic development in humans. Consistent to reported skeletal and cardiovascular defects of complete NXN knockout mice causing embryonic lethality (Funato et al., 2010).

3.3.3 Mechanisms of NXN

Detailed molecular mechanisms of NXN are still less well studied. NXN was reported to mediate the canonical WNT pathway as well as the WNT/planar cell polarity (PCP) pathway (Funato et al., 2008; J. J. White et al., 2018).

3.3.3.1 The role of NXN in the canonical WNT pathway

The functionality of Nucleoredoxin was investigated in the cascade of the canonical WNT-pathway which is a mechanism involved in cell proliferation and differentiation. The canonical WNT pathway is also known as the β-catenin dependent pathway. Studies revealed interaction of NXN with the dishevelled protein (DVL) (Funato, Michiue, Asashima, & Miki, 2006). DVL is essential for the WNT signaling pathway although its concrete mechanisms are still undiscovered (Sharma, Castro-Piedras, Simmons, & Pruitt, 2018). At the activation state of the canonical WNT cascade, WNT binds to the transmembrane Frizzled (Fzd) receptor which activates DVL. This results into the inhibition of the β-catenin destruction complex consisting of the tumor suppressor adenomatous polyposis coli (APC), glycogen synthase kinase 3β (GSK3β) and the scaffold protein AXIN. More and more β-catenin molecules accumulate in the cytosol which translocate into the nucleus to activate transcription factors such as T-cell factor/lymphocyte enhancer factor (TCF/LEF) (K. Yang et al., 2016). NXN was reported to inhibit the canonical WNT pathway by associating to the PDZ binding domain of DVL which is essential for anchoring cytoskeletal components to membrane receptors. In vivo experiments uncovered the association of NXN as a competitive inhibition of WNT-β-catenin activators such as the GSK-3 binding protein Frat1. This association was reported to be redox-sensitive. NXN was reported to dissociate from DVL under oxidative conditions through H_2O_2 treatment in cells (Funato et al., 2006).

3.3.3.2 Non-neuronal interaction partners of NXN

Studies of adipogenic differentiation in mice also describe the involvement of NXN in the WNT/β-catenin cascade. An inhibition of the WNT/β-catenin signaling with NXN through DVL were suggested to result in decreased levels of β-catenin and an induction of peroxisome proliferator-activated receptors γ (PPARγ), a transcription factor responsible for the differentiation of adipocytes. Obesity and tendencies to glucose intolerance were described in mice with adipose-specific overexpressed NXN (Adipo-Nrx). Further investigations revealed elevated inflammation and fibrosis in the adipose tissue of Adipo-Nrx mice. Correlating to their in vitro studies showing a lower differentiation rate of preadipocytes into matured adipocytes in NXN-knockdown cells (Bahn et al., 2015). NXN was reported to have inhibitory effects on the signaling cascade of toll- like- 4 receptors (TLR4). TLR4-receptors are responsible for inflammatory and immunity processes. Lipopolysaccharide (LPS) stimulate TLR4-receptors which provokes the activation of the transcription factor nuclear factor kappa-light-chain-enhancer of activated B cells (NF-κB) through myeloid differentiation primary response gene (MyD88). In-vitro studies of embryonic fibroblasts derived from NXN deficient mice evaluated higher levels of NF-κB activation at LPS stimulation due to the absence of NXN (Hayashi et al., 2010). Several studies investigated the processes of liver fibrosis especially caused by chronic abuse of alcohol and found involvements of NXN. Acetaldehyde, a metabolite of ethanol, provokes oxidative stress which in vitro reduces the association rate of NXN with DVL in a WNT independent manner. The accumulation of acetaldehyde resulted in the translocation of β-catenin into the nucleus of human hepatic stellate cells, which led to the activation transcription factors responsible for fibrogenic events (Arellanes-Robledo et al., 2013).

3.3.3.3 neuronal interaction partners of NXN

NXN is described as an oxidoreductase in neuronal cells, which rather has oxidating than reducing activities towards thiols from various proteins (Urbainsky et al., 2018). Mass spectrometry data revealed possible enhancing effects of H_2O_2 related oxidation of target proteins in the presence of NXN. Peroxiredoxin 1 (PRDX 1) was identified as a potential interaction partner oxidizing NXN for further effects on proteins related to morphological changes and signal transduction of neuronal cells. Their data suggested that NXN acts as an oxidase in neuronal pathways. NXN is

expressed unspecific in the periphery but predominant in skin and testis. Interestingly, mRNA of NXN was also reported to be located in dorsal root ganglia, some parts of the brain and limb buds of murine embryos (Kurooka et al., 1997). In-vitro studies report an inhibitory effect of NXN on protein phosphatase 2A (PP2A) activity (Lechward et al., 2006). PP2A in neurons is essential for the dephosphorylation of AMPAR to reverse LTP and generate LTD (J. Wang et al., 2019). PP2A is involved in synaptic plasticity but also various cell signaling pathways (Nematullah, Hoda, & Khan, 2018). Little analysis of functionality of NXN in neuronal pathways has been done so far.

3.3.3.4 Linkage of the canonical WNT pathway and neuronal plasticity

Wnt7a was described to affect neuronal plasticity in both direction (up- and downscaling) (Ciani et al., 2011). At the presynaptic site, Wnt7a regulated growth cone (Ciani et al., 2011; Galjart, 2005) and neurotransmitter release (Ahmad-Annuar et al., 2006) by initiating the canonical WNT pathway (Salinas, 2007) mediated through DVL1 (Fig.3.5). At the postsynaptic site, Wnt7a initiated WNT signaling through DVL1 (Dickins & Salinas, 2013) to activate Camk2 resulting in LTP generation. This mechanism was reported to enhance dendritic spine remodeling (Ciani et al., 2011; McLeod et al., 2018) in terms of spine density and maturation (Viale et al., 2019) by increasing AMPAR insertion at the postsynaptic membrane (McLeod et al., 2018). Regulatory activities of NXN on neuronal plasticity involved transcription factors were discovered, such as the cAMP response element-binding protein (CREB) and activator protein 1 (AP-1) (Hirota et al., 2000). Our interest was to study the interaction of NXN with Camk2a to reveal the functional role of NXN in neuroplasticity and thereby the connection to neurodevelopmental diseases.

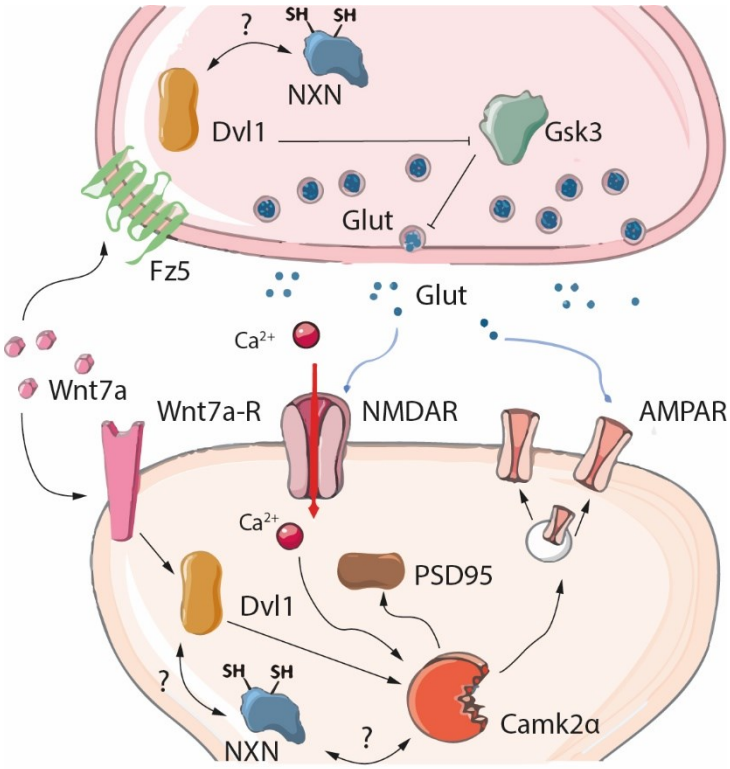

Fig 3.5 Linkage between Wnt7a initiating the canonical WNT pathway and Camk2a mediated neuronal plasticity. Wnt7a is a bidirectional signaling molecule meaning that it regulates mechanisms at the presynaptic and postsynaptic site. Wnt7a can be found at hippocampal and cerebellar synapse. At the presynapse, Wnt7a binds to Fz5 which induces the divergent-canonical WNT pathway by DVL1 activation leading to the inhibition of Gsk3β. Thus, inhibitory effects of Gsk3β are neutralized leading to a clustering of presynaptic components as well as synaptic vesicles. At the postsynaptic membrane, Wnt7a binds to its receptor and promotes PSD-95 recruitment, spine stabilization and remodeling activities through stimulating DVL1 and Camk2. Frizzled 5 receptors (Fz5), Dishevelled protein-1 (DVL1), Glycogen synthase kinase-3 ß (Gsk3β), postsynaptic density protein 95 (PSD95) adapted from (Dickins & Salinas, 2013).

4. Materials And Methods

LacZ histochemistry, RNA and protein analysis of NXN expression were conducted by Lucie Valek and IntelliCage parameters were analyzed as described in (Tran et al., 2021) by Irmgard Tegeder.

4.1 Mice

Experiments were approved by the local Ethics Committee for Animal Research (Darmstadt, Germany) and are adhered to standards of the Society of Laboratory Animal Science (GV-SOLAS) as well as the guidelines of Animal Research: Reporting of in Vivo Experiments (ARRIVE) to comply with European and German directives for animal welfare in science. Behavioral mice experiments were initiated at the youngest age of 8–12 weeks. Mice were acclimatized to the experiment rooms, cages or mazes before starting experiments. They had free access to food and water and were maintained in climate-controlled rooms (20–24 °C with 45–65 % humidity) at a 12 h light-dark cycle.

4.1.1 Generation conditioned NXN deficiency in neurons of mice

The Cre/loxP technology was used to create the conditioned pan-neuronal knockout of nucleoredoxin (NXN). In NesNXN$^{-/-}$ mice the essential exon 2 in the *nxn* gene (ENSMUSG00000020844) is deleted. Floxed nucleoredoxin mice were obtained from the European Conditional Mouse Mutagenesis Program (EUCOMM; Nxn^{tm1a}(EUCOMM)$^{Wtsi/leg}$). Mice carry a conditional-ready allele which was inserted by homologous recombination (Fig. 4.1).

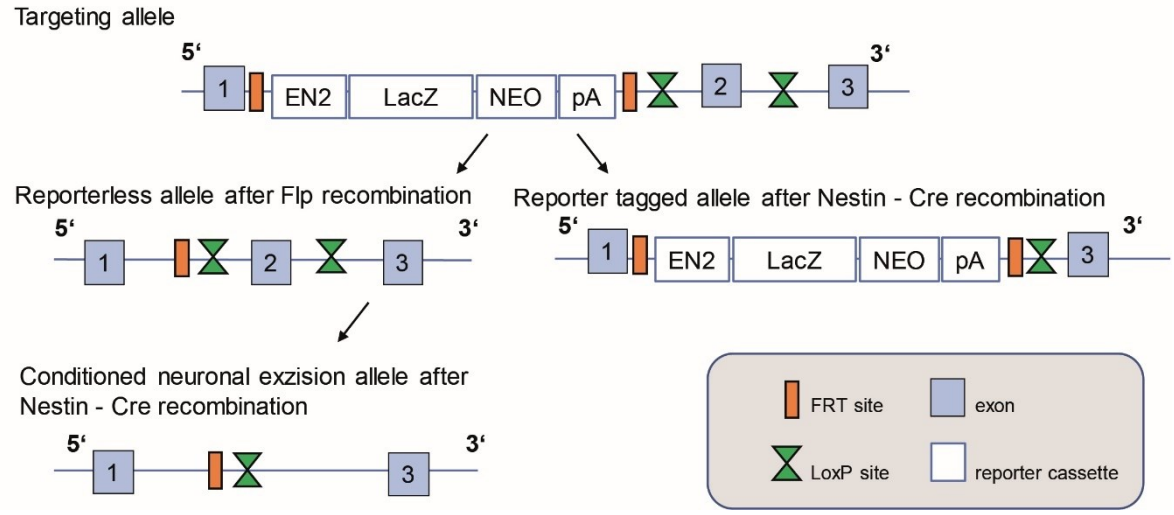

Fig 4.1 Gene construct of the conditioned knockout of NXN. The targeting allele is a promoterless selection cassette and is composed of a reporter cassette which was flanked by Flippase recognition target (FRT) sites, prior to the floxed exon 2 which is essential for NXN functionality. A reporterless floxed allele can be generated by flippase recombinase (Flp) expression. The subsequent Nestin-Cre recombinase expression results in a pan-neuronal deficiency of NXN. Reporter tagged allele had a reporter cassette composed of Engrailed 2 (EN2) as the promoter of Frt sites followed by a lacZ sequence, neomycin and polyA. Reporter mice were generated by the recombination with Nestin-Cre.

The first gene construct of the target allele was composed of a flippase recognition target (FRT) flanked reporter cassette prior to exon 2 flanked by loxP sites. The reporter cassette was removed by breeding with flippase recombinase (Flp)-mice (Fig. 4.1) to generate reporterless NXN-flfl mice. They were subsequently mated with Nestin-Cre mice (The Jackson Laboratory, B6.Cg(SJL)-Tg(Nes-cre)1Kln/J) for exicision of exon 2 to create NesNXN$^{-/-}$ mice. Reportedly, Cre-recombinase activity starts with embryonic day 11 (Harno, Cottrell, & White, 2013) and continues until the postnatal state (Liang, Hippenmeyer, & Ghashghaei, 2012). NesNXN$^{-/-}$ mice have a C57BL6N genetic background. The successful pan-neuronal deletion was confirmed at RNA and protein level.

4.1.2 Genotyping

Mice were genotyped using the KAPA2G Fast HotStart Genotyping kit (Sigma, #KK5621) for tail tip biopsies or ear punches. Tissue samples were lysed by heating in a ThermoMixer (Eppendorf, Hamburg) at 70 °C for 10 min after adding 50 µl of a master mix for DNA extraction containing a thermostable protease, followed by an additional heating step at 95 °C for 5 min to inactivate enzymes.

PCR-grade water	44 µl
10X KAPA Express Extract Buffer	5 µl
1 U/µl KAPA Express Extract Enzyme	1 µl

Tab. 4.1 DNA extraction (each sample)

For DNA amplification a PCR master mix containing DNA polymerase and primers were prepared and 2 µl of DNA extract was added to each reaction.

PCR-grade water	6 µl
2X KAPA2G Fast (HotStart) Genotyping Mix with dye	10 µl
10 µM Primer Forward	1 µl
10 µM Primer Reverse	1 µl
Sample	2 µl

Tab. 4.2 PCR master mix (20 µl reaction)

Eppendorf tubes were centrifuged briefly to set the sample mix at the bottom of the tubes. Cycling protocol was set up in the PCR depending on the used primers.

Initial denaturation	94 °C for 3 min	1 cycle
Denaturation	94 °C for 45 s	35 cycles
Annealing	55 °C for 45 s	
Extension	72 °C for 1 min	
Final extension	72 °C for 10 min	1 cycle
Hold	10 °C	
Cycling protocol for Cre		
Initial denaturation	94 °C for 5 min	1 cycle
Denaturation	94 °C for 30 s	34 cycles
Annealing	58 °C for 30 s	
Extension	72 °C for 45 s	
Final extension	72 °C for 5 min	1 cycle
Hold	10 °C	
Cycling protocol for NXN		

Primer name	**Sequence**	**Product size (bp)**
CB1 Forward	gct gtc tct ggt cct ctt aaa	400
CB1 Reverse	ggt gtc acc tct gaa aac aga	
Cre Forward	gaa agc agc cat gtc caa ttt act gac cgt	250
Cre Reverse	gcg cgc ctg aag ata tag aag a	
NXN Forward	ttc cca ggt tct cag ctt cc	204
NXN Reverse	cat ctt gga gtg caa tga gac c	
CAS_R1_Term	tcg tgg tat cgt tat gcg cc	

Tab. 4.3 List of primer sequences for genotyping.

PCR products were then analyzed with agarose electrophoresis analysis. For this purpose, a 1.5 % agarose gel was prepared in a 1x TBE buffer. 5 µl ROTI®Gelstain dye (Carl Roth, Karlsruhe) was added per 100 ml agarose gel as a substitute for ethidium bromide. PCR products and the DNA ladder mix (100-10000 bp) were loaded to the gel. The electrophoresis was run for approximately 30-45 min at 100 V. UV- signal was visualized by the Molecular Imager® Gel Doc XR system (Biorad, Munich) and analyzed with Quantity One® 1-D analysis software (Biorad, Munich).

4.2 Immunhistochemical analysis

4.2.1 LacZ histochemistry (conducted by Lucie Valek)

The lacZ reporter gene is controlled by the promoter of NXN. The β-galactosidase expression (β -Gal) is stained as a blue signal by oxidation with 5-bromo-4-chloro-3-indolyl-β-D-galactopyranoside (X-Gal) reagent. Tissue embedded after

preparation as described in 4.2.2 (Perfusion and Immunofluorescence of brain tissue) was postfixed in 2 % PFA for 5 min and washed with 2 mM $MgCl_2$ in 1xPBS solution. Slides were then rinsed three times in detergent buffer (2 mM $MgCl_2$, 0.1 % sodium deoxycholate, 0.02 % Nondiet P40 in 1x PBS pH 7.5) at room temperature for 5 min. Staining solution composed of 0.5 mg/ml nitrotetrazolium blue chloride (NTB) and 5 µg/ml phenazine methosulfate (PMS) in detergent washing solution was incubated at 37 °C. Incubation time was optimized for each tissue. Slides were rinsed 3 times with 1xPBS for 5-10 min to stop the reaction. Subsequent counter-staining was conducted by rinsing in eosin solution. Finally, slides were dehydrated with an increasing ethanol dilution gradient and then rinsed in xylene before embedding in Pertex (MEDITE, Orlando, USA) mounting medium. Microscopy was performed with a BZ-9000 inverted fluorescence microscope (Keyence, Osaka, Japan) with automated image stitching function (conducted by Lucie Valek) (Tran et al., 2021).

4.2.2 Perfusion and Immunofluorescence of brain tissue

Mice were euthanized by gradual induction of carbon dioxide (CO_2) into an enclosed chamber. For perfusion a pump was used to guarantee the evenness of perfusion rate. Heart was punctuated with the perfusion needle into the left ventricle while the right atrium was cut open to release washed-out blood from the system. Mice were perfused with 0.9 % sodium chloride solution (NaCl) first to remove blood from the blood vessels which would influence the quality of fixation. Each adult mouse was perfused with approximately 50 ml NaCl. The perfusion rate was kept at a low level to prevent damages to blood vessels. Approximately 50 ml of 2 % ROTI®Histofix was perfused to fixate tissue. Organs were dissected and kept in 2 % PFA on ice. Post-fixation of mice brain was done overnight at 4 °C. Tissue was subsequently dehydrated in a gradually increasing concentration of sucrose beginning with 10 %, 20 % and ending with 30 %. Sucrose concentration was elevated each time the tissue settled down due to higher density. After dehydration step tissue was embedded in glycerol-based Tissue-Tek® O.C.T.™ and kept at -80 °C until cryostat sectioning. Embedded tissue was prechilled to -20 °C for at least 1 hour before sectioning. Samples were cut in the cryostat to 10 µm sections at -20 °C and air dried at room temperature before freezing slides at -80 °C. For immunofluorescence stainings, slides were washed in 1x PBS at room temperature to rehydrate tissue and eliminate embedding material. Tissue was permeabilized by incubating

samples in 0.1 % Triton X-100 (PBSTx) for 20 min at room temperature. To reduce unspecific binding of antibodies, a blocking buffer consisting of 3 % albumin fraction V (BSA) in PBSTx was added to the slides and incubated for 2 hours at room temperature. After the blocking step, samples were incubated with the primary antibodies overnight at 4 °C. Slides were immersed in 1x PBS and incubated with secondary antibodies for 2 hours at room temperature. Antibodies were diluted to the desired concentration in 1 % BSA/PBSTx solution. Primary antibodies included NXN, Camk2a, NeuN (Tab. 4.4). Secondary antibodies were labeled with fluorochromes (Invitrogen, Sigma, Life Technologies). Slides were mounted with an aqueous mounting medium (aqua-Poly/Mount). Stained tissue slices were analyzed on an inverted fluorescence microscope (BZ-9000, KEYENCE, Germany and Axio Imager Z1, Zeiss, Germany). Tiled images were obtained to reconstruct whole brain regions.

Primary antibody					
Antibody	**Manufacturer**	**Product Nr**	**Dilution**	**Species reactivity**	**Type**
NXN	Sigma	HPA023566	1:200	rabbit	pab
Camk2a	Invitrogen	MA1-048	1:500	mouse	mab
NeuN	Millipore	MAB377	1:200	mouse	mab
MAP-2 Alexa488	Sigma	MAB3418X	1:400	mouse	mab
Secondary antibody					
Antibody	**Manufacturer**	**Product Nr**	**Dilution**	**Species reactivity**	**Type**
Alexa Fluor 488	Invitrogen	A27034	1:800	rabbit	pab
Alexa Fluor 488	Invitrogen	A11029	1:800	mouse	pab
Cy3	Sigma	C2181	1:800	mouse	pab
Alexa Fluor 647	Thermo Fisher	A-21235	1:500	mouse	pab

Tab. 4.4 List of antibodies used for immunofluorescence stainings. pab (polyclonal antibody), mab (monoclonal antibody)

4.2.3 Immunofluorescence of primary neuronal culture

Primary neurons were cultured for 14 days as described in 2.3 (Cell culture) For localization of NXN and Camk2a, primary cultures were washed with pre-warmed PBS and fixed in 4 % paraformaldehyde (PFA) for 25 min at room temperature. Cover slips were then washed with 1x PBS and permeabilized with 0.01 % Triton X-100 at room temperature for 15 min. Blocking and staining procedures were conducted as described for tissue samples in 2.2.2 (Perfusion and Immunofluorescence of brain tissue). Microtubule-associated protein 2 (MAP2)

conjugated Alexa-488 antibody was additionally incubated overnight at 4 °C. Cover slips were washed with 1x PBS and DAPI was added for 10 min. Cover slips were mounted with Aqua-Poly/Mount after neurons were washed with PBS again. Images were captured on the confocal microscope Zeiss LSM 800 (Zeiss, Jena, Germany).

4.2.4 In-situ proximity ligation assay of primary cortical neurons

Primary cortical neurons were used for the proximity ligation assay (PLA) to elucidate the colocalization of NXN and Camk2a. Fixation and permeabilization was performed as described in 2.2.2 (Perfusion and Immunofluorescence of brain tissue). Duolink™ In Situ PLA® kit was used to conduct PLA experiments. Cover slips were incubated with Duolink® blocking buffer for 1 hour at 37 °C. Primary antibodies were diluted in Duolink antibody diluent to the same concentration as used in immunofluorescence staining (Tab. 4.4) and incubated overnight at 4 °C. Cover slips were washed with buffer A provided in the Duolink™ In-Situ PLA® kit. PLA probes were incubated for 1 h at 37 °C in a preheated humidity chamber. Probes matched to the hosts of primary antibody (anti-mouse PLUS probe to bind on primary antibody anti-Camk2a, anti-rabbit MINUS probe to bind primary antibody anti-NXN). Ligase was diluted and was put on neurons for 30 min at 37 °C after washing steps with buffer A. After the hybridization step, a diluted amplification solution, containing the polymerase, was incubated for 100 min at 37 °C in the humidity chamber. The rolling circle amplification was stopped by washing with buffer B provided in the kit. As indicated by the manufacturer, the polymerase only starts the rolling circle amplification (RCA) when targeted proteins are localized closer than < 40 nm to each other. Cy3-labeled complementary oligonucleotides bind to the single strand DNA product which enables the fluorescent detection of PLA signals as dots. The Alexa488-conjugated MAP2 antibody was incubated on PLA samples overnight and washed with washing buffer B. The Duolink® in situ mounting medium, containing DAPI for nuclear counterstaining, was used afterwards. Slides were sealed with nail polish and stored at -20 °C until imaging. Images were captured with the confocal microscope Zeiss LSM 800 (Zeiss, Jena, Germany) at 40x magnification.

4.3 Cell culture

4.3.1 Primary culture of cortical and hippocampal neurons

Glial cells and neurons were isolated from cortical and hippocampal tissue of P0 postnatal pups after decapitation. Hippocampal and cortical neurons were isolated with the same protocol whereas the maintaining buffer differs from each other (Tab. 4.5). Primary neuronal cultures need factors of astroglia cells to survive and for synaptogenesis (Eroglu & Barres, 2010). Adding these factors from used astroglia cell medium gets even more essential after adding cytosine arabinoside (Ara-C) treatment to inhibit the differentiation of astrocytes. AraC is anti-mitotic and can prevent glial contamination in primary neuronal cultures by adding early after plating, but neurons must stabilize first to prevent toxic effects on the culture (Moutin et al., 2020). Even the maintenance medium for the neurons is serum-free to prevent contamination of the cultures with astrocytes. Supplements are therefore provided by collecting used medium from primary cultures of glial cells. This step is optimally done before the planned isolation of hippocampal and cortical tissue. Glial cells were isolated from cortical tissue and the isolation procedure is equal to those for primary neurons except the medium.

	Dissociation medium (DM)	**Maintenance medium (NGM /MEM++)**	**Conditioned Maintenance medium (NGM con)**
Glial cells	MEM, 10 % horse serum,	MEM, 30 mM Glucose, 50 µg/ml Pen-Strep, 10 % horse serum	
Cortical neurons	NB, 10 % FCS	NB, B27 (1 ml/50 ml), 1 % Glutamax, 50 µg/ml Pen-Strep	NGM, 15 % glial medium
Hippocampal neurons	NB, 10 % FCS	NB, B27 (1ml/50ml), 1 % Glutamax, 50 µg/ml Pen-Strep	NGM, 30 % Glial medium, 15 % cortical medium

Tab. 4.5 Composition of cell culture media of primary glial cells, cortical and hippocampal neurons.

Before the day of preparation glass cover slips were covered with poly-D-lysin (100 µg/ml diluted in sterile PBS) overnight at 4 °C. Coated coverslips were washed with sterile PBS and prewarmed to room temperature immediately before plating neurons. Tissue was collected in ice cold PBS until finishing preparation of all pups (around 5-8 pups per breeding). Tissue was incubated with 1 mg/ml papain (Sigma) activated with L-cysteine (30 min, 37 °C at 5 % CO2) and shook every 10 min. Digestion was stopped by adding dissociation medium (DM). After the tissue settled down to the bottom of falcon tubes, the supernatant was discarded, and new DM was added. Wash step was repeated twice. Maintenance medium (NGM/MEM++)

was added to the tissue for trituration with a 1000 µl pipette tip. During trituration (10 times per sample), it was ensured to prevent foam development. Samples were kept on ice for 3 min to let larger pieces of tissue settle down. The supernatant was transferred to a new falcon tube and centrifuged (800 rpm, 5 min, 4 °C). Pellet was resuspended in NGM/MEM++ and diluted to a concentration of (5 x 105 cells/ml) after counting with trypan blue dye in a hemocytometer. Cell suspension was plated on coated cover slips and incubated for 2 h at 37 °C at 5 % CO2. After cells adhered, 600 µl maintenance medium was added to each well of a 12-well plate. 4 µM AraC treatment was added to the primary neuronal culture at the 3rd day in vitro. Additional 600 µl conditioned maintenance medium was added on the 4th and 7th day after the plating and then once a week. Primary neurons were cultured for 14 d where dendritic spines began to mature.

4.4 Assays

4.4.1 Immunoprecipitation and Camk2 activity assay

Cerebellum samples were dissected after decapitation of mice. Tissue was homogenized rapidly in ice cold non-denaturing lysis buffer (Tab. 4.6) with a potter tissue homogenizer and centrifuged for 40 min at 4 °C with 12000 rpm. The supernatant was discarded, and the pellet was resuspended. Samples were aliquoted on ice and kept in -80 °C for measurements. Total protein concentrations were determined with bicinchoninic acid assay (BCA assay). 2700 µg whole protein extract was incubated with 19 µl anti-Camk2a antibody for 1 h at 4 °C. 125 µl beads were added to each sample and incubated overnight at 4 °C. Samples were centrifuged at 2500 rpm for 5 min. Supernatant was then discarded and a lysis buffer was added to wash the beads. Wash and centrifugation steps were repeated 3 times. The end of a 1000 µl pipette tip was cut open to guarantee a gentle resuspension of the pellet through careful agitation. The pellet was resuspended in 125 µl buffer.

20 mM	Tris HCl
137 mM	NaCl
1 %	TritonX-100
2 mM	EDTA
1X	protease inhibitor cocktail (Sigma)
1X	phosphatase inhibitor cocktail (Sigma)

Tab. 4.6 Composition of non-denaturing lysis buffer

The CaM kinase II Assay Kit is a phosphocellulose assay which was designed to measure activities of purified Camk2 samples. The Assay was performed with two assay buffers, kinase buffer including Ca^{2+}/Calmodulin (Tab. 4.7) to measure Camk2's total activity and kinase buffer without Ca^{2+} and Calmodulin to determine the autonomous activity of Camk2.

Ca^{2+}/Calmodulin plus kinase buffer		**without Ca^{2+}/Calmodulin kinase buffer**	
1.25 mM	ATP	1.25 mM	ATP
125 mM	$CaCl_2$	100 mM	EGTA
200 ng/ml	Calmodulin	As Calmodulin substitute	ddH2O

Tab. 4.7 Composition of Ca2+/CaM containing assay buffer and Ca2+/CaM negative assay buffer.

Each well was filled with beads-antibody-enzyme-complex which was isolated from the brain tissue as described above. The well preparation was conducted in ice. Camk2 activities of the enzyme samples were elucidated under different treatments (1µM recombinant NXN, 1mM H_2O_2, vehicle). A positive control 15mUnits Camk2 (MBL, Woburn) and a negative control without enzyme was included in the measurements. Each well was set with a total volume of 10µl sample, which was composed of the purified enzyme and the treatment or vehicle. The reaction was started by adding 90 µl kinase buffer to each well (Tab. 4.7). After the incubation step (30 min at 30 °C), wells were washed five times as described in the manufacturer's protocol. The solution of a horseradish peroxidase (HRP) conjugated detection antibody was added to each sample and incubated at room temperature for 60 min. After another wash step with 5 repetitions, substrate reagent provided in the kit was given to the wells and incubated for 5 min at room temperature. Stop solution was given on time to each well to prevent signals over the limit. Absorbance was measured within 30 min after adding the stop solution at 450 nm with the plate reader, Infinite 200 PRO Reader (Tecan, Crailsheim). The absorbance of samples was conducted as triplicates.

Samples	**Beads**	**Kinase buffer (+/-)**	**0,23 µg/µl rNxn (1 µM final conc.)**	**5 mM H2O2 (1 mM final conc)**
A	5 µl	3.2 µl	0 µl	0 µl
B	5 µl	2 µl	1.19 µl	0 µl
C	5 µl	3.2 µl	0 µl	2 µl
D	5 µl	2 µl	1.19 µl	2 µl
Positive control	0.5 µl	9.5 µl	0 µl	0 µl

Negative control	0 µl	10 µl	0 µl	0 µl

Tab. 4.8 Sample preparation for each sample well

4.4.2 Isolation of mitochondria from brain tissue

Isolated mitochondria from brain tissues of age-matched mice were used to assess oxygen consumption rates with the Seahorse XFe96 Analyzer (Agilent, Santa Clara). Mitochondria were isolated through discontinuous Percoll® (Merck, Darmstadt) density gradient centrifugation (Sims & Anderson, 2008). Percoll® stock solutions were diluted with the isolation buffer (Tab. 4.9) and adjust to pH 7.4 with 0.1 M HCl. The isolation buffer was stable for 3 days at 4 C.

10 mM	Tris-HCl
1 mM	EDTA-K+
320 mM	Sucrose
pH 7.4 adjusted with 0.1 M HCl	

Tab. 4.9 Components of the isolation buffer for tissue homogenization.

Prior to the tissue dissection, a Percoll® gradient made of 26 % and 40 % Percoll® was generated freshly. Careful layering was necessary to prevent the Percoll® dilutions from being mixed and to generate a clean gradient. The discontinuous density gradient was built at a regular and slow flow rate through the apparatus shown in Fig. 4.2. Percoll® gradient was kept on ice and protected from shaking disturbances.

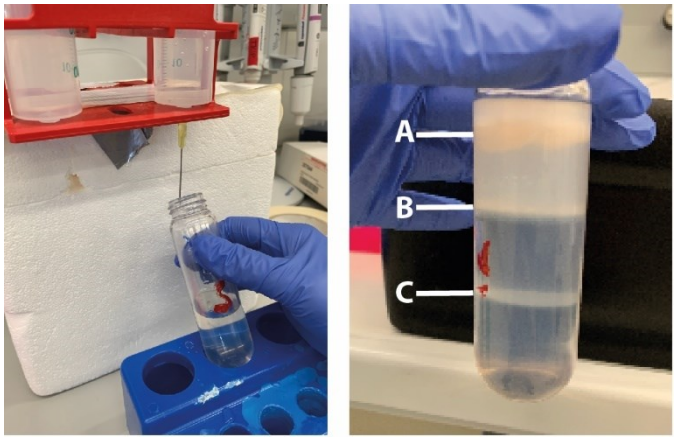

Fig 4.2 Generation of the density gradient. A 50 ml perfusion syringe with a cannula (ø 0,90 x 40 mm) was held in an elevated falcon stand to generate the density gradient (left). Centrifugation through the discontinuous density gradient generated 3 layers (right). Myelin is accumulated in the upper layer (A), the middle layer (B) contains mainly synaptosome, myeline and some mitochondria followed by the third layer (C) highly enriched with mitochondria.

Mice were sacrificed through decapitation. Brain tissues were dissected rapidly in an ice-cold isolation buffer. Meninges was removed and the brain was washed with

an isolation buffer to eliminate blood. Tissue was cut in small pieces and transferred to a 4 ml isolation buffer mixed with protease inhibitor in a glass Weathon® dounce tissue grinder (DWK Life Sciences, Mainz). Tissue was homogenized on ice four times with the loose glass pestle, followed by eight strokes with the tight pestle. Each stroke was executed without pressure and with pauses to keep the sample temperature low. The same volume of 24 % Percoll® (pH 7.4, ~ 4 ml) was given to the sample to create a 12 % Percoll® suspension. Homogenate was layered on the top of the prepared discontinuous gradient. Each tube contained 10 ml of 40 % Percoll®, 14 ml 26 % Percoll® solution and 8 ml 12 % Percoll® -homogenate mixture. Tubes were centrifuged in the fixed-angle rotor (JA-30.50, Beckman Coulter) for 20 min at 4°C with 55600 g. Centrifugation created three phases (Fig. 4.2). The mitochondrial layer between the 2nd and 3rd phase was transferred by a glass pipette and washed twice with isolation buffer by resuspending and centrifuging for 15 min at 4°C with 30300 g. Finally, mitochondria were resuspended in the mitochondrial assay solution (MAS) composed of 220 mM mannitol, 70 mM sucrose, 10 mM KH_2PO_4, 5 mM $MgCl_2$, 2 mM HEPES and 1 mM EGTA (Tab. 4.10). MAS was generated without BSA to determine the whole protein concentration through BCA assay.

4.4.3 Seahorse analysis of oxygen consumption in isolated mitochondria

Oxygen consumption ratio (OCR) was measured in fresh mitochondrial lysates from brain tissues. Isolated mitochondria from frozen tissue samples would develop an uncoupled electron transport chain due to damages of mitochondrial membrane (Acin-Perez et al., 2020). Time span between mice sacrifices and measurement of respiratory activity took maximal 5 h. XF Sensor Cartridge (Agilent) was hydrated in XF calibrant buffer in a non-CO2 incubator at 37°C, one day prior to the assay. MAS buffer was prepared fresh on the day of preparation (Tab. 4.10).

220 mM	Mannitol
70 mM	Sucrose
10 mM	Potassium dihydrogen phosphate
5 mM	Magnesium chloride
2 mM	HEPES
1 mM	EGTA
pH 7.4	

Tab. 4.10 Composition of 1X mitochondrial assay solution (MAS buffer).

MAS was used to resuspend mitochondrial pellets and to generate the 10x stock solutions of the substrates and inhibitors to load the ports of XF Sensor Cartridge. After isolation of mitochondria from brain tissue and protein concentration determination, 5 µg of each sample was added to each well of a seahorse XF cell culture plate (Agilent, Santa Clara). This 96-well plate was centrifuged in a plate centrifuge (20 min at 4 °C with 2000 g). The generation of a monolayer of attached mitochondria to the well surfaces was confirmed through microscopy with at least 20X magnification. Assay buffer consisting of 1X MAS and 0.2 % fatty acid free BSA was added to the plate and incubated for 5 min at 37 °C in a non-CO2 incubator. 10x stocks of substrates and inhibitors in MAS without BSA were loaded into the ports of the hydrated cartridge (Tab. 4.11). The cartridge was calibrated before measurements.

Port	Compound	10x stock solution	Final conc (µM)
A	ADP/pyruvate/malate	45 mM/ 100 mM / 50 mM	4.5 mM/ 10 mM/ 5 mM
B	Oligomycin	30 µM	3 µM
C	FCCP	40 µM	4 µM
D	Rotenone/AA	20 µM/40 µM	2 µM/ 4 µM

Tab. 4.11 Concentrations of substrates and inhibitors of mitochondrial respiration loaded to the defined ports. Abbreviations: adenosine diphosphate (ADP), FCCP (carbonyl cyanide-p-trifluormethoxyphenylhydrazone), antimycin A (AA).

10 mM pyruvate, 5 mM malate and 4.5 mM adenosine diphosphate (ADP) were injected to measure the basal respirational activity of isolated mitochondria. 3 µM oligomycin was used to assess ATP generation and proton leakage. Subsequently, 4 µM FCCP (carbonyl cyanide-p-trifluormethoxyphenylhydrazone) was added to assess maximum uncoupled respiration. Residual non-mitochondrial respiration was determined after inhibition of complex I with 2 µM rotenone and complex-III with 4 µM antimycin A (AA). OCR was measured for 3 cycles at baseline measurements and after each injection. Injection protocol was programmed as previously defined (Tab. 4.12). A mix step was included after every injection. OCR Data analysis was performed using the Seahorse XF Wave software.

	Baseline	Port A	Port B	Port C	Port D	End
Mix	00:01:30	00:00:30	00:00:30	00:00:30	00:00:30	00:00:30
Wait	00:00:30	00:00:00	00:00:00	00:00:00	00:00:00	00:00:30
Measure	00:03:00	00:03:00	00:06:00	00:03:00	00:03:00	00:09:00
Cycles	3	3	3	3	3	3

Tab. 4.12 Agent injection scheme of substrates and inhibitors for seahorse assay (hh:mm:ss).

4.5 RNA analysis

Brain regions were dissected after sacrificing mice through decapitation. Dissection was proceeded on ice and snap frozen in liquid nitrogen. Tissue samples were kept at -80 °C for long term storage. RNA was isolated with RNEasy kit. The Isolation is based on spin column centrifugation to reach a high purity of RNA. The RNA binding capacity of spin columns is limited. Therefore, the volume of lysis buffer was adapted to the tissue weight (600 µl lysis buffer for 30 mg tissue) to reach the optimal RNA yield and purity. RNA was isolated after the manufacturer's protocol. Gained total RNA concentrations were determined with ThermoFisher NanoDrop™ One/OneC through spectrophotometric measurements. RNA quality was declared through the purity ratio. RNA samples are pure when their ratio of the absorbance of 260 nm and 280 nm was equal 2 (260/280 ratio). Total RNA samples were transcribed to cDNA by a reverse transcriptase of the Verso cDNA Synthesis kit (Thermo scientific). A master mix consisting of synthesis buffer, dNTP mix, hexamer primer, oligo(dT) primer, verso enzyme mix and RT-enhancer (Tab. 4.13) was prepared and added to the RNA samples.

4 µl	Synthesis Buffer 5x
2 µl	dNTP Mix
0.7 µl	Hexamer primer
0.3 µl	Oligo(dT) primer
1 µl	Verso enzyme mix
1 µl	RT-Enhancer
800 ng	RNA sample

Tab. 4.13 Verso master mix (20µl reaction) shown for one RNA sample.

Cycling program was set as recommended in the manufacturer's manual (Tab. 4.14) in the Eppendorf mastercycler. Generated cDNA samples were stored at -20 °C until usage for RT-qPCR experiments.

cDNA synthesis	42 °C	30 min	1 cycle
Inactivation	95 °C	2 min	1 cycle
Hold	4°C		

Tab. 4.14 Reverse transcription cycling program

RT-qPCR was conducted by using SYBR™ Select Mastermix which contains the AmpliTaq® DNA Polymerase, SYBR® GreenER™ dye and other components needed for the reaction. Primers were designed specifically for targeted RNA

samples. A mixture of SYBR™ Select Mastermix, primers and RNA-free water was added to 1 µl cDNA. RT-qPCR experiments were conducted with QuantStudio™ 5 system. The efficiency of the primers was tested with a range of cDNA concentrations. Efficacy reaching 10±100 % were accepted as efficient.

PP1A Fw	GCTGGACCAAACACAAACGG
PP1A Rev	GCCATTCCTGGACCCAAAAC
mNXNFW	GGAGGTGCTCAATGACGAGGA
mNXNRev	CACAAAGAACAACAGCGGCG

Tab. 4.15 Primer sequences of PP1A and murine NXN (mNXN)

In wells with negative controls, the cDNA was substituted with RNA-free water and tested for each primer pair to exclude misinterpreted results through primer dimers. Melting temperature of the products were conducted (Tm NXN=88 °C, Tm PP1A=82.5 °C). Each sample was pipetted as 3 replicates. Primers for murine NXN and peptidylprolyl isomerase A (PP1A) as the housekeeping gene (S. Watson et al., 2007) was used for RNA analysis. Total volume included 10 µl per well.

UDG Activation	50 °C	2 min	Hold
Amplitaq DNA polymerase, UP Activation	95 °C	2 min	Hold
Denature	95 °C	15 s	40 cycles
Anneal/Extend	60 °C	1 min	

Tab. 4.16 RT-qPCR cycling program defined for experiment in the QuantStudio™ 5 system

4.6 Behavioral experiments

4.6.1 Phenomaster

TSE Phenomaster® can track metabolic and activity behavior at home cage environments through an automatic monitoring system. Drinking and feeding behavior were monitored with high-precision weight sensors for liquid and food dispensers, which are integrated into the lid of the cage. Mice were adapted to the drinking bottles for one week in their home cage. A running wheel was accessible in the Phenomaster® cage to allow a voluntary use which was tracked continuously. Mice were habituated in the Phenomaster® cages for 2 consecutive days before starting measurements. Drinking, feeding and voluntary wheel running were recorded for 24 hours. Eleven mice per group with an age of 8-16 weeks were observed in the Phenomaster cage (male NesNXN$^{-/-}$ mice n=5 and female NesNXN$^{-/-}$ mice n=6 compared with male NXNflfl n=5 and female control mice n=6).

4.6.2 Open field test

TSE VideoMot2 (TSE Systems GmbH, Bad Homburg, Germany) was used to track locomotion in the open field. The camera was connected to a computer outside of the enclosure. This automatic tracking system allows to observe behavioral patterns of mice in the absence of the experimenter. Mice were acclimatized from transport in their home cages to the experiment room for at least 1 hour but no habituation to the apparatus prior to measurements was necessary. Mice were placed in the center of the open field box (50 × 50 cm width, 38 cm height). Recordings were started immediately, while mice moved freely in the open field. Virtual zones were defined as center and border regions. 9-11 weeks old NesNXN$^{-/-}$ mice (5 male, 2 female) and male NXN-flfl mice (n=7) of the same age were tracked for 10 min.

4.6.3 Elevated Plus Maze

Elevated plus maze (EPM) experiments were also tracked with the TSE VideoMot2 (TSE Systems GmbH, Bad Homburg, Germany) tracking system. Mice were acclimatized from transport in their home cages to the experiment room for at least 1 hour. Mice were not habituated to the apparatus before the experiment. The EPM contained 2 open arms crossed by 2 closed arms, which were grey untransparent walls (10 cm width, 50 cm length). The maze was raised 50 cm above the ground. Tracking was initiated immediately after placing the mouse in the center of the maze. Each tracking trial lasted 10 min. Locomotion, visits to zones and times spent in zones were analyzed with VideoMot2 which uses 2-point tracking (TSE Systems). 9-11 weeks old NesNXN$^{-/-}$ mice (5 male, 2 female) and male NXN-flfl mice (n=7) of the same age were tracked at naïve status and 14 days after paw inflammation.

4.6.4 Sociability and social memory test

The social discrimination task assesses social cognition and memory according to standard protocol in a three-chamber paradigm, which is also known as Crawley's protocol for sociability and preference of social novelty (Kaidanovich-Beilin, Lipina, Vukobradovic, Roder, & Woodgett, 2011). Mice were observed in a box with 3 equally designed chambers of same size (18.5 × 38 cm). The middle chamber was connected to the outer chambers by doors, which can be closed. A cylindrical enclosure was placed into the corners of each outer compartment, and mice were habituated to the environment one week before test start. On the experiment day, mice were acclimatized to the middle chamber for 5 min with closed doors. The trial

started when the doors were lifted, and mice were allowed to explore the chambers and enclosures for 10 min. One enclosure was empty, whereas the other enclosure contained a stimulus mouse. Subsequently, a second mouse was added to the still empty enclosure showing responses to social novelty and movement tracking was recorded for 10 min. Normally, mice are more interested in the social partner relative to an empty compartment (social cognition) and spend more time with a novel partner relative to a familiar one (social memory). The trials were recorded with a video camera and analyzed with VideoMot2 software (TSE Systems GmbH, Bad Homburg, Germany). 8-13 weeks old female NesNXN$^{-/-}$ mice (n=7) and female NXN-flfl mice (n=7) were observed.

4.6.5 IntelliCage

The IntelliCage (NewBehavior AG, Zurich, Switzerland) (Albuquerque, Haussler, Vannoni, Wolfer, & Tegeder, 2013; Hardt et al., 2017; Hardt et al., 2018; Krackow et al., 2010) consists of four operant corners, each with two water bottles, sensors, light-emitting-diodes (LEDs) and doors that control the access to the water bottles. The automatic system enables the observation of 16 mice at a time in a cage (20 × 55 × 38 cm, Tecniplast, 2000P) without interfering into the environment. Four triangular red shelters (Tecniplast) are placed in the center to serve as sleeping quarters and as stands to reach the food rack. The floor is covered with standard bedding. Mice are tagged with radio-frequency identification (RFID)-transponders, which are read with an RFID antenna integrated at corner entrance. RFID transponder was implanted subcutaneous after sedating mice with isoflurane. Inside the corners are two entries to drinking bottles, which can be opened and closed by automated doors. Mice have to make nosepokes (NP) to open the doors for water access. The IntelliCage is controlled by a computer with IntelliCage Plus software, which executes pre-programmed experimental tasks and schedules. The IntelliCage experiments were conducted with female mice to avoid fights which is known to commonly occur between males. Up to 16 mice were housed per cage (8/8 and 7/8 of each genotype). Mice in cage-1 were 5-6 months old upon start, mice in cage-2 were 11-12 months old.

Task name	Task description	Duration	Readouts, cognitive dimensions and interpretation
Free adaptation (FA)	Habituation to the system with free access to every corner, with all doors open, and water and food ad libitum.	8 days	Exploratory behavior, general activity, circadian rhythms, social structure
Nosepoke adaptation (NP)	The first nosepoke of a visit opened the door for 5 s. To drink more, the animals had to leave the corner and start a new visit.	6 days	Exploratory behavior, general activity, circadian rhythms, social structure
Place preference learning (PPL)	Mice were allowed to drink in one out of 4 corners. Only the first correct nosepoke of a visit opened the door. LEDs in 3 colors (green, red, yellow) turn on upon entry to the correct corner. Each 4 mice assigned to one correct corner	8 days	Simple spatial preference learning activity and exploration
Place preference REVERSAL (PPLrev)	Protocol as in “place preference learning” but with the opposite corner being correct.	7 days	Cognitive flexibility of Reversal Learning requires the dorsal and ventral hippocampus and their functional interactions with the prefrontal cortex (Avigan, Cammack, & Shapiro, 2020; Vila-Ballo et al., 2017)
Place preference REVERSAL 2 (PPLrev2)	Protocol as in “place preference learning” but new assignment of correct corner and only one side in this corner was correct. Each 5-6 mice were assigned to one correct corner. One corner was excluded	13 days	Reversal Learning plus only one side out of 8 sides correct.
NP random side (NPrd)	Upon corner entry, one side was randomly assigned to be correct, which was indicated by LED. NP opened the door on this correct side. The other side remained closed.	7 days	Requires attention to LED and decision for correct side according to LED. Requires functions of the hippocampus and medial PFC (Cho & Jeantet, 2010; Jackson, Kesner, & Amann, 1998)
Place avoidance acquisition (PAA)	Mice had to avoid one specific previously preferred corner. NP in this corner was punished with an air-puff and a red LED was switched on upon visit to this corner. Avoidance acquisition was for 24h, followed by a one-day home cage interval. Each 4 mice assigned to one forbidden corner	1 day	Spatial avoidance learning is sensitive to genetic differences and hippocampal lesions (Voikar et al., 2010)
Place avoidance extinction (PAEx)	During avoidance extinction, water was available in each corner on NP without any punishment. Only the red LED still announced the previously punished corner.	6 days	Retention of avoidance behavior. Avoidance memory. Duration of avoidance reflects caution over curiosity
Final free adapation (FAfin) with one sweet corner	Final free access protocol with all doors open, and water and food ad libitum. In one corner sweet water was provided.	7 days	Exploratory behavior, sweet preference, general activity, circadian rhythms, social structure

Tab. 4.17 Chronologic description of IntelliCage tasks.

The numbers and duration of corner visits, nosepokes, and licks are automatically recorded without the need for handling of the mice during the recording times. IntelliCage tasks address a number of different aspects of cognition as well as

circadian rhythms and social interactions and are run sequentially. The tasks are described in Tab. 4.17 and abbreviations of behavioral parameters are summarized in our previous publication (Tran et al., 2021). The tasks followed established protocols (Albuquerque et al., 2013; Hardt et al., 2017).

Mice were adapted to the system for 8 days with free access to food and to the water bottles at every corner through opened doors. This free adaptation (FA) was followed by 6-days nosepoke adaptation (NP) during which the doors were closed, the first nosepoke of the visit opened the door for 5 s and in order to drink more, the animals had to leave the corner and start a new visit. In the place preference learning (PPL) task mice had to learn to prefer a specific corner for 8 days, where they got the water reward. Each 4 mice were assigned to one corner and the PPL module was active for 24 h. Only the first correct nosepoke opened the door, and any incorrect nosepoke had no effect. After conditioning to the corner, PPL reversal learning (PPLrev) was assessed by switching the rewarding corner to the opposite side for 7 days, and another corner switch for 13 days (PPLrev2). Subsequently, LED attention and visual discrimination were assessed in an NP protocol for 7 days, where an LED was randomly switched on either on the right or left side upon corner entry, and only the LED side was set to correct. Salience based motivation has been assigned to cortical regions and the nucleus accumbens (LeGates et al., 2018; Ventura, Morrone, & Puglisi-Allegra, 2007). Flexible spatial reversal learning requires the dorsal and ventral hippocampus and their functional interactions with the prefrontal cortex (Avigan et al., 2020; Vila-Ballo et al., 2017), and is partially lost with disturbances of adult hippocampal neurogenesis (Garthe, Behr, & Kempermann, 2009). In place avoidance learning (PAL), mice had to learn to avoid one punished corner, which was randomly assigned to each 4 mice. The punishment consisted of an airpuff (~ 0.8 bar, 1 s) and was coupled with a red LED. The avoidance acquisition lasted for 24h. At completion, mice returned to their home cages for 1 day with water restriction for the last 18 h prior to their return to their IntelliCage for the analysis of the extinction of the avoidance behavior for 6 days (PAEx). The temporary water restriction ensured that all mice were equally thirsty and highly motivated to get water upon re-entry of the IntelliCage. The IntelliCage was not cleaned during the home cage stay to maintain the environmental and olfactory cues. In PAEx all doors opened in response to a nosepoke and no air-puff was applied. Only the red LED still reminded the mice of the previously 'punished'

corner. Conditioned place avoidance in the IntelliCage is sensitive to functions of the hippocampus (Krackow et al., 2010) and reminiscent of fear conditioning in classical foot-shock based tests of hippocampal functions. Finally, the last NP protocol was run with tap water on one side and sweet water on the other side of each corner to assess the sugar appeal (7 days).

4.7 Statistical analysis

Group data are presented as mean ± SD or median ± IQR for non-parametric data as specified in the respective figure legends. Data were analyzed with SPSS 24 and Graphpad Prism 8.4 or 9.0 and Origin Pro 2020. Data were mostly normally distributed, or log-normally distributed. For testing the null-hypothesis that groups were identical, two groups were compared with 2-sided, unpaired Student's t-tests. The Mann Whitney U test (2 groups) was used as a non-parametric alternative in case of violations of t-test requirements. Time course data or multifactorial data were submitted to 2-way analysis of variance (ANOVA) using e.g. the factors 'time' and 'genotype'. In case of significant differences, groups were mutually compared at individual time points using post hoc t-tests according to Dunnett, i.e. versus the control group, or according to Šidák. Asterisks in figures show multiplicity-adjusted P-values. Multivariate behavioral parameters were used to reduce the dimensionality. To assess different behavioral readouts together, data were normalized and are expressed as percentage of the 90%-quantile. Canonical discriminant analysis (CanDisc) was employed to separate treatment groups and assess the predictability of group membership. Polar plots were created in Origin Pro 2021. Chi-square automatic interaction detection (CHAID) was used to generate decision trees, which is based on Bonferroni adjusted significance testing. Behavioral parameters were introduced as independent variables, and then stepwise removed to find the strongest discriminant candidates. IntelliCage data were analyzed with IntelliCage Plus® software (TSE) and with FlowR (NewBehavior) (Krackow et al., 2010; Voikar et al., 2018) for analyses of time courses and circadian parameters by Irmgard Tegeder (Tran et al., 2021). Data were exported to tab separated txt files for further analyses in Excel, Prism, SPSS and OriginPro. The mean behavioral for each task module for each mouse was used for fitting with Friedmann splines and 2-way ANOVA for “modul” by “genotype”

(conducted by Irmgard Tegeder). The mean behavior per mouse for each parameter over the total observation time was used for comparisons of box plots and distributions.

5. Results

5.1 NXN expression pattern in murine brain

Previous studies suggested that NXN is essential for brain development. We analyzed the expression pattern of NXN with NXN-lacZ-reporter-mice. In agreement with images provided by the mouse phenotype database (http://www.mouse-phenotype.org), we observed the expression of NXN in cerebellum, hippocampus and cortex of adult mouse brain with X-Gal stainings (Fig. 5.1). Expression of β-galactosidase (β -Gal) was also found in sensory ganglia and nerves, in the peripheral nervous system and in heart and skeletal muscle (not shown). Co-Immunofluorescence stainings show corresponding localization of NXN in different brain regions. In the cerebellum Camk2a is localized in Purkinje cells and NXN in granule cells going together with β-galactosidase expressions. NXN was localized in stratum granulosum and hilus of the dentate gyrus. NXN and Camk2a were also found in the cornu ammonis areas (CA) CA3 and CA1, where pyramidal neurons are known to be located. Cortex shows localization of NXN in Camk2a-positive neurons. The wide neuronal expression suggested a dominant function in murine adult brain. Therefore, we generated the pan-neuronal Nestin-Cre driven NXN knockout mice (NesNXN$^{-/-}$).

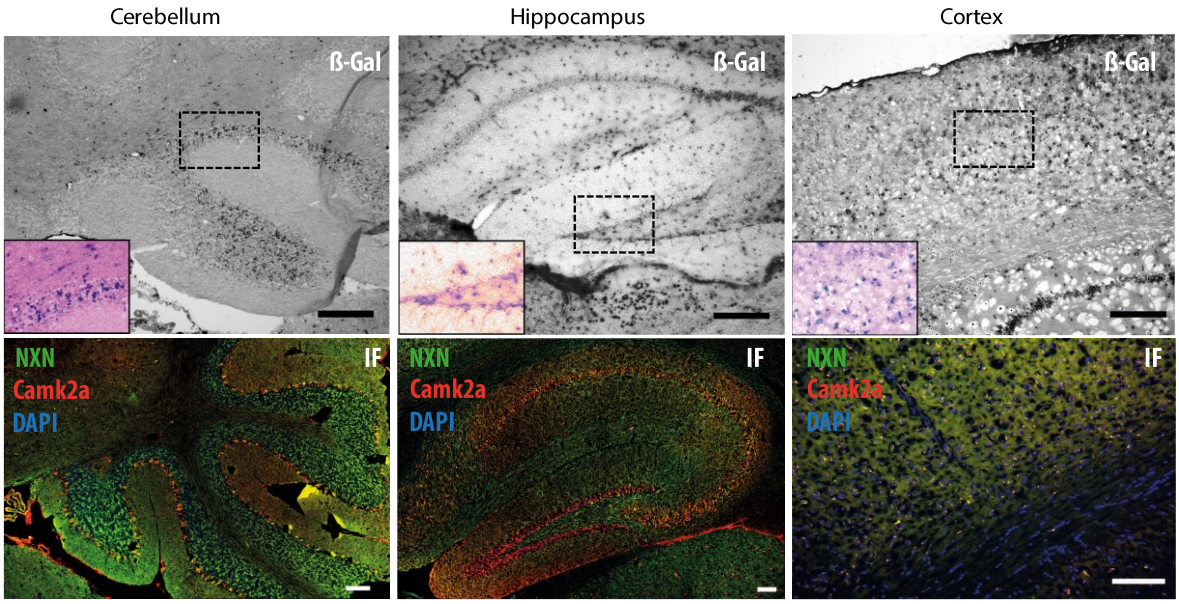

Fig 5.1 IHC analyzes visualize expression of NXN in LacZ reporter mice (conducted by Valek; Tran et al, 2021) and immunofluorescence stainings (IF) of NXN (green) and Camk2a (red) in adult murine brain tissue. Yellow colored regions mark colocalization of NXN and Camk2a. LacZ reporter gene expression analysis through X-gal stainings (grey) and immunofluorescence stainings (colored) represent the expression of NXN in the cerebellum and Camk2a is localized in purkinje cells. Corresponding to the β-galactosidase (β-

Gal) expression, NXN is localized in stratum granulosum and hilus of the dentate gyrus of hippocampal regions. NXN and Camk2a were also found in CA3 and CA1 regions. Cortex shows localization of NXN in Camk2a-positive neurons. Dashed rectangles show the areas used for zoom-ins shown in the left of X-Gal stainings.The scale bars display 100 µm.

The lateral septum nuclei (LS) circuits with the limbic system such as the amygdala were reported to regulate motivation and goal-directed behavior (Luo, Tahsili-Fahadan, Wise, Lupica, & Aston-Jones, 2011; Risold & Swanson, 1997). RT-PCR analysis of the amygdala and the LS revealed a reduction of NXN expression in NesNXN$^{-/-}$ mice compared to NXN-flfl mice ranging between 53-64 % (Fig. 5.2B). Immunofluorescence signals of NXN in the dorsal and ventral part of LS was in agreement with the β-Gal signals in LacZ reporter mice (shown in the Supplement of (Tran et al., 2021)) revealing NXN expression in the LS (Fig. 5.20A).

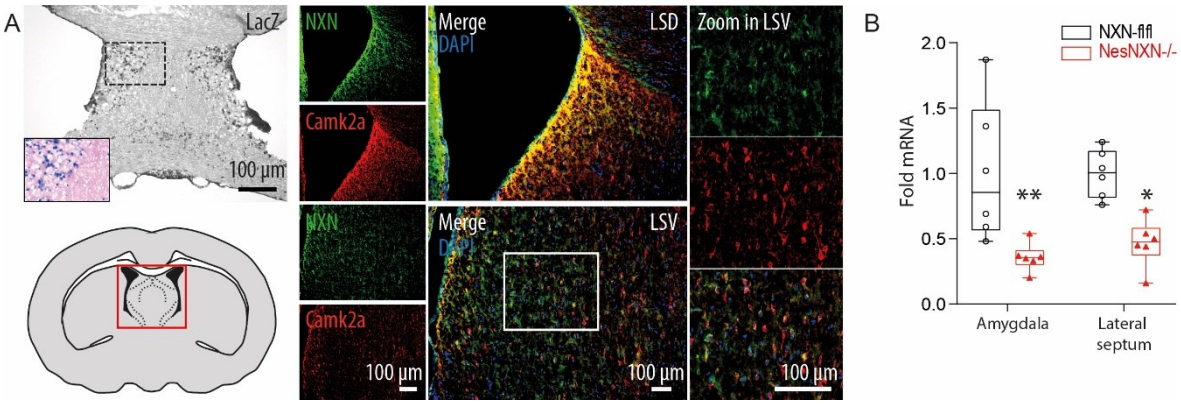

Fig 5.2 Analysis of NXN expression in lateral septum nuclei which is the brain region involved circuits for explorational goal-directed behavior (Luo et al., 2011). A Lateral septum shows colocalization of NXN and Camk2a in immunofluorescence stainings. Sketch of coronal brain section with lateral septum is shown below the positive LacZ staining of Nxn. B qRT-PCR analysis of amygdala and lateral septum revealed significant reduction of NXN mRNA fold. Each scatter represents one mouse. Genotypes were compared with 2-way ANOVA for "fold mRNA x genotype"; post-hoc analyses for each time point using Šidák multiple comparison test; P*< 0.05). Abbreviation: Lateral septum dorsal (LSD), lateral septum ventral (LSV)

Growth curves and body weight revealed a statistically lower body weight in young NesNXN$^{-/-}$ mice, which disappeared beyond 9-10 weeks of age (Fig 5.3). The behavioral studies were conducted with mice beyond youth, and not affected by weight differences. NesNXN$^{-/-}$ mice were healthy throughout life. This allowed us to study functions of for various aspects of behavior in adult mice up to old age.

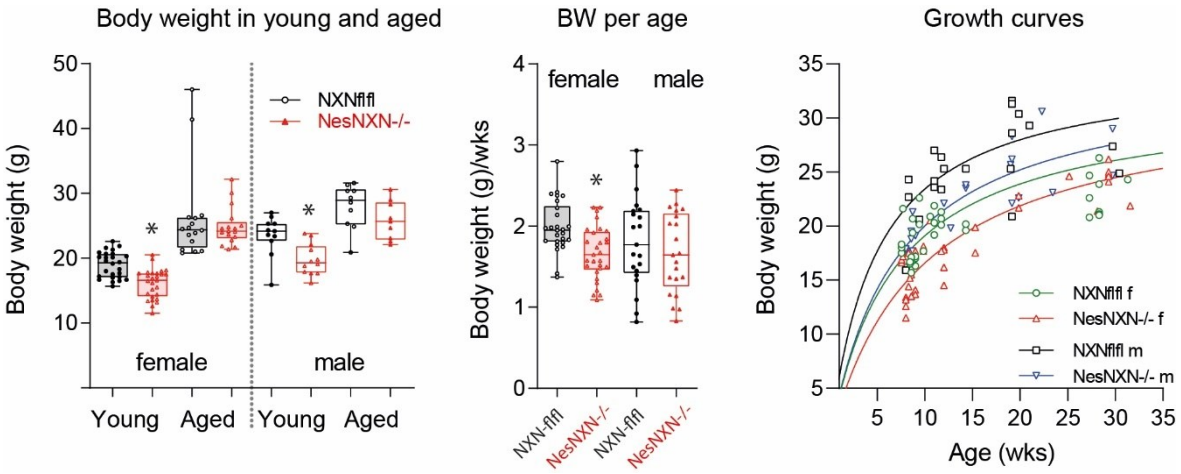

Fig 5.3 Body weight of female NesNXN$^{-/-}$ young mice is reduced but normalizes by ageing. Body weights of NesNXN-/- and NXN-flfl mice are shown at different ages. Young mice were 7-9 weeks and aged mice were 25-50 weeks old. Growth curves were fitted to an exponential increase. Each scatter represents a mouse. Data were compared with 2-way or one-way ANOVA and subsequent posthoc analysis using an adjustment of alpha according to Šidák. Asterisks show significant differences between genotype, *P<0.05.

5.2 NXN interacts with Camk2a sustaining its activity

Camk2a was identified as a potential interaction partner of NXN through investigation in previous studies by using a yeast-2-hydrid assay. Camk2a has a number of redox-sensitive cysteines (Scheving et al., 2012; Valek, Heidler, Scheving, Wittig, & Tegeder, 2019) and regulates neuronal plasticity (Coultrap et al., 2014; Ninan & Arancio, 2004). The functional implications of the NXN-Camk2a interaction were studied in a Camk2a kinase assay (Fig. 5.4). Camk2a was extracted from brain lysates through pulldown with antibody conjugated agarose beads to concentrate and purify the assay samples. Brain samples were dissected from NXN-flfl mice (control group) and NesNXN$^{-/-}$ mice. There was no difference at baseline measurements of total (at presence of calmodulin/Ca^{2+}) or autonomous (without calmodulin/Ca^{2+}) Camk2a activity between genotypes. Hydrogen peroxide (H_2O_2) had no effect, but recombinant NXN (rNXN) significantly increased Camk2a activity. This boost was lower in samples obtained from NXN-deficient brains (Fig. 5.4B), suggesting a lower redox-sensitive proportion of Camk2a activity in samples of NXN-deficient mice.

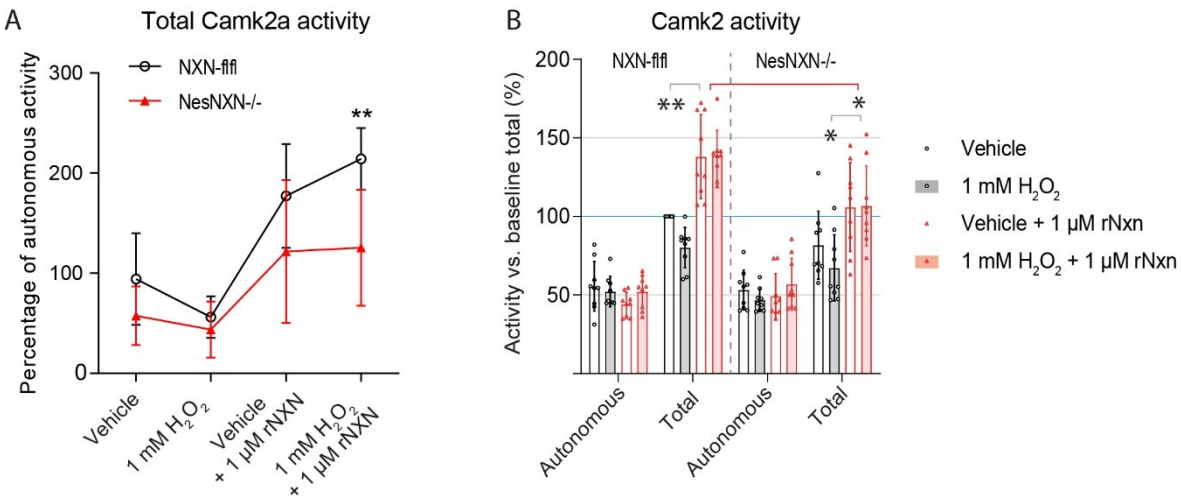

Fig 5.4 NXN preserves Camk2a activity in the presence of H_2O_2. Camk2a activity assay in Camk2-enriched mouse brain lysates of NXN-flfl and NesNXN$^{-/-}$ mice. The "autonomous" activity was assessed in the absence of calmodulin/without Ca^{2+}, the "total" activity was measured with assay buffer containing calmodulin/Ca^{2+}. The tissue was obtained from three mice per genotype, each split into three samples. A Graph shows the total activity relative to the autonomous activity of each mouse as mean ± 95% CI at treatment with assay buffer as vehicle, 1 mM H_2O_2, 1 µM recombinant NXN (rNXN) and a combination of H_2O_2 and rNXN. B Bar graph shows the activities of Camk2 normalized to the total activity of NXN-flfl at vehicle treatment as the baseline. Data were compared with 2-way ANOVA and subsequent posthoc analysis with an adjustment of alpha according to Tukey. Asterisks denote statistical significance at * $P < 0.05$ (adjusted P Value)

For further confirmation and subcellular localization of the interaction between NXN and Camk2a, we performed a proximity ligation assay (PLA) in primary cortical neurons cultured from floxed control (NXN-flfl) and NesNXN$^{-/-}$ newborn mice. Positive PLA signals were detected as red dots because Cy3-labeled complementary oligonucleotides bind to the RCA products (Fig. 5.5A). One PLA signal represents a closer proximity of 40 nm between one molecule of NXN to one molecule of Camk2a (Fig 5.5C). The PLA signals mainly occurred along axons and dendrites, and the quantification revealed a significant reduction in NesNXN$^{-/-}$ mice as compared to NXN-flfl control mice (Fig. 5.5B). As expected from the Western Blot studies of the knockout mice, PLA signals were not completely absent in neurons of NesNXN$^{-/-}$ mice (not shown, supplement of (Tran et al., 2021).

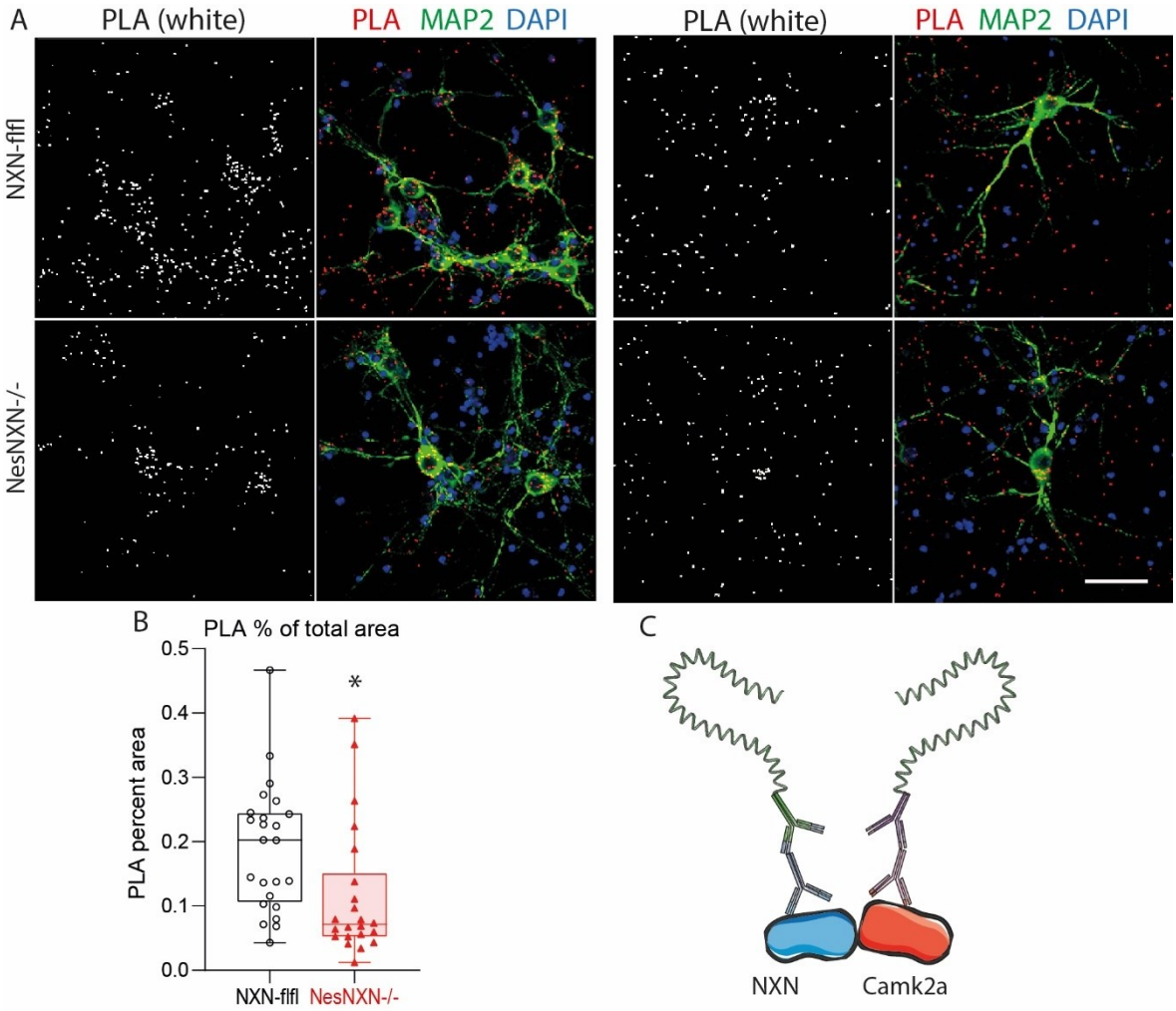

Fig 5.5 More PLA signals in primary cortical neurons of NXN-flfl mice than in neurons of NesNXN$^{-/-}$ mice. **A** Representative image with low (right) and high (left) densities of murine primary cortical neurons show the proximity ligation assay (PLA, white/red) of NXN and Camk2a in NXN-flfl and NesNXN-/- mice. PLA signals require the proximity of the candidate proteins. MAP-2 immunoreactivity (green) and DAPI (blue) were used to ensure comparable numbers of neurons. **B** Box and whiskers plot shows PLA signals conducted from three NXN-flfl and NesNXN-/- mice, each split into 3 cultures. PLA counts were normalized to the area. Quantification was conducted with the "Particle counter" in ImageJ after background subtraction and default threshold setting. Data were compared with 2-tailed, unpaired Student's t-test. *P < 0.05. **C** Sketch of plus and minus PLA probes

coupled with oligonucleotides docking on primary antibody of different host species that are bound to target proteins. The sample is ready for rolling circle amplification (adapted from the manual by Merck).

Additionally, immunofluorescent signals of NXN staining were also found in NesNXN$^{-/-}$ primary cortical neurons in agreement with PLA experiments. Insert display zoomed images of soma (Fig. 5.6).

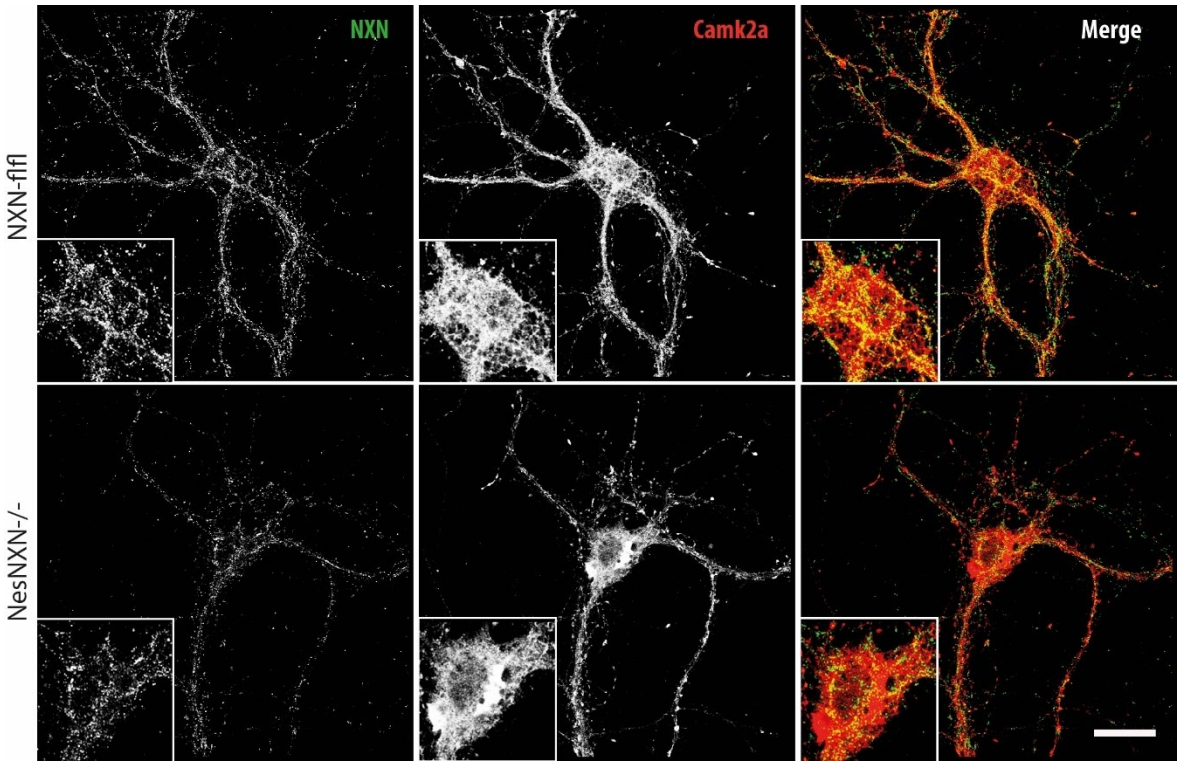

Fig 5.6 Camk2a-positive neurons in primary cortical cultures. Representative immunofluorescence staining of primary cortical neurons of NesNXN-/- mice are compared to Nxn-flfl mice. NXN and Camk2a are shown in gray, while merged channels are colored with NXN (green) and Camk2a (red) and colocalization is recognizable with the yellow color. Images were taken with 40X oil magnification at confocal microscope LSM800. Scale bar is 20 µm.

5.3 NXN in neuronal fibers sustains neuronal respiratory activity

Camk2a is expressed at postsynaptic sites in dendritic spines and is crucial for NO-dependent forms of neuronal plasticity (Coultrap & Bayer, 2014; Fang, Wu, Lin, & Willis, 2002; Glazewski, Bejar, Mayford, & Fox, 2001; Lledo et al., 1995). NXN was localized in cerebellum, hippocampus and cortex corresponding to matching results from X-Gal-stainings (Fig. 5.1). Those brain regions are widely known for long term potentiation mechanisms and are regions with high neuroplastic events (Scelfo, Sacchetti, & Strata, 2008). Predominant immunoreactive signals of NXN were detected in neuronal fibers (Fig. 5.7B) but only few in neuronal bodies. Co-immunofluorescence studies of NXN and Camk2a in tissue (Fig. 5.7A, B) and primary neurons (Fig. 5.8) revealed a neighboring expression of the candidates mainly in neuronal fibers, neurites and axons in agreement with PLA experiments.

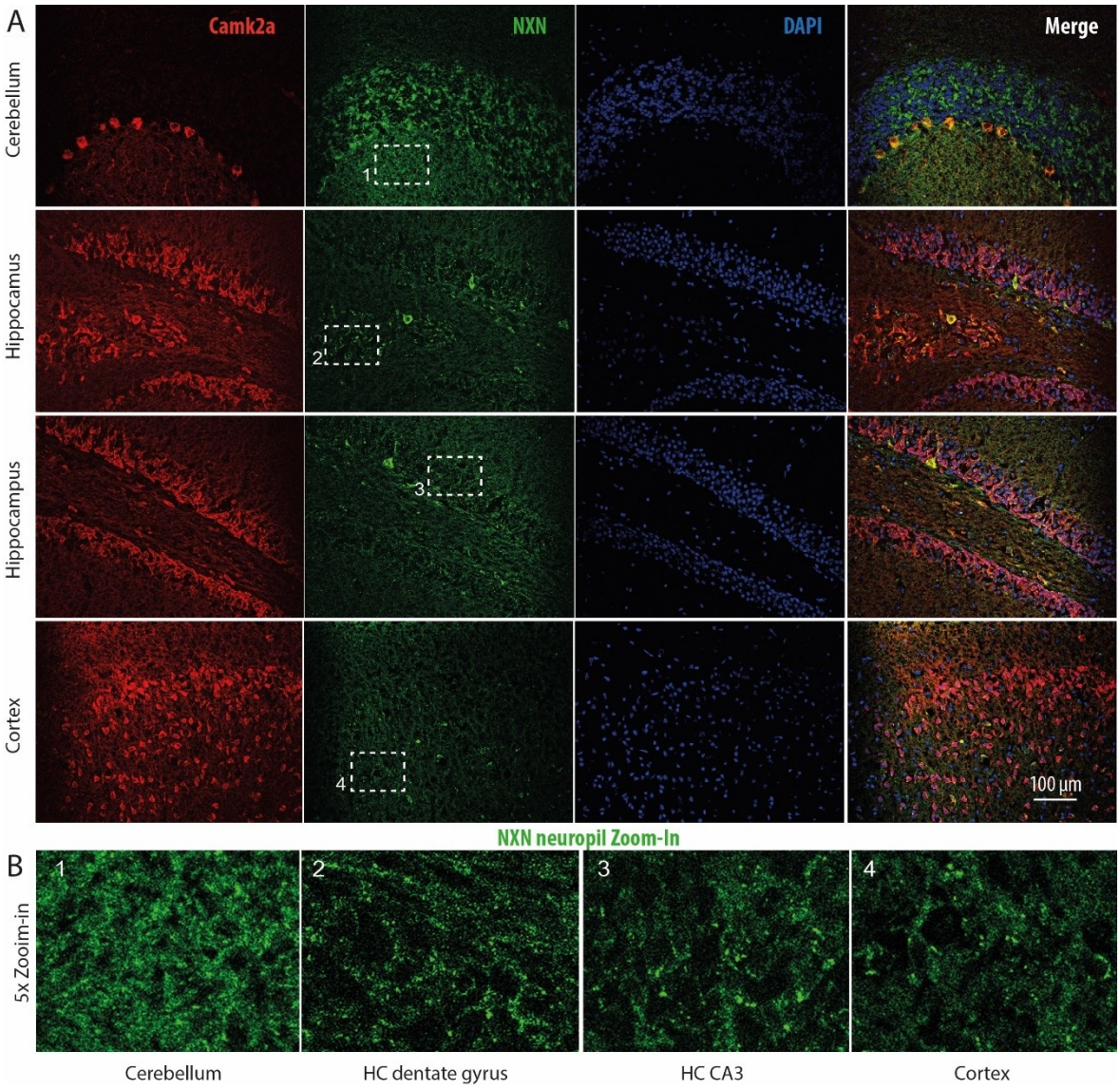

Fig 5.7 NXN is localized in neuronal fibers of different brain regions. A Immunofluorescence analysis of NXN and Camk2a in NXN-flfl mice cerebellum, hippocampus and cortex. Dashed rectangles show the areas used for **B** zoom-ins. Scale bars as depicted.

Immunofluorescent staining of matured primary hippocampal neurons shows localizations of Camk2a and NXN, which were also interestingly found in dendritic spines (Fig. 5.8). The squared inserts in the zoom-in shows a dendritic spine. The overlay of NXN (green) and Camk2a (red) signals are yellow-colored areas. Dendritic spines are postsynaptic sites with high plasticity which is regulated through LTP as described in Fig. 3.4.

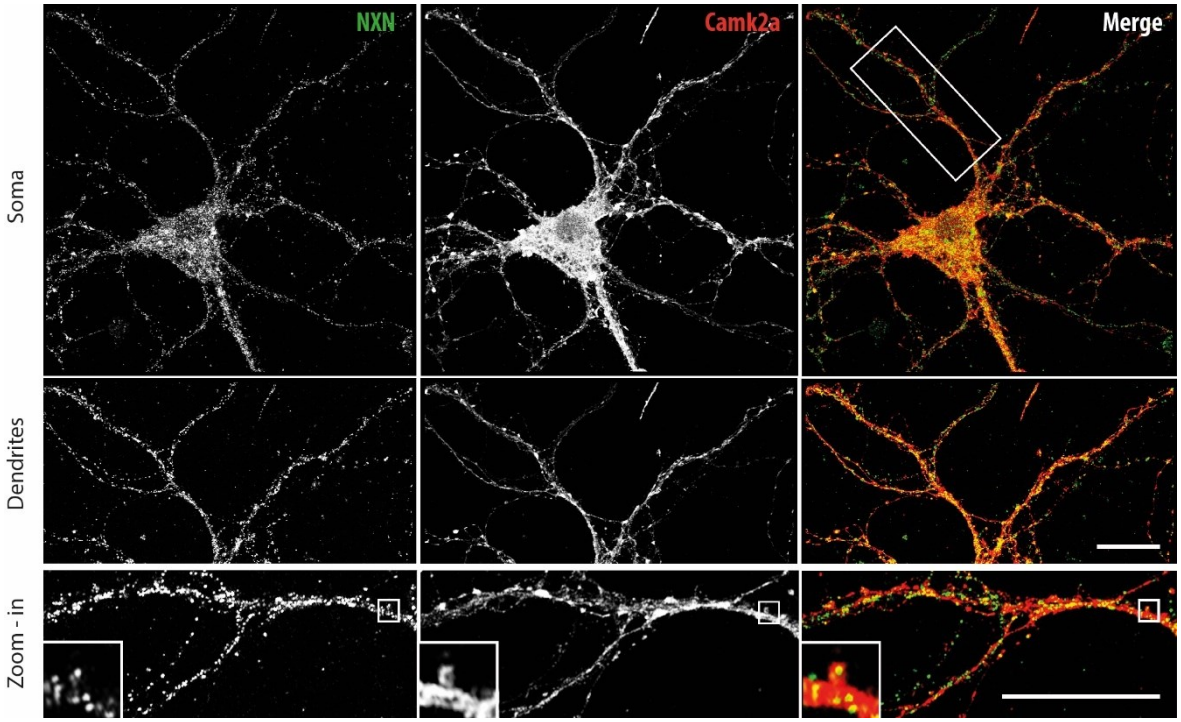

Fig 5.8 NXN is expressed in dendritic spines. Zoom-in of a dendritic spine shows colocalization of Nxn and Camk2a in some primary hippocampal neurons of NXN-flfl. NXN and Camk2a are shown in gray scale images. Merged channels are colored with NXN (green) and Camk2a (red). Colocalizations are apparent as yellow-colored regions. Images were taken with 40X oil magnification at confocal microscope LSM800. Scale bar is 20 µm.

The PLA signals along axons suggested a similar distribution of NXN, and a putative redox modulation of spine biology. To assess the functional implications of NXN in neuronal fibers we measured the respiratory oxygen consumption using a “substrate-uncoupler-inhibitor-titration” protocol assuming NXN would affect the respiratory turn-over of oxygen as an oxidoreductase. Mitochondrial protein of NesNXN$^{-/-}$ and NXN-flfl mice brains was subjected to a Seahorse SUIT analysis. Inhibitors and substrates of respiratory activity were added to the samples automatically. Baseline respiration was equal in both groups, but oxygen consumption was reduced in mitochondrial enriched extracts of NesNXN$^{-/-}$ brains

after adding ADP substrate to measure ATP-coupled respiration. Residual non-mitochondrial respiration, after adding rotenone and antimycin A to block complex I and III, did not differ between genotypes. The data reveal a reduced respiratory rate and suggest lower ATP generation in the absence of NXN in neurons (Fig. 5.9).

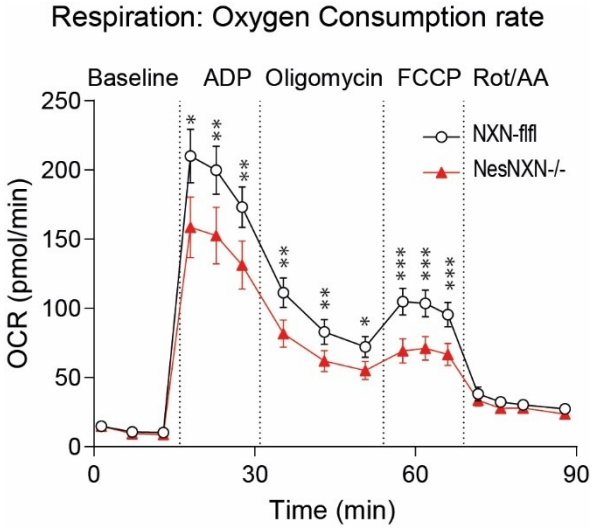

Fig 5.9 Respiratory activity in NesNXN$^{-/-}$ mice is reduced in brain tissue. Mitochondrial respiration was measured in a Seahorse analyzer through automatic injection of 4 different treatments into the sample plate. The “substrate-uncoupler-inhibitor-titration” protocol measured basal respiration, then coupled respiration by adding ADP substrate, followed by oligomycin to assess ATP generation and proton leakage, subsequent FCCP to assess maximum uncoupled respiration, and finally rotenone (Complex-I inhibitor) plus antimycin A (Complex-III inhibitor) to assess residual non-mitochondrial respiration. OCR shown as mean ± 95% CI was analyzed with the Wave® software. The analysis was done with n=94 NXN-flfl samples and n=69 NesNXN-/- samples combined from experiments of each three mouse brains. Time courses were compared by 2-way ANOVA for "group" X "stimulus" and posthoc analysis using an adjustment of alpha according to Šidák. Asterisks reveal significant differences between groups. *P<0.05, **P<0.01, ***P<0.001.

5.4 NesNXN$^{-/-}$ mice show reduced exploratory behavior and low interest in the reward

A number of studies have investigated the impact of Camk2a on the development of social behavior and exploratory behavior beside learning and memory mechanisms, because of its essential role in LTP generation in association with synaptic remodeling and stabilization (Harda et al., 2018; Rivera et al., 2020; Robison, 2014; Stephenson et al., 2017). The interaction of NXN with Camk2a and the impaired ATP consumption in neuronal mitochondria of NesNXN$^{-/-}$ mice (Fig. 5.9) would agree with slowing or dampening effects of NXN deficiency on cognitive behavior. The IntelliCage system enables an undisrupted tracking of each mouse through the implanted RFID transponder. Behavior of NesNXN$^{-/-}$ and NXN-flfl mice were observed continuously in IntelliCages with minimal interference from the experimenter. Tracking lasted over nine weeks and the mice were subjected to

different tasks ranging from simple free adaptation to complex reversal learning. Primary readouts for multiple behavioral features were visits of corners and nosepokes at the doors, as well as licks from drinking bottles. Overall activity of mice can be indicated by the total number of visits with licks per hour (Visits/h) (Fig. 5.11A) and the ratio of nosepoke counts during visits with nosepokes (NP/NPVisit) (Fig. 5.10). Both read-outs showed no difference between genotypes throughout the experiments. Additionally, daytime to nighttime fluctuations (12 h bins) were similar and regular in both genotypes. NP/NPVisit (Fig. 5.10) is a constant behavioral indicator that is reduced in models of dementia (Hardt et al., 2017) or traumatic brain injury (Vogel et al., 2020). The unaltered NP/NPVisit ratio (Fig. 5.10) throughout the experiment suggests that NesNXN$^{-/-}$ mice have no cognitive or social or motor disability.

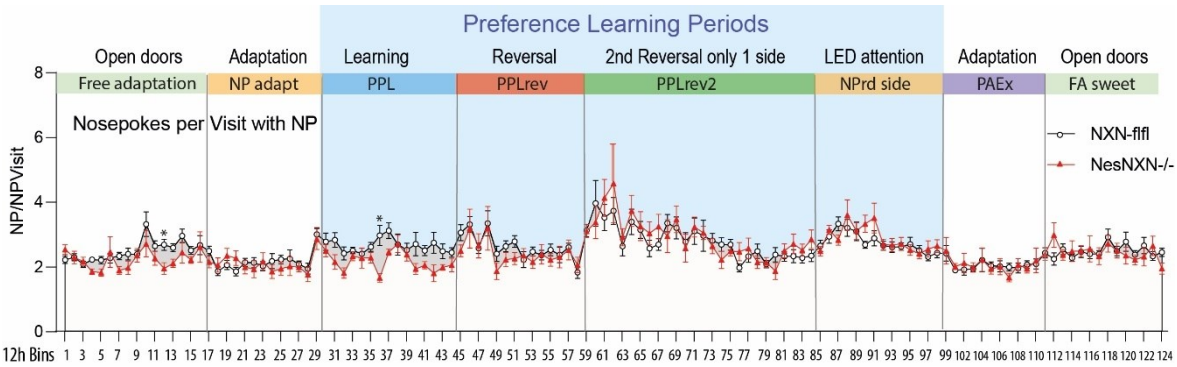

Fig 5.10 Time course of nosepoke ratio from nosepoke per visit in IntelliCages. The x-axis represents the days of experiment. No difference was observed between genotypes at nosepoke/visit with nosepoke. The data show means ± sem of 14-15 mice per group. The fluctuation of the behavior reveals nighttime and daytime differences (12h Bins). Data were compared with 2-way ANOVA for the factors “time” X “genotype” and posthoc comparison for “genotype” with adjustment of alpha according to Šidák.

However, exploratory visits (Fig. 5.11) which is indicated by the number of non-goal directed visits of NesNXN$^{-/-}$ mice was interestingly reduced throughout the experiment. Reduction of explorative behavior of NesNXN$^{-/-}$ mice was especially observed at non-learning periods, where nosepokes are made during exploration instead of getting reward. Non-goal directed visits (Fig. 5.11B) are represented by the number of visits with nosepokes but without licking at the drinking bottle (NPVisits/h). Correspondingly, the exploratory index (Fig. 5.11C) was significantly reduced, which is shown as the ratio between exploratory visits (NPVisits) versus goal-directed visits (visits with licks, LVisits). During the initial easy place preference learning periods (PPL and PPLrev), NesNXN$^{-/-}$ mice showed a higher accuracy agreeing with lower exploration (Fig. 5.11D). The proportion of correct nosepokes

(Fig. 5.11D) likely result from lower exploratory behavior.

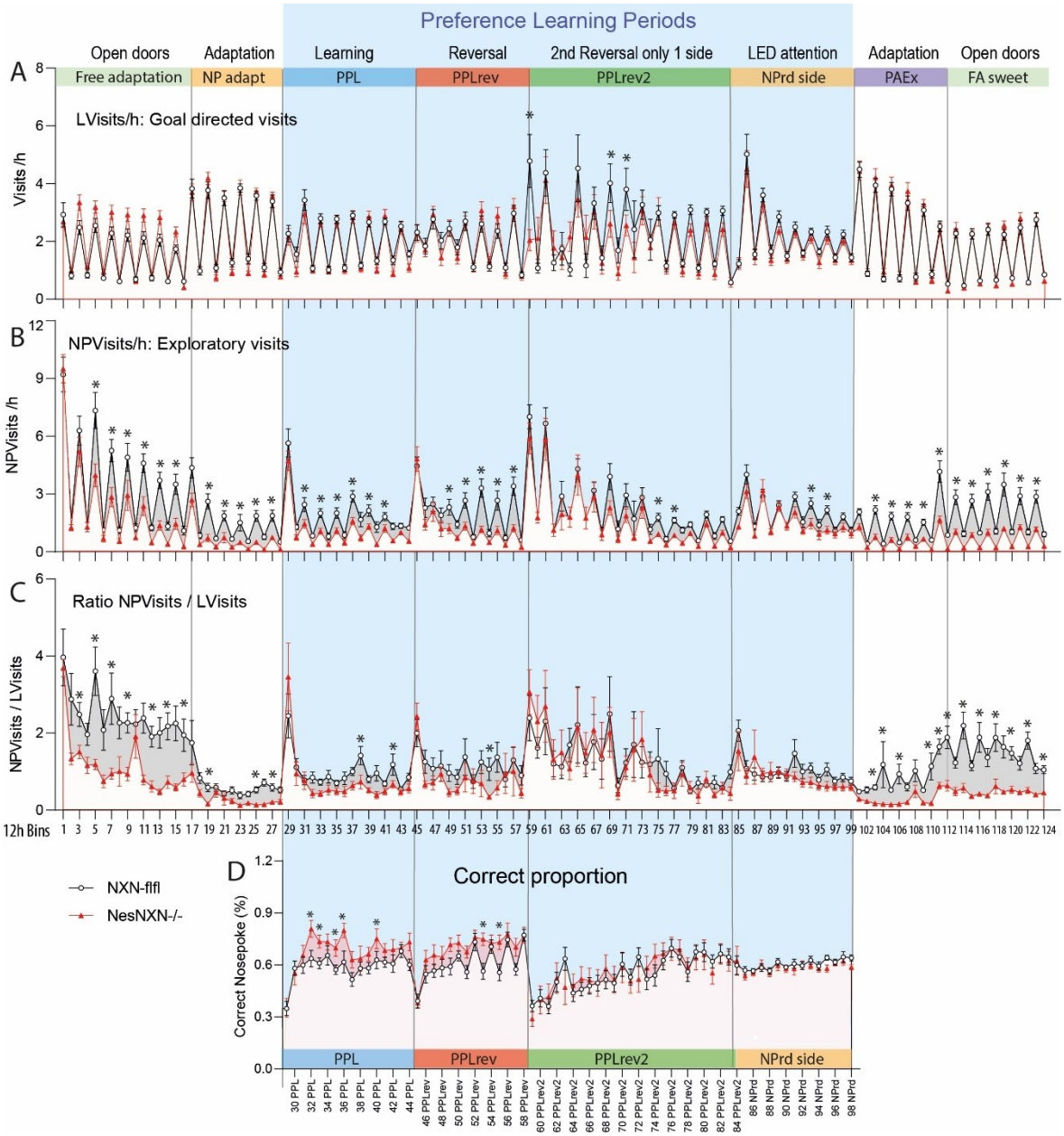

Fig 5.11 Exploratory and goal directed activity of NesNXN$^{-/-}$ versus NXN-flfl mice in IntelliCages. A: Time course of goal directed visits with licks per hour (LVisits/h). **B**: Time course of exploratory visits with nosepokes but without licks (NPVisits/h). **C**: Time course ratio of exploratory visits (NPVisits) versus goal-directed visits (visits with licks, LVisits) **D**: Proportion of correct corner visits during place preference learning tasks. The data show means ± sem of 14-15 mice per group. The fluctuation of the behavior reveals nighttime and daytime differences (12h Bins). Data were compared with 2-way ANOVA for the factors "time" X "genotype" and posthoc comparison for "genotype" with adjustment of alpha according to Šidák.

Enhanced accuracy, which was observed during the initial simple PPL period, was not apparent during difficult tasks of place preference learning phase (PPLrev2). The number and duration of licks during the visits with successful licks at drinking bottles (Licks/LVisits) was lower in NesNXN$^{-/-}$ mice compared to NXN-flfl mice (Fig. 5.12) which can interpreted as a reduced interest in reward and a restriction of licks to the need. Although NesNXN$^{-/-}$ mice were attracted to sweet water shown by

increased licks in the final free adaptation protocol of sweet (FA sweet), they were still less interested than the control group (Fig. 5.12).

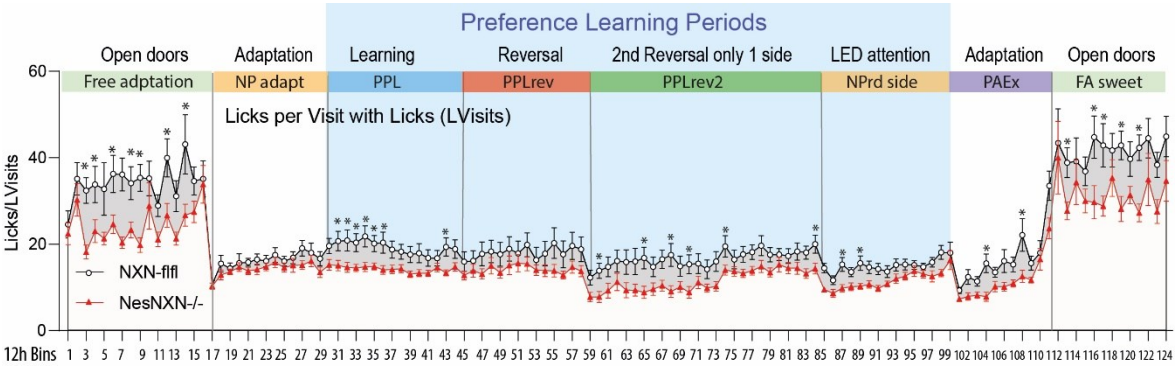

Fig 5.12 The number of licks per visit reveals reward collection for successful goal-directed LVisits. Licks/LVisits was reduced in NesNXN$^{-/-}$ compared to the control group. Graph shows the mean duration of licking during successful LVisits during the place preference learning periods. The data show means ± sem of 14-15 mice per group. The fluctuation of the behavior reveals nighttime and daytime differences (12h Bins). Data were compared with 2-way ANOVA for the factors “time” X “genotype” and posthoc comparison for “genotype” with adjustment of alpha according to Šidák.

Violin plots were used to display twenty behavioral parameters summarized over the full time course to investigate behavioral patterns of NesNXN$^{-/-}$ mice (Fig. 5.13). The violin plots show multiplicity adjusted statistics as color shaded background of the respected plot and reveal the major difference between genotypes. Blue colored graphs (Fig. 5.13) show a reduction of exploratory, non-goal-directed NPVisits, overall visiting activity and licking of NesNXN$^{-/-}$ mice. Orange-colored plots display an increased regularity and unevenness, which both point to strong habits of NesNXN$^{-/-}$ mice. High “Regularity” indicates a low frequency of diagonal transitions and “Unevenness” shows strong usage of specific corners instead of equal usage of all four corners. In adaptive and free protocols, “Unevenness” shows spontaneous strong habits and agrees with a low exploratory drive.

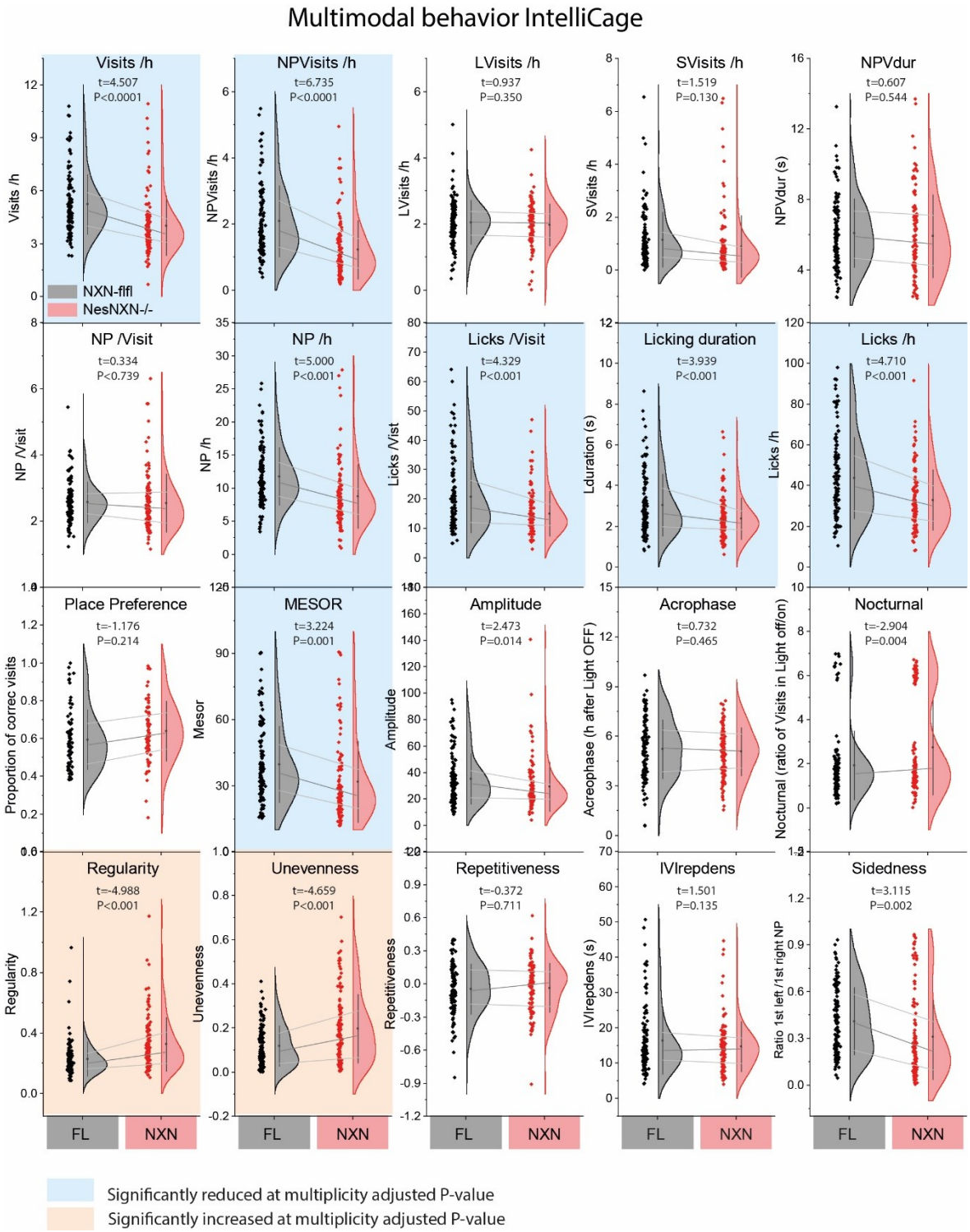

Fig 5.13 IntelliCage behavior of NesNXN$^{-/-}$ versus NXN-flfl mice averaged over different tasks. To compare behavior across modules/tasks the averages for each mouse per period were pooled and were plotted as half violin plots that show the Gauss distribution. The box within the violin is the interquartile range, the median is the dot. The lines connect the mean and the quartiles. The left scatters show individual results, each mouse represented by eight dots for each of the modules/tasks. The data were compared per 2-tailed, unpaired Student's t-test for each parameter. Asterisks show statistically significant differences between genotypes. *P< 0.05; **P<0.01; ***P<0.001.

5.5 Learning and memory in NesNXN$^{-/-}$ mice

Spatial learning behavior was assessed with protocols of place preference learning (PPL), reversal PPL (PPLrev, PPLrev2) as well as place avoidance acquisition (PAA) and extinction (PAex) experiments. NesNXN$^{-/-}$ mice made fewer trials but with similar number of successful visits during the periods of initial PPL (Fig. 5.14A). This correlates with the learning probability curves which were significantly steeper in NesNXN$^{-/-}$ mice during simple PPL tasks compared to the control group (Fig. 5.14B). The observed learning advantage was not present in more challenging tasks, where the correct corner was switched to the opposite side or a corner, that had not been rewarded before (PPLrev and PPLrev2). The learning probability curve represents the proportion of visits to correct corners relative to the number of trials. Thereby, NesNXN$^{-/-}$ mice needed fewer trials to reach 35% accuracy, which was defined as the learning threshold (10% above random success). No differences between genotypes were found in PAA and in PAex tasks and the final free adaptation (FAfin) with sweetened water (Fig. 5.15). Place avoidance was trained by conditioning the entry of forbidden corners with an unpleasant airpuff, whereas all corners were freely accessible during subsequent PAex period. Only LED signals were presented during PAex. Memory of previously punished corners was not different between genotypes which is shown in the proportion of visits to correct corners (Fig. 5.15A) and to previously punished corners (Fig 5.15B). During the FAfin period, mice had access to sweetened water in one corner. Both genotypes show similar attraction to sweetened water as shown in the learning probability curve of FAfin (Fig. 5.15C), whereas Licks/LVistis was reduced in NesNXN$^{-/-}$ mice compared to control mice, as described above (Fig. 5.12).

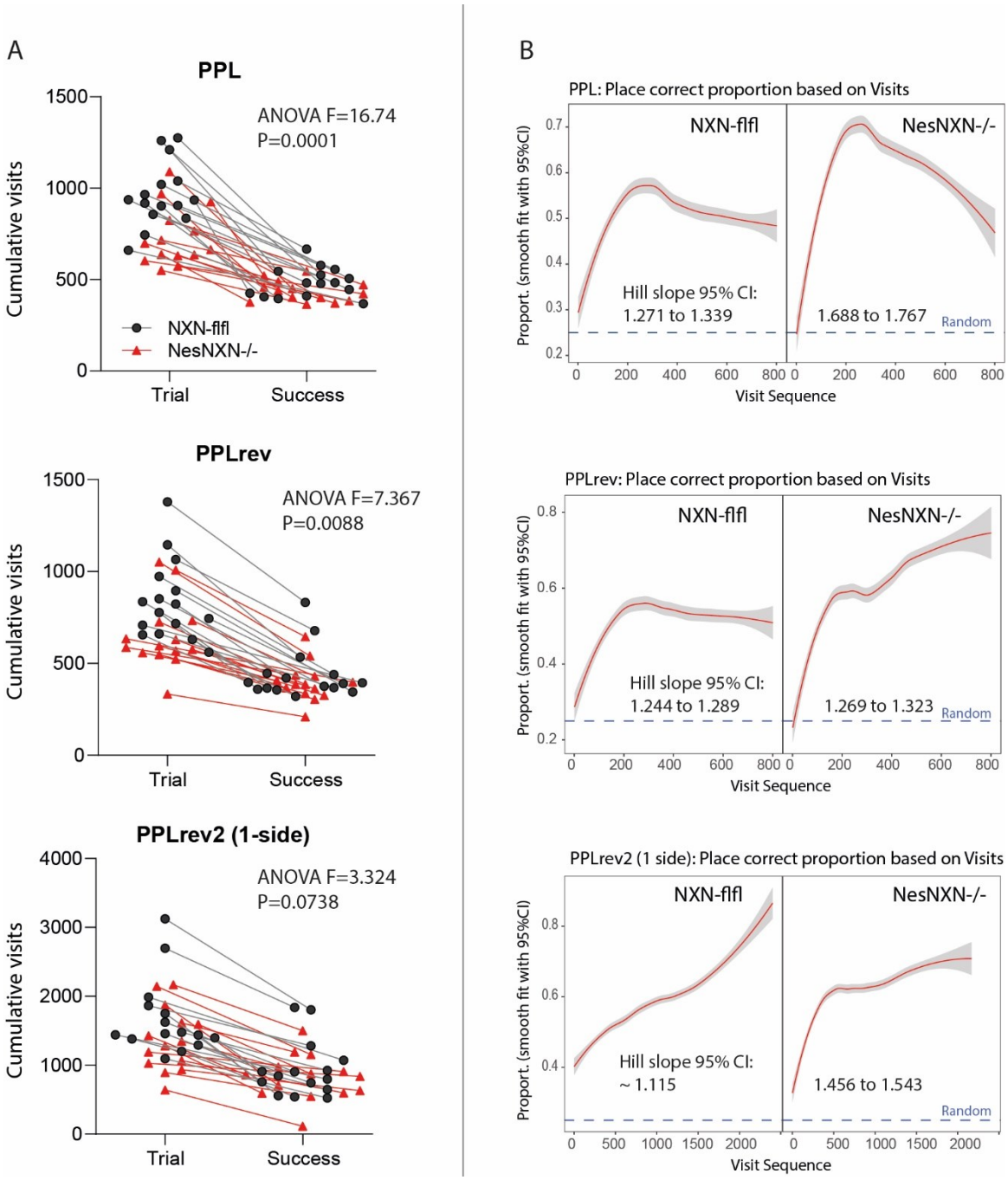

Fig 5.14nSpatial learning behavior during PPL and PPL reversal tasks in IC. **A**: Paired scatter/line plots show the numbers of trials versus successes for place preference learning and reversal learning tasks in IntelliCages. The groups comprised 14-15 mice per genotype. Each scatter shows a mouse. Data were compared with 2-way ANOVA for "trial/success" versus "genotype and reveal a lower number of trials of NesNXN$^{-/-}$ mice but similar successes. **B**: Learning probability curves show the proportion of correct corner visits relative to the trial number during place preference learning and PPL reversal learning (PPLrev, PPLrev2) tasks. The learning probability curves were significantly steeper during PPL in NesNXN$^{-/-}$ as revealed by non-overlapping 95% confidence levels for the Hill factor (Hill factor 95% CI given in the figures). NesNXN$^{-/-}$ needed fewer trials to reach 35% accuracy which was defined as the learning threshold (10% above random success). Place preference learning (PPL), PPL reversal learning and second reversal learning (PPLrev and PPLrev2).

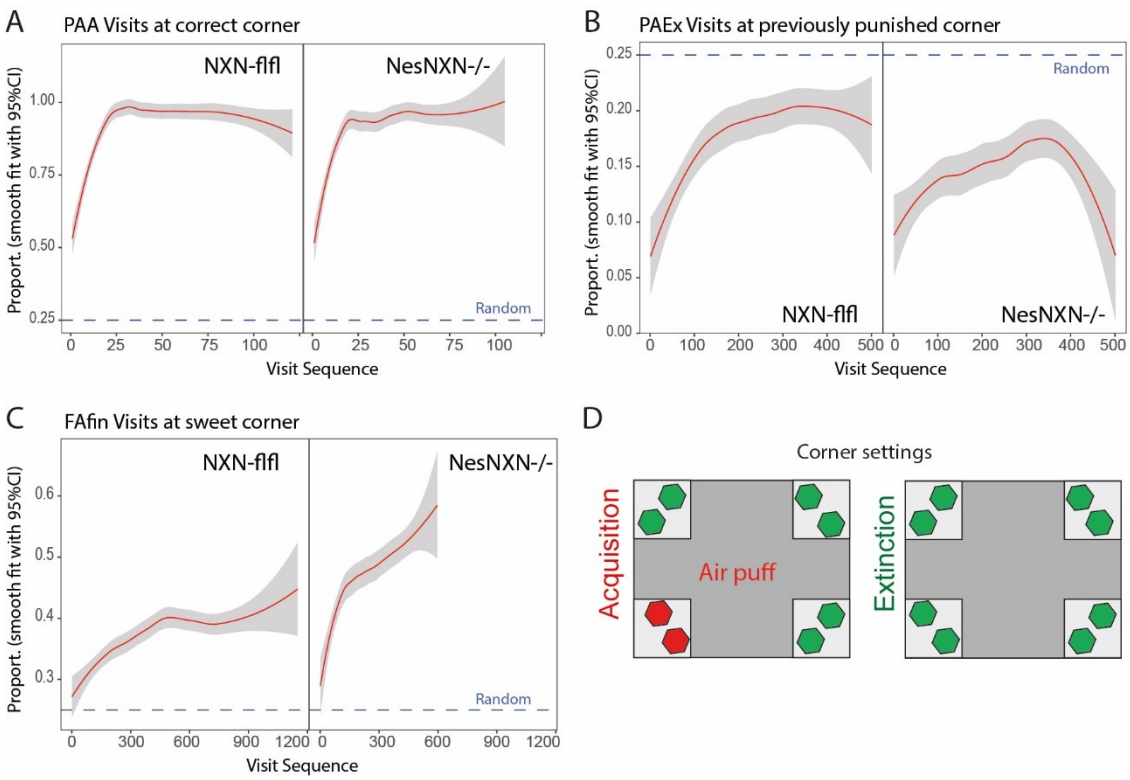

Fig 5.15 Learning probability curves show the proportion of correct corner visits. Behavior of gentotypes did not differ during **A** place avoidance acquisition (PAA), **B** place avoidance extinction (PAEx) and **C** final free adaptation with one corner providing sweetened water. In PAEx, all corners are allowed, and only LED signals reminded of the previously forbidden/punished corner. The proportion of correct corners in this task reveals the maintenance of the memory for the previously punished corner. **D** Sketch shows the experiment set up during PAA and PAEX tasks. Thereby, nosepokes at the forbidden corner would trigger an air puff as punishment signal. Additionally, LED lights are switched on with the air puff to support the mice's memory. In PAEx, all corners are freely accessible, but the LED signal reminds of the previously punished corner. The groups comprised 14-15 mice per genotype.

The proportion of correct nosepokes and correct visits during avoidance learning and extinction was also alike (Fig. 5.16). We infer that NesNXN$^{-/-}$ mice are goal-directed and "habit-loving" but less curious or "adventurous", leading to a mild advantage in easy preference learning but not in reversal learning or avoidance learning and memory.

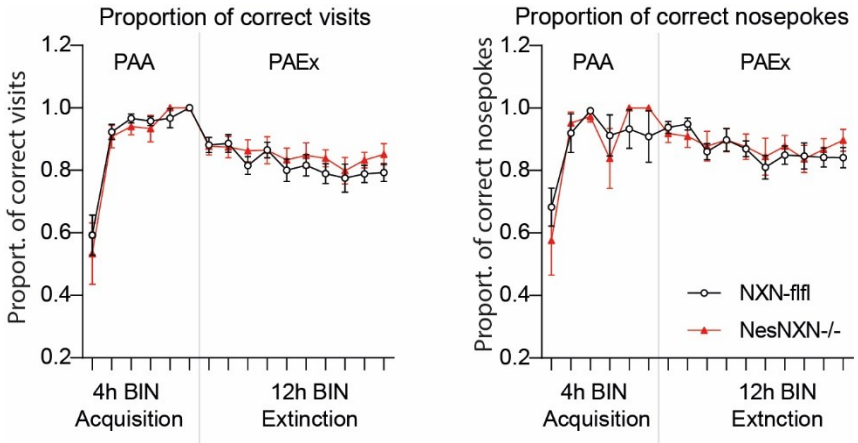

Fig 5.16 Time courses of the proportion of correct visits and correct nosepokes during place avoidance acquisition (PAA) and place avoidance extinction (PAEx). The data show means ± SEM of 14-15 mice per group. There were no differences between genotypes.

5.6 Lower interests in novel environments and low voluntary wheel running

The IntelliCage data suggested that NesNXN$^{-/-}$ mice were less interested in objects or environment and had a low exploratory and rewarding behavior. To further dissect the behavioral dimensions which were affected we used Maze tests and rewarding voluntary wheel running (VWR). There were no differences in feeding and drinking (Fig. 5.17A), but VWR was reduced in NesNXN$^{-/-}$ mice (Fig. 5.17B) supporting the presumption of a low rewarding exploratory and playful behavior of NesNXN$^{-/-}$ mice. In contrast, we did not observe differences of RotaRod running (not shown), where mice are forced to run.

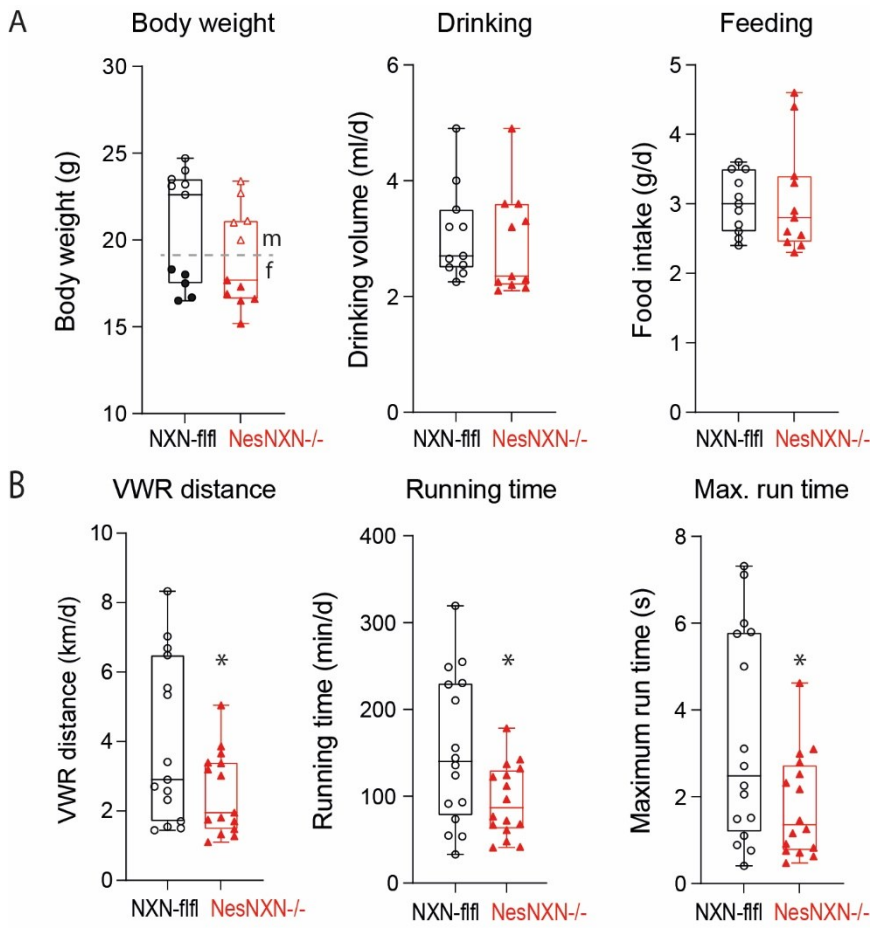

Fig 5.17 Phenomaster shows same food and drink intake but reduced voluntary wheel running of NesNXN$^{-/-}$ compared to Nxn-flfl. Running wheel and precision scales for food and water bottles are tracked in home cage environment. Data of **A** body weights, drinking, feeding and **B** voluntary wheel running (VWR) of NXN-flfl and NesNXN-/- mice in phenomaster cages are shown in box plots. Graph reveal the means ± SEM of 11 mice per genotype, and were compared with 2-tailed, unpaired Student's t-tests. The asterisks denote statistical significance, *P<0.05.

In the open field test (OFT), NesNXN$^{-/-}$ mice explored the center of the field less than the controls revealed by shorter paths in the center compartment (Fig. 5.18A). Overall paths were equivalent again showing that NesNXN$^{-/-}$ mice had no motor deficit. Similarly, total paths were equivalent in the EPM test (Fig. 5.18B) to observe anxiety and in 3-chamber tests of social cognition and memory (Fig. 5.19B). The EPM did not show any differences and suggest that low exploratory behavior of NesNXN$^{-/-}$ mice was not caused by anxiety.

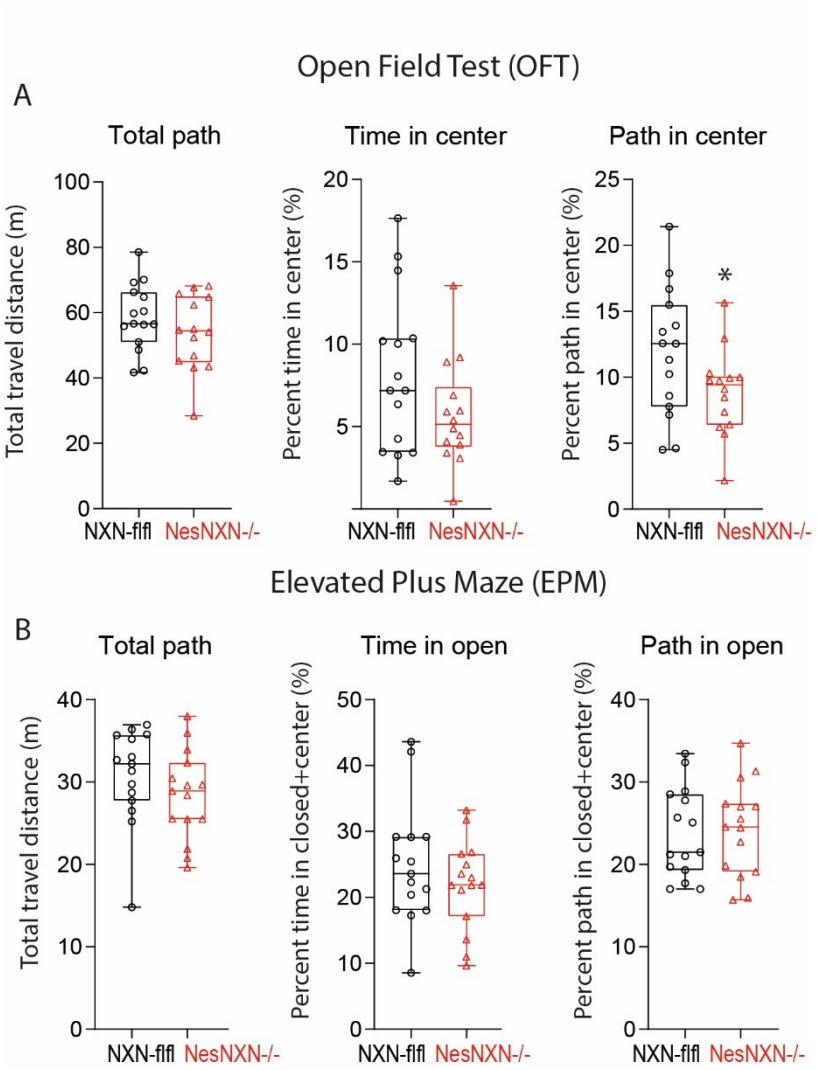

Fig 5.18 NesNXN$^{-/-}$ show lower explorative behavior in open field test (OFT) and no abnormal anxiety behavior in the elevated plus maze (EPM) compared to NXN-flfl. A Total path in OFT reflects the overall activity while time and path in the center region reveals exploratory behavior which were not significantly different between genotypes. **B** Total path during EPM experiments show no differences in overall activity between genotypes. Relative time spent in open arm show no difference in explorative and risk taking behavior. Each scatter represents one mouse. Box plots visualize data with each sample at min and max. 14 to 15 mice per genotype were compared with 2-tailed, unpaired Student's t-tests. The asterisks denote statistical significance, *P<0.05.

The sociability test shows a stronger relative interest of NesNXN$^{-/-}$ mice for social partners over the empty compartment (Fig. 5.19A). Social interest was rather

increased, whereas preferences for the compartment with the familiar mouse versus the novel social partner was similar between genotypes (Fig 5.19B). The behavior reveals no autism-like features in the NesNXN$^{-/-}$ group, as described in mice with alterations of dendritic spine plasticity and remodeling (Bowling & Klann, 2014; Pathania et al., 2014). It is of note, that a loss-of-function mutation of Camk2a leads to autism like behavior in mice (Stephenson et al., 2017). Hence, we conclude that NXN is not essential for maintenance of Camk2a activity needed for social behavior in mice.

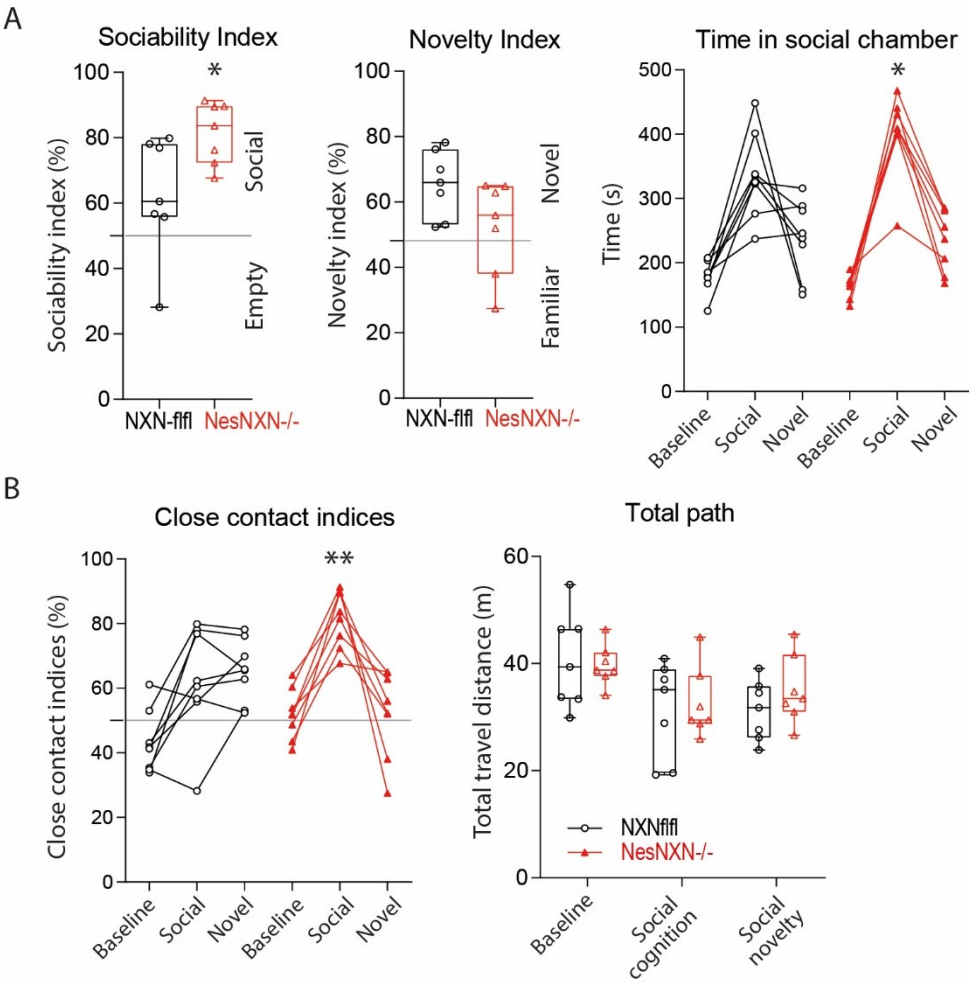

Fig 5.19 Sociability and social novelty/memory of NXN-flfl and NesNXN$^{-/-}$ mice were conducted in a 3-chamber maze test with two social compartments. A NesNXN-/- show stronger preference to the social chamber than to the empty compartment shown with the sociablity index which were calculated as [Tsocial/(Tsocial-Tempty)*100]. The novelty index calculated as [TNovel/(TFamiliar+TNovel)*100] reveals insignificant differences in relative time spent at familiar mouse against novel mouse between genotypes. Time in the social chamber with the social compartment reveals the social interest relative to the interest in an object. (social SC vs familiar SM) **B** Close contact indices show significant preference of NesNXN-/- to social mice in presence to an empty environment than to the novel mouse in presence of a familiar mouse. Tracked movements in total path are equal in both genotypes and reflect the overall activity. Each scatter represents one mouse. Data were compared with 2-way ANOVA and subsequent posthoc test according to Šidák (three time points) or by 2-tailed, unpaired Student's t-tests. *P<0.05.

6. Discussion

Redox homeostasis is essential for various cell signaling mechanisms throughout the whole organism. Various studies focused on the signaling role of NXN as an oxidoreductase involved in embryonic development or adipocyte differentiation through the canonical WNT pathway (Bahn et al., 2015; J. J. White et al., 2018). Only limited data are available so far giving information about the role of NXN in functional mechanisms in neurons (Urbainsky et al., 2018). Interestingly, our previous experiments revealed Camk2a as a prey in a Yeast-2-Hybrid-screening with NXN as a bait using a total brain library (Tran et al., 2021). This has prompted us to investigate the impact of NXN on neuronal plasticity, because Camk2a is the key protein for neuronal plasticity through regulating LTP and LTD during neuronal activity (Coultrap et al., 2014; Lamsa, Irvine, Giese, & Kullmann, 2007). A possible interaction of NXN with Camk2a suggested the involvement of NXN in neuronal plasticity pointing at a putative new mechanism of behavioral abnormalities of psychiatric diseases. The goal of this study was to find further evidence for the interaction of NXN with Camk2a and to investigate the impact of the neuronal deficiency of NXN on behavioral patterns in mice. The key finding of this study is the in-vitro interaction of NXN and Camk2a. But in-vivo, the redox-regulative interaction showed only moderate influence in our NesNXN$^{-/-}$ mouse model, such as reduced explorative behavior and no impact on cognitive functionality.

6.1 Expression pattern of NXN in the nervous system

In this study we confirmed the expression pattern of NXN from our previous studies where we found NXN in different brain regions and in the peripheral nervous system. The broad neuronal expression of NXN suggested a dominant function in the murine adult brain. Thus, we generated a mouse model to achieve a pan-neuronal depletion of NXN expression through the Nestin-Cre driver and mating with mice carrying floxed alleles. The neuronal deficiency of NXN in NesNXN$^{-/-}$ mice was confirmed in previous studies at RNA level and protein level in different brain tissues, spinal cord and DRGs (Tran et al., 2021). NXN expression was successfully reduced by 80-90 % at RNA level as expected from the efficient Nestin-Cre driven pan-neuronal conditioned deletion (Dubois, Hofmann, Kaloulis, Bishop, & Trumpp, 2006), hence the incomplete reduction at protein level of 50 % is pointing to compensatory

mechanisms. Additionally, remaining NXN expression in the central nervous system of NesNXN$^{-/-}$ mice can be contributed by glial and vascular cells (not evident in histologic studies) or incomplete Cre-recombinase mediated transformation. We did not achieve the expected complete deletion of NXN, which is a limitation of our studies. In comparison to reported perinatal lethality of complete NXN knockout (Funato et al., 2010), our NesNXN$^{-/-}$ mice have only shown a significant reduction of bodyweight after birth. This phenotype disappeared at the age of 9-10 weeks. Nevertheless, the partial deletion of NXN in our transgenic mouse model prevented embryonic lethality as occurring in complete NXN knockout mice (Funato et al., 2010). This gave us the opportunity to investigate NXN-dependent behavior in adult mice even though NXN was not completely absent in neurons.

6.2 NXN as a modulator of the redox-sensitive Camk2a

Camk2a elevates the translocation of AMPAR on the postsynaptic membrane for faster NMDAR resulting in long-term potentiation. (M. J. Robinson, Warlow, & Berridge, 2014; Xiong et al., 2019). Camk2a is also important for structural plasticity to control the volume and shape of dendritic spines(M. Matsuzaki, N. Honkura, G. C. R. Ellis-Davies, & H. Kasai, 2004; Gisela Zalcman, Noel Federman, & Arturo Romano, 2018). In this process, proteins involved in depolymerization of F-actin, such as cofilin, are phosphorylated and subsequently activated by Camk2a resulting in spine enlargement (Poncer et al., 2002). Additionally, nitric oxide synthase is phosphorylated and thereby activated by Camk2a resulting in the production of nitric oxide (NO) to induce synaptic strength and neuronal plasticity (Coultrap & Bayer, 2014; Feil & Kleppisch, 2008).

We found evidence for the interaction between NXN and Camk2a during this study through close localization of NXN and Camk2a. NXN was found in dendritic spines of primary hippocampal neurons, while conducting a co-staining of microtubule - associated protein 2 (MAP-2) which stabilizes microtubules of differentiated neurons (Soltani et al., 2005). Dendritic spines are protrusions of dendrites and represent the postsynaptic site of synapses (Borczyk, Sliwinska, Caly, Bernas, & Radwanska, 2019). The morphology of a dendritic spine is known to be correlated to the synaptic function (Alvarez & Sabatini, 2007; Bourne & Harris, 2008). As expected, we also found Camk2a in dendritic spines at primary neurons (Feng, Raghavachari, & Lisman, 2011). The close localization of NXN and Camk2a was

furtherly confirmed through the proximity ligation assay in primary cortical neurons. In this assay, the RNA-probe amplification only occurs if target proteins are found at close proximity (<40 nm) to generate a fluorescent signal.

In this study, we have shown the functional interaction of Camk2a and NXN during oxidative stimulation with H_2O_2. Camk2 activity in brain lysates of NesNXN$^{-/-}$ mice and samples from control mice were indifferent at baseline measurements and upon oxidative stimulation with H_2O_2. But significant difference between genotypes showed up with treatments with recombinant NXN significantly increased Camk2a activity. The boost of Camk2a activity was lower in NXN-deficient brains, suggesting a lower redox-sensitive proportion of Camk2a activity in samples of NXN-deficient mice. Redox modification with S-nitrosylation and further oxidation can enhance autonomous activity of Camk2a (Coultrap & Bayer, 2014; Scheving et al., 2012).

We hypothesize that NXN enhances the oxidation of Camk2a especially at the redox-sensitive cysteines which elevates its activity (Coultrap & Bayer, 2014) possibly by strengthening autophosphorylation (Buard et al., 2010; Giese et al., 1998). Cysteine sites, Cys280 and Cys289, are close to the autophosphorylation site T286 of Camk2a which is responsible for the autonomous activity (Coultrap & Bayer, 2014). The autonomous activity of Camk2 is maintained after intracellular Ca^{2+} level drops to baseline levels and has been believed to be responsible for biochemical memory (Lisman et al., 2002). Calmodulin trapping mediated by autophosphorylation of T286 increased the affinity of CaM to Camk2a (Meyer et al., 1992) for faster activation. Alteration of Camk2a phosphorylation through redox mechanisms at cysteine residues can potentially influence its activity (Klomsiri, Karplus, & Poole, 2011). Similar effects were reported in cardiovascular models showing Camk2a activation with ROS by increasing the autonomous activity (Erickson et al., 2011; Erickson et al., 2008). Autonomy of Camk2a is physiologically needed to induce LTP and LTD during neuronal plasticity (Chang et al., 2019; Coultrap et al., 2014) which has an impact on exploratory behavior (Stephenson et al., 2017), learning (Coultrap & Bayer, 2014; Giese, Fedorov, Filipkowski, & Silva, 1998).

Mitochondrial dysfunction in neurons is widely linked to neurodegenerative diseases, such as Alzheimer, Parkinson, and Huntington disease (Norat et al., 2020), because mitochondria are the major energy sources. Neurons and astrocytes

are the cells with highest energy demand with low capacity for energy storage (Dienel, 2019; Hyder et al., 2013; Peters et al., 2004), therefore insufficient respiratory activity in mitochondria for ATP production can indicate pathologic conditions. Endogenous ROS are generated through mitochondrial ETC and OXPHOS mechanisms, but excessive levels of ROS can contribute to further mitochondrial damages which enhances toxic ROS accumulation (R. R. Robinson et al., 2019). Our seahorse SUIT analysis revealed a significant reduction of the oxygen consumption rate (OCR) in mitochondria of NesNXN$^{-/-}$ mice brains after adding substrate and inhibitory components of the respiratory activity. Mitochondrial metabolism is linked to neuronal plasticity, hence mitochondrial $O2^{-\bullet}$ induced the phosphorylation of proteins to generate LTP, such as Camk2 and PKA, after NMDAR activation (Hongpaisan, Winters, & Andrews, 2004). This has led to the suggestion that NXN deficiency, even if only partial, would impact the mice behavior caused by alterations of energy production.

6.3 Neuronal deficiency of NXN reduces exploratory behavior

LTP mediated learning and memory mechanisms of Camk2a were investigated in the hippocampal area while other brain regions are recently in focus (Butler et al., 2017; Robison, 2014). Irregularities in the functions of Camk2a are involved in numerous psychiatric diseases, such as autism spectrum disorder (Stephenson et al., 2017), schizophrenia (Dadheech, Mishra, Gautam, & Sharma, 2008) and addiction (Easton et al., 2014; Mijakowska et al., 2017; Salling et al., 2016). To focus on the phenotype of our NesNXN$^{-/-}$ mice, we studied their behavior in IntelliCage and video-tracked experiments in classical maze tests. Our goal was to examine the impact of NXN deficiency in neurons on cognitive, exploratory, and social behavior.

IntelliCage systems enabled the observation of a large group of mice (16 mice each cage) in their home cage environment with minimized observer handling. NesNXN$^{-/-}$ mice were found to have a reduced explorative drive preferring strong habits compared to NXN-flfl mice whereas the cognitive behavior was normal. Indeed, data during complex learning periods did not show alterations in goal-directed activity and learning was indifferent between genotypes. NesNXN$^{-/-}$ mice even showed higher accuracy in simple learning tasks resulting from reduced try-and-error behavior. High explorative motivation in mice comes at the expense of accuracy (Mechan, Wyss, Rieger, & Mohajeri, 2009).

The predominant feature of NesNXN$^{-/-}$ mice in IntelliCage experiments was a reduction of non-goal-directed behavior. The apparent advantage of NesNXN$^{-/-}$ mice disappeared with the level of difficulty of the task. Exploratory behavior is a rewarding playful behavior particularly in young mice which depends on Camk2a (Easton et al., 2011) and diminishes continuously with the age of mice (Albuquerque et al., 2013; Mechan et al., 2009) to save energy for required activity. NesNXN$^{-/-}$ mice had no disadvantage in health, but translated to human low exploratory behavior can also be associated with a reduction of pleasure and curiosity. Hence, exploratory activity and play behavior are seen as indicators of pleasure and satisfaction (Boissy et al., 2007; Spangenberg & Wichman, 2018). When mice are satiated and do not need to look for food, as in IntelliCages, where food pellets are presented ad libitum, explorative behavior can mirror information-gathering behavior (Inglis, Langton, Forkman, & Lazarus, 2001). Thus, partial deletion of NXN in neurons revealed subtle effects on mouse behavior, although loss-of-function models of Camk2a reported severe phenotypes regarding autism-like behavior (Stephenson et al., 2017) and defects of learning and memory (Yamagata et al., 2009). We tracked the locomotor activity in the open-field test (OFT). The interpretation of the OFT is seen controversially regarding exploratory behavior (Perals, Griffin, Bartomeus, & Sol, 2017). However, the data from OFT support IntelliCage results by showing a significant reduction of traveled distance in the center in NesNXN$^{-/-}$ versus NXN-flfl mice. Elevated Plus Maze did not show any differences and suggest that low exploratory behavior of NesNXN$^{-/-}$ mice was not caused by anxiety.

Analyses in Phenomaster cages allowed automated assessments of food and drink intake as well as voluntary physical activity in a home cage environment, similar to IntelliCages. The use of the voluntary wheel is seen as a rewarding and playful activity (Spangenberg & Wichman, 2018) . Voluntary wheel running (VWR) was significantly diminished in NesNXN$^{-/-}$ mice compared to NXN-flfl mice, whereas drinking and feeding data were equal. NesNXN$^{-/-}$ mice were less motivated to use the VWR and maximal speed was significantly reduced. The reduced VWR strengthens our conclusion of a low rewarding exploratory and playful behavior in mice with neuronal deficiency of NXN. VWR was not affected by locomotive impairment, because we did not observe differences of forced running on the RotaRod running from previous studies (not shown).

Interestingly, there are studies for addictive behavior which use mouse models with Camk2a mutations. Addictive drugs, such as cocaine, enhance the activation of Camk2a and its autophosphorylation in the striatum (S. L. White, Schmidt, Vassoler, & Pierce, 2013). Studies in mice suggested a mechanism involving dopamine and serotonin and subsequent neuronal activity in the reward system, which was attenuated in Camk2a autophosphorylation-deficient mice in models of cocaine (Easton et al., 2014) or alcohol addiction (Mijakowska et al., 2017; Salling et al., 2016). Therefore, we infer that NXN sustains the motivational and exploratory drive which possibly is caused by activating Camk2a and keeping it at the oxidative state.

The recognition of social novelty involves dopaminergic systems in the prefrontal cortex (D. J. Watson et al., 2012). The major feature of autism spectrum disorder (ASD) and schizophrenia are deficits in social behavior (Chevallier, Kohls, Troiani, Brodkin, & Schultz, 2012). Impairment of social cognition, repetitive behavior and motoric stereotypy are also behavioral abnormalities of ASD (Bicks, Koike, Akbarian, & Morishita, 2015; Moy et al., 2008). In this study we investigated social cognition and social memory of NesNXN$^{-/-}$ mice relative to the interest in an object. Our sociability test revealed a difference in social interest between the genotypes. NesNXN$^{-/-}$ mice preferred the social partner over the empty compartment, whereas novelty seeking did not differ between genotypes.

Our sociability data of NesNXN$^{-/-}$ mice did not reveal autistic features, as seen in Camk2a deficient mice (Harda et al., 2018; Stephenson et al., 2017) or in mice with deficits in spine maturation and stabilization as observed in neurodevelopmental diseases (Courchet et al., 2018; Pathania et al., 2014). Interestingly, there are also ASD models of mice which revealed the linkage between the WNT signaling to dysregulations of synaptic structure and spine maturation (Medina et al., 2018). In these studies, downregulation of canonical WNT activities in young mice caused dysfunctional spine plasticity which was observed as an abnormal behavior in spatial exploration and memory in their later life (Viale et al., 2019). Dishevelled protein-1 (DVL1), which was described as an interaction partner of NXN in multiple studies (Funato et al., 2008; Hayashi et al., 2010; J. J. White et al., 2018), was not found in our Yeast-2-Hybrid screen. But NXN may have further target proteins for direct or indirect redox regulation, which are still unidentified. The interaction of NXN with WNT might contribute to alterations of neuronal plasticity. Various studies suggested an involvement of canonical and non-canonical WNT pathways at LTP

generation (Fig. 3.5) (Dickins & Salinas, 2013; McLeod & Salinas, 2018; McQuate, Latorre-Esteves, & Barria, 2017). For future experiments, it would be interesting to investigate the impact of NXN deletion on LTP and LDP pathways and the redox regulative impact of NXN on the autophosphorylation of Camk2a.

In conclusion, we observed a significantly reduced exploratory behavior and a reduced motivation for rewarding activities at the VWR in NesNXN$^{-/-}$ mice. We did not observe severe in vivo effects on cognitive and social behavior in our mice likely owing to a partial deletion of NXN in neurons. Remaining activity of NXN was likely sufficient to prevent serious neurodevelopmental diseases with mutations of Camk2 or WNT signaling. The observed loss of explorative behavior of NesNXN$^{-/-}$ mice likely results at least in part from the interaction and redox modification of Camk2a, but further unidentified target proteins may contribute to the phenotype. Our data revealed the function of NXN as a non-essential redox modulator of Camk2a in neurons. The behavioral phenotype neuronal NXN deficiency may be compensated via alternative redox cycles such as TXN or GSH which can even act as a back-up for each other (Branco et al., 2017; Ren et al., 2017).

7. Zusammenfassung

Oxidativer Stress wird mit neurodegenerativen Erkrankungen wie Alzheimer Demenz und Parkinson, aber auch mit neurologischen Entwicklungsstörungen wie Autismus-Spektrum-Störungen in Verbindung gebracht (Kandlur, Satyamoorthy, & Gangadharan, 2020; Matson & Williams, 2014). Eine Vielzahl an Erkrankungen kann durch das Ungleichgewicht der Redox-Homöostase verursacht werden. Hierbei sind ROS (reaktive Sauerstoffspezies) vermehrt vorhanden und können durch das Antioxidative System nicht mehr ausreichend reduziert werden (Eisner et al., 2018). Da im Gehirn die Speicherkapazität von Energie begrenzt ist (Peters et al., 2004), besteht ein kontinuierlicher Energiebedarf, der sowohl während der Aufrechterhaltung überlebenswichtiger Mechanismen als auch während hoher neuronaler Aktivitäten erzeugt wird (Hyder et al., 2013). ROS entsteht dabei als Nebenprodukt der mitochondrialen Zellatmung, welches eine Ansammlung von ROS (reaktive Sauerstoffspezies) zur Folge haben kann.

Befindet sich die ROS-Konzentration im physiologischen Bereich, können durch Oxidation der Signalproteine verschiedene Signalwege in den Neuronen aktiviert werden. Dazu gehören u.a. die Signalwege der axonalen Wegfindung, neuronale Netzwerkbildung und synaptische Plastizität (Oswald et al., 2018). Nucleoredoxin (NXN) ist ein Thioredoxin-ähnliches Protein, welches als Oxidoreduktase agiert (Urbainsky et al., 2018). Die genauen Funktionsmechanismen von NXN in den Neuronen sind bislang wenig untersucht. In der Proteinstruktur von NXN sind zwei konservierte Cysteine enthalten, die für die redoxregulierende Funktion wesentlich sind und somit Parallelen zum Thioredoxin aufweisen (Funato & Miki, 2007). Das Thioredoxin- und das Glutathion-System spielen als Reduktionssysteme von Disulfiden eine wesentliche Rolle in redox-modulierten Signalwegen (Drechsel & Patel, 2010; Holmgren, 2000).

Mit dem Yeast-2-Hybrid-Screen identifizierten wir als potenziellen Interaktionspartner die Calcium-Calmodulin-abhängige Proteinkinase 2a (Camk2a). Camk2a spielt eine Hauptrolle im Signalweg der synaptischen Plastizität, die während neuronaler Aktivitäten stattfindet. Mit Hilfe von NXN-LacZ-Reportermäusen konnten wir eine Expression des NXN-Reporters in verschiedenen Arealen nachweisen, die für verschiedene Aspekte des Verhaltens von Bedeutung

sind (Tran et al., 2021). Dies Färbungen zeigten eine Lokalisierung von NXN in Hirnregionen und im peripheren Nervensystem. Die neuronale Expression von NXN und die mögliche Interaktion mit Camk2a veranlassten uns daher, die Funktion von NXN in den Neuronen genauer zu untersuchen. Das Ziel dieser Arbeit war es, die Interaktion von Camk2a und NXN mit weiteren Experimenten zu bestätigen. Zusätzlich untersuchten wir die Auswirkungen des pan-neuronalen Mangels an NXN auf das Verhalten unserer transgenen Mäuse.

Für unser Mausmodell generierten wir pan-neuronale NXN-knockout Mäuse. Dabei wurde das Cre/loxP-System verwendet, um mithilfe der Nestin gesteuerten Cre Rekombinase einen Neuronen-spezifischen Knockout zu generieren (NesNXN$^{-/-}$). Der "knockout" war auf Protein-Ebene inkomplett und weist auf unbekannte Kompensationsmechanismen hin, verhinderte jedoch die embryonale bekannte fetale/embryonale Letalität, die bei vollständigen NXN-Knockout-Mäusen berichtet wurde (Funato et al., 2010). Demzufolge ermöglichte uns der partielle NXN-Knockout das Verhalten von adulten Mäusen zu untersuchen.

Im Proximity Ligation Assay (PLA) wurden weniger Signalpunkte in den kortikalen Primärneuronen der NesNXN$^{-/-}$ detektiert als in den NXN-flfl Mäusen. Ein Signalpunkt im PLA entsteht, wenn sich die beiden Zielproteine in unmittelbarer Nachbarschaft befinden, um eine Rolling-Circle-Amplifizierung zu ermöglichen. Die Interaktion von Camk2a und NXN wurde durch den PLA weiter gestützt. Parallel zum PLA wiesen wir Camk2a und NXN durch Immunfluoreszenzfärbungen in den kortikalen Primärkulturen nach. Camk2a und NXN Signale wurden u.a. im Soma und in den dendritischen Dornen gefunden.

Exzitatorische Neuronen des Kortex verbinden sich über dendritische Dornen mit weiteren exzitatorische Neuronen (Keller, 2002). Dendritische Dornen sind Fortsätze der Dendriten der exzitatorischen Neuronen. Sie sind in geringerem Umfang auch an inhibitorischen Neuronen zu finden (Keck et al., 2011). Sie spielen eine entscheidende Rolle in der neuronalen strukturellen Plastizität. Dabei ändert sich ihre Anzahl und Morphologie je nach der Funktionalität. Pilzförmige Dornen haben beispielsweise die längste Lebenszeit und kommen bei starken Neuronen Verknüpfungen vor (Frank et al., 2018). Die Langzeitpotenzierung (LTP) ist eine Beschreibung der funktionellen Plastizität und beeinflusst die Morphologie und Dichte der dendritischen Dornen (Ciani et al., 2011; McLeod et al., 2018; Viale et

al., 2019). Camk2a ist hierbei das Schlüsselenzym zur Generierung des LTP. In dem Zusammenhang werden mehr AMPA-Rezeptoren (α-Amino-3-hydroxy-5-methyl-4-isoxazolpropionsäure) an die postsynaptische Membran transloziert. Dadurch kann bei einer glutamatergen Stimulierung die postsynaptische Membran stärker depolarisiert werden, die zu einer Öffnung der NMDA-Rezeptoren führt (McLeod et al., 2018).

Mithilfe des Camk2-Aktivitätsassay wurde die funktionale Interaktion von Camk2a und NXN untersucht. Dabei wurde Camk2a aus Gehirn-Proteinlysaten der NXN-flfl und NesNXN$^{-/-}$ Mäuse angereichert. Die Aktivität von Camk2a wurde unter verschiedenen Bedingungen mit Stimulation durch rekombinantes NXN oder H_2O_2 Behandlung bestimmt. Die Ergebnisse deuten auf eine erniedrigte Redox-Sensitivität der Camk2a Aktivität in den NesNXN$^{-/-}$ Mäusen hin. Obwohl über die Funktionsmechanismen von NXN noch wenig bekannt ist, wird NXN in verschiedenen Studien als kompetitiver Inhibitor des kanonischen WNT-Signalweges beschrieben (Funato et al., 2006; Funato et al., 2010). Für den inhibitorischen Effekt ist NXN am Dishevelled (DVL) Protein gebunden und hemmt dessen Funktion, die für den WNT-Signalweg essentiell ist. Unter oxidativen Bedingungen dissoziiert NXN vom DVL zur Aktivierung der DVL-Funktion (Funato et al., 2006). Im Yeast-2-Hybrid-Screen konnte DVL nicht als Interaktionspartner im Nervensystem gefunden werden, jedoch könnte ein interessanter Zusammenhang zwischen dem kanonischen und nicht-kanonischen WNT Signalweg und der LTP während der Neuroplastizität bestehen (Dickins & Salinas, 2013; McLeod & Salinas, 2018; McQuate et al., 2017).

Endogenes ROS wird während der mitochondrialen Zellatmung produziert und bewirkt physiologische Funktionen. Jedoch können durch Störungen im Glukose Metabolismus nicht nur unzureichend ATP produziert, sondern auch toxische ROS Ansammlungen verursacht werden (R. R. Robinson et al., 2019). Seahorse Analysen der mitochondrialen Atmung zeigten eine reduzierte respiratorische Aktivität in den Mitochondrien der NesNXN$^{-/-}$ Gehirne, welches ein Indikator für mitochondriale Dysfunktionen in den Neuronen sein könnte, wie sie bei verschiedenen neurodegenerativen Erkrankungen beobachtet werden, z. B.: Alzheimer, Parkinson und Huntington-Krankheit (Norat et al., 2020).

Verhaltensstudien zeigten entgegen unseren Erwartungen nur schwache Auswirkungen auf den Phänotyp des panneuronalen NXN Knockouts.

Sowohl kognitive Fähigkeiten als auch das Sozialverhalten waren bei den NesNXN$^{-/-}$ Mäusen unauffällig. Die NesNXN$^{-/-}$ Mäuse wiesen keine autistischen Merkmale auf, wie sie bei Camk2a defizienten Mäusen (Harda et al., 2018; Stephenson et al., 2017) beobachtet wurden. Transgene Mäuse, die eine Mutation des Camk2a an T286 tragen, wiesen mit der fehlenden Autophosphorylierung ein erniedrigtes Angstverhalten im Elevated Plus Maze (EPM) auf (Gustin et al., 2011). Das EPM wird für gewöhnlich zur Untersuchung des Angstverhalten bei Mäusen verwendet (Walf & Frye, 2007), jedoch zeigten die NesNXN$^{-/-}$ Mäuse keine Unterschiede zur Kontrollgruppe. Der schwache Effekt auf das Sozial- und Angstverhalten der NesNXN$^{-/-}$ Mäuse leitet zu der Annahme, dass NXN einen nicht essentiellen partiellen Einfluss auf Camk2a und demzufolge auf die Neuroplastizität ausübt.

Im Phenomaster zeigten die NesNXN$^{-/-}$ Mäuse eine erniedrigte Motivation für die Nutzung des Laufrads (voluntary wheel running), welches als belohnende und Spiel-Aktivität gilt. Trink- und Essverhalten waren im Phenomaster zwischen den beiden Genotypen gleich.

Zudem wiesen die NesNXN$^{-/-}$ Mäuse ein reduziertes Explorationsverhalten auf, welches mithilfe der IntelliCage Versuche erfasst werden konnte. Im IntelliCage können das Verhalten und die kognitiven Fähigkeiten einer größeren Gruppe an Mäusen (16 Mäuse pro Käfig) beobachtet werden, ohne dass der Experimentator eingreifen muss. Reduziertes Explorations- und Motivationsverhalten in den NesNXN$^{-/-}$ Mäusen kann auf eine Anhedonie und reduzierte Neugier hinweisen.

Das beobachtete veränderte Verhaltensmuster der NesNXN$^{-/-}$ Mäusen ist möglicherweise das Ergebnis der Interaktion zwischen NXN und Camk2a, sowie einer verminderten Oxidation von Camk2a und weiteren unbekannten Zielproteinen von NXN. Unsere Ergebnisse lassen schlussfolgern, dass NXN in den Neuronen kein essenzieller Redox-Modulator von Camk2a ist, jedoch wesentlich zur Modifikation des explorativen Verhaltens beiträgt. Der Phänotyp der NesNXN$^{-/-}$ Mäuse könnte möglicherweise durch unbekannte Mechanismen kompensiert werden, da die Regulation des Redoxstatus von Camk2a durch verschiedene Redoxin wie das Thioredoxin und das Glutathion System mit-kontrolliert werden

lann. Diese Redox-Systeme könnten als gegenseitiges Backup fungieren (Branco et al., 2017; Ren et al., 2017).

8. References

Abraham, W. C., Jones, O. D., & Glanzman, D. L. (2019). Is plasticity of synapses the mechanism of long-term memory storage? *NPJ Sci Learn, 4*, 9. doi:10.1038/s41539-019-0048-y

Acin-Perez, R., Benador, I. Y., Petcherski, A., Veliova, M., Benavides, G. A., Lagarrigue, S., . . . Shirihai, O. S. (2020). A novel approach to measure mitochondrial respiration in frozen biological samples. *EMBO J, 39*(13), e104073. doi:10.15252/embj.2019104073

Ahmad-Annuar, A., Ciani, L., Simeonidis, I., Herreros, J., Fredj, N. B., Rosso, S. B., . . . Salinas, P. C. (2006). Signaling across the synapse: a role for Wnt and Dishevelled in presynaptic assembly and neurotransmitter release. *J Cell Biol, 174*(1), 127-139. doi:10.1083/jcb.200511054

Albuquerque, B., Haussler, A., Vannoni, E., Wolfer, D. P., & Tegeder, I. (2013). Learning and memory with neuropathic pain: impact of old age and progranulin deficiency. *Front Behav Neurosci, 7*, 174. doi:10.3389/fnbeh.2013.00174

Alvarez, V. A., & Sabatini, B. L. (2007). Anatomical and physiological plasticity of dendritic spines. *Annu Rev Neurosci, 30*, 79-97. doi:10.1146/annurev.neuro.30.051606.094222

Aoyama, K., & Nakaki, T. (2015). Glutathione in Cellular Redox Homeostasis: Association with the Excitatory Amino Acid Carrier 1 (EAAC1). *Molecules, 20*(5), 8742-8758. doi:10.3390/molecules20058742

Arellanes-Robledo, J., Reyes-Gordillo, K., Shah, R., Dominguez-Rosales, J. A., Hernandez-Nazara, Z. H., Ramirez, F., . . . Lakshman, M. R. (2013). Fibrogenic actions of acetaldehyde are beta-catenin dependent but Wingless independent: a critical role of nucleoredoxin and reactive oxygen species in human hepatic stellate cells. *Free Radic Biol Med, 65*, 1487-1496. doi:10.1016/j.freeradbiomed.2013.07.017

Avigan, P. D., Cammack, K., & Shapiro, M. L. (2020). Flexible spatial learning requires both the dorsal and ventral hippocampus and their functional interactions with the prefrontal cortex. *Hippocampus*. doi:10.1002/hipo.23198

Bahn, Y. J., Lee, K. P., Lee, S. M., Choi, J. Y., Seo, Y. S., & Kwon, K. S. (2015). Nucleoredoxin promotes adipogenic differentiation through regulation of Wnt/beta-catenin signaling. *J Lipid Res, 56*(2), 294-303. doi:10.1194/jlr.M054056

Barcomb, K., Buard, I., Coultrap, S. J., Kulbe, J. R., O'Leary, H., Benke, T. A., & Bayer, K. U. (2014). Autonomous CaMKII requires further stimulation by Ca2+/calmodulin for enhancing synaptic strength. *FASEB J, 28*(8), 3810-3819. doi:10.1096/fj.14-250407

Bayer, K. U., Löhler, J., Schulman, H., & Harbers, K. (1999). Developmental expression of the CaM kinase II isoforms: ubiquitous γ- and δ-CaM kinase II are the early isoforms and most abundant in the developing nervous system. *Molecular Brain Research, 70*(1), 147-154. doi:10.1016/s0169-328X(99)00131-X

Beckhauser, T. F., Francis-Oliveira, J., & De Pasquale, R. (2016). Reactive Oxygen Species: Physiological and Physiopathological Effects on Synaptic Plasticity. *J Exp Neurosci, 10*(Suppl 1), 23-48. doi:10.4137/JEN.S39887

Belanger, M., Allaman, I., & Magistretti, P. J. (2011). Brain energy metabolism: focus on astrocyte-neuron metabolic cooperation. *Cell Metab, 14*(6), 724-738. doi:10.1016/j.cmet.2011.08.016

Benhar, M. (2018). Roles of mammalian glutathione peroxidase and thioredoxin reductase enzymes in the cellular response to nitrosative stress. *Free Radic Biol Med, 127*, 160-164. doi:10.1016/j.freeradbiomed.2018.01.028

Bhattacharyya, M., Lee, Y. K., Muratcioglu, S., Qiu, B., Nyayapati, P., Schulman, H., . . . Kuriyan, J. (2020). Flexible linkers in CaMKII control the balance between activating and inhibitory autophosphorylation. *Elife, 9*. doi:10.7554/eLife.53670

Bhattacharyya, S., Biou, V., Xu, W., Schluter, O., & Malenka, R. C. (2009). A critical role for PSD-95/AKAP interactions in endocytosis of synaptic AMPA receptors. *Nat Neurosci, 12*(2), 172-181. doi:10.1038/nn.2249

Bicks, L. K., Koike, H., Akbarian, S., & Morishita, H. (2015). Prefrontal Cortex and Social Cognition in Mouse and Man. *Front Psychol, 6*, 1805. doi:10.3389/fpsyg.2015.01805

Boissy, A., Manteuffel, G., Jensen, M. B., Moe, R. O., Spruijt, B., Keeling, L. J., . . . Aubert, A. (2007). Assessment of positive emotions in animals to improve their welfare. *Physiol Behav, 92*(3), 375-397. doi:10.1016/j.physbeh.2007.02.003

Bolduc, J. A., Nelson, K. J., Haynes, A. C., Lee, J., Reisz, J. A., Graff, A. H., . . . Lowther, W. T. (2018). Novel hyperoxidation resistance motifs in 2-Cys peroxiredoxins. *J Biol Chem, 293*(30), 11901-11912. doi:10.1074/jbc.RA117.001690

Borczyk, M., Sliwinska, M. A., Caly, A., Bernas, T., & Radwanska, K. (2019). Neuronal plasticity affects correlation between the size of dendritic spine and its postsynaptic density. *Sci Rep, 9*(1), 1693. doi:10.1038/s41598-018-38412-7

Bourne, J. N., & Harris, K. M. (2008). Balancing structure and function at hippocampal dendritic spines. *Annu Rev Neurosci, 31*, 47-67. doi:10.1146/annurev.neuro.31.060407.125646

Bowling, H., & Klann, E. (2014). Shaping Dendritic Spines in Autism Spectrum Disorder: mTORC1-Dependent Macroautophagy. *Neuron, 83*(5), 994-996. doi:10.1016/j.neuron.2014.08.021

Branco, V., Coppo, L., Sola, S., Lu, J., Rodrigues, C. M. P., Holmgren, A., & Carvalho, C. (2017). Impaired cross-talk between the thioredoxin and glutathione systems is related to ASK-1 mediated apoptosis in neuronal cells exposed to mercury. *Redox Biol, 13*, 278-287. doi:10.1016/j.redox.2017.05.024

Brandes, N., Schmitt, S., & Jakob, U. (2009). Thiol-based redox switches in eukaryotic proteins. *Antioxid Redox Signal, 11*(5), 997-1014. doi:10.1089/ARS.2008.2285

Brennan, A. M., Suh, S. W., Won, S. J., Narasimhan, P., Kauppinen, T. M., Lee, H., . . . Swanson, R. A. (2009). NADPH oxidase is the primary source of superoxide induced by NMDA receptor activation. *Nat Neurosci, 12*(7), 857-863. doi:10.1038/nn.2334

Butler, R. K., Ehling, S., Barbar, M., Thomas, J., Hughes, M. A., Smith, C. E., . . . Lascelles, B. D. X. (2017). Distinct neuronal populations in the basolateral and central amygdala are activated with acute pain, conditioned fear, and fear-conditioned analgesia. *Neurosci Lett, 661*, 11-17. doi:10.1016/j.neulet.2017.09.025

Chang, J. Y., Nakahata, Y., Hayano, Y., & Yasuda, R. (2019). Mechanisms of Ca(2+)/calmodulin-dependent kinase II activation in single dendritic spines. *Nat Commun, 10*(1), 2784. doi:10.1038/s41467-019-10694-z

Chevallier, C., Kohls, G., Troiani, V., Brodkin, E. S., & Schultz, R. T. (2012). The social motivation theory of autism. *Trends Cogn Sci, 16*(4), 231-239. doi:10.1016/j.tics.2012.02.007

Cho, Y. H., & Jeantet, Y. (2010). Differential involvement of prefrontal cortex, striatum, and hippocampus in DRL performance in mice. *Neurobiology of Learning and Memory, 93*(1), 85-91. doi:10.1016/j.nlm.2009.08.007

Ciani, L., Boyle, K. A., Dickins, E., Sahores, M., Anane, D., Lopes, D. M., . . . Salinas, P. C. (2011). Wnt7a signaling promotes dendritic spine growth and synaptic strength through Ca(2)(+)/Calmodulin-dependent protein kinase II. *Proc Natl Acad Sci U S A, 108*(26), 10732-10737. doi:10.1073/pnas.1018132108

Citri, A., & Malenka, R. C. (2008). Synaptic plasticity: multiple forms, functions, and mechanisms. *Neuropsychopharmacology, 33*(1), 18-41. doi:10.1038/sj.npp.1301559

Colbran, R. J. (1993). Inactivation of Ca2+/calmodulin-dependent protein kinase II by basal autophosphorylation. *J Biol Chem, 268*(10), 7163-7170.

Collingridge, G. L., Peineau, S., Howland, J. G., & Wang, Y. T. (2010). Long-term depression in the CNS. *Nat Rev Neurosci, 11*(7), 459-473. doi:10.1038/nrn2867

Coultrap, S. J., & Bayer, K. U. (2012). CaMKII regulation in information processing and storage. *Trends Neurosci, 35*(10), 607-618. doi:10.1016/j.tins.2012.05.003

Coultrap, S. J., & Bayer, K. U. (2014). Nitric oxide induces Ca2+-independent activity of the Ca2+/calmodulin-dependent protein kinase II (CaMKII). *J Biol Chem, 289*(28), 19458-19465. doi:10.1074/jbc.M114.558254

Coultrap, S. J., Freund, R. K., O'Leary, H., Sanderson, J. L., Roche, K. W., Dell'Acqua, M. L., & Bayer, K. U. (2014). Autonomous CaMKII mediates both LTP and LTD using a mechanism for differential substrate site selection. *Cell Rep, 6*(3), 431-437. doi:10.1016/j.celrep.2014.01.005

Courchet, V., Roberts, A. J., Meyer-Dilhet, G., Del Carmine, P., Lewis, T. L., Jr., Polleux, F., & Courchet, J. (2018). Haploinsufficiency of autism spectrum disorder candidate gene NUAK1 impairs cortical development and behavior in mice. *Nat Commun, 9*(1), 4289. doi:10.1038/s41467-018-06584-5

D'Autreaux, B., & Toledano, M. B. (2007). ROS as signalling molecules: mechanisms that generate specificity in ROS homeostasis. *Nat Rev Mol Cell Biol, 8*(10), 813-824. doi:10.1038/nrm2256

Dadheech, G., Mishra, S., Gautam, S., & Sharma, P. (2008). Evaluation of antioxidant deficit in schizophrenia. *Indian J Psychiatry, 50*(1), 16-20. doi:10.4103/0019-5545.39753

Dickins, E. M., & Salinas, P. C. (2013). Wnts in action: from synapse formation to synaptic maintenance. *Front Cell Neurosci, 7*, 162. doi:10.3389/fncel.2013.00162

Dienel, G. A. (2019). Brain Glucose Metabolism: Integration of Energetics with Function. *Physiol Rev, 99*(1), 949-1045. doi:10.1152/physrev.00062.2017

Drechsel, D. A., & Patel, M. (2010). Respiration-dependent H2O2 removal in brain mitochondria via the thioredoxin/peroxiredoxin system. *J Biol Chem, 285*(36), 27850-27858. doi:10.1074/jbc.M110.101196

Du, Y., Zhang, H., Zhang, X., Lu, J., & Holmgren, A. (2013). Thioredoxin 1 is inactivated due to oxidation induced by peroxiredoxin under oxidative stress and reactivated by the glutaredoxin system. *J Biol Chem, 288*(45), 32241-32247. doi:10.1074/jbc.M113.495150

Duan, Y., Gross, R. A., & Sheu, S. S. (2007). Ca2+-dependent generation of mitochondrial reactive oxygen species serves as a signal for poly(ADP-ribose) polymerase-1 activation during glutamate excitotoxicity. *J Physiol, 585*(Pt 3), 741-758. doi:10.1113/jphysiol.2007.145409

Dubois, N. C., Hofmann, D., Kaloulis, K., Bishop, J. M., & Trumpp, A. (2006). Nestin-Cre transgenic mouse line Nes-Cre1 mediates highly efficient Cre/loxP mediated recombination in the nervous system, kidney, and somite-derived tissues. *Genesis, 44*(8), 355-360. doi:10.1002/dvg.20226

Dwivedi, D., Megha, K., Mishra, R., & Mandal, P. K. (2020). Glutathione in Brain: Overview of Its Conformations, Functions, Biochemical Characteristics, Quantitation and Potential Therapeutic Role in Brain Disorders. *Neurochem Res, 45*(7), 1461-1480. doi:10.1007/s11064-020-03030-1

Easton, A. C., Lourdusamy, A., Havranek, M., Mizuno, K., Solati, J., Golub, Y., . . . Muller, C. P. (2014). alphaCaMKII controls the establishment of cocaine's reinforcing effects in mice and humans. *Transl Psychiatry, 4*, e457. doi:10.1038/tp.2014.97

Easton, A. C., Lucchesi, W., Schumann, G., Giese, K. P., Muller, C. P., & Fernandes, C. (2011). alphaCaMKII autophosphorylation controls exploratory activity to threatening novel stimuli. *Neuropharmacology, 61*(8), 1424-1431. doi:10.1016/j.neuropharm.2011.08.036

Eisner, V., Picard, M., & Hajnoczky, G. (2018). Mitochondrial dynamics in adaptive and maladaptive cellular stress responses. *Nat Cell Biol, 20*(7), 755-765. doi:10.1038/s41556-018-0133-0

Engert, F., & Bonhoeffer, T. (1999). Dendritic spine changes associated with hippocampal long-term synaptic plasticity. *Nature, 399*(6731), 66-70. doi:10.1038/19978

Erickson, J. R., He, B. J., Grumbach, I. M., & Anderson, M. E. (2011). CaMKII in the cardiovascular system: sensing redox states. *Physiol Rev, 91*(3), 889-915. doi:10.1152/physrev.00018.2010

Erickson, J. R., Joiner, M. L., Guan, X., Kutschke, W., Yang, J., Oddis, C. V., . . . Anderson, M. E. (2008). A dynamic pathway for calcium-independent activation of CaMKII by methionine oxidation. *Cell, 133*(3), 462-474. doi:10.1016/j.cell.2008.02.048

Eroglu, C., & Barres, B. A. (2010). Regulation of synaptic connectivity by glia. *Nature, 468*(7321), 223-231. doi:10.1038/nature09612

Erondu, N. E., & Kennedy, M. B. (1985). Regional distribution of type II Ca2+/calmodulin-dependent protein kinase in rat brain. *J Neurosci, 5*(12), 3270-3277.

Fahlke, C., Kortzak, D., & Machtens, J. P. (2016). Molecular physiology of EAAT anion channels. *Pflugers Arch, 468*(3), 491-502. doi:10.1007/s00424-015-1768-3

Fang, L., Wu, J., Lin, Q., & Willis, W. D. (2002). Calcium-calmodulin-dependent protein kinase II contributes to spinal cord central sensitization. *J Neurosci, 22*(10), 4196-4204. doi:20026343

Feil, R., & Kleppisch, T. (2008). NO/cGMP-dependent modulation of synaptic transmission. *Handb Exp Pharmacol*(184), 529-560. doi:10.1007/978-3-540-74805-2_16

Feng, B., Raghavachari, S., & Lisman, J. (2011). Quantitative estimates of the cytoplasmic, PSD, and NMDAR-bound pools of CaMKII in dendritic spines. *Brain Res, 1419*, 46-52. doi:10.1016/j.brainres.2011.08.051

Finelli, M. J. (2020). Redox Post-translational Modifications of Protein Thiols in Brain Aging and Neurodegenerative Conditions-Focus on S-Nitrosation. *Front Aging Neurosci, 12*, 254. doi:10.3389/fnagi.2020.00254

Frank, A. C., Huang, S., Zhou, M., Gdalyahu, A., Kastellakis, G., Silva, T. K., . . . Silva, A. J. (2018). Hotspots of dendritic spine turnover facilitate clustered spine addition and learning and memory. *Nat Commun, 9*(1), 422. doi:10.1038/s41467-017-02751-2

Funato, Y., Michiue, T., Asashima, M., & Miki, H. (2006). The thioredoxin-related redox-regulating protein nucleoredoxin inhibits Wnt-beta-catenin signalling through dishevelled. *Nat Cell Biol, 8*(5), 501-508. doi:10.1038/ncb1405

Funato, Y., Michiue, T., Terabayashi, T., Yukita, A., Danno, H., Asashima, M., & Miki, H. (2008). Nucleoredoxin regulates the Wnt/planar cell polarity pathway in Xenopus. *Genes Cells, 13*(9), 965-975. doi:10.1111/j.1365-2443.2008.01220.x

Funato, Y., & Miki, H. (2007). Nucleoredoxin, a novel thioredoxin family member involved in cell growth and differentiation. *Antioxid Redox Signal, 9*(8), 1035-1057. doi:10.1089/ars.2007.1550

Funato, Y., Terabayashi, T., Sakamoto, R., Okuzaki, D., Ichise, H., Nojima, H., . . . Miki, H. (2010). Nucleoredoxin sustains Wnt/beta-catenin signaling by retaining a pool of inactive dishevelled protein. *Curr Biol, 20*(21), 1945-1952. doi:10.1016/j.cub.2010.09.065

Galjart, N. (2005). CLIPs and CLASPs and cellular dynamics. *Nat Rev Mol Cell Biol, 6*(6), 487-498. doi:10.1038/nrm1664

Garthe, A., Behr, J., & Kempermann, G. (2009). Adult-generated hippocampal neurons allow the flexible use of spatially precise learning strategies. *PLoS One, 4*(5), e5464. doi:10.1371/journal.pone.0005464

Garthwaite, J. (2008). Concepts of neural nitric oxide-mediated transmission. *Eur J Neurosci, 27*(11), 2783-2802. doi:10.1111/j.1460-9568.2008.06285.x

Gegg, M. E., Beltran, B., Salas-Pino, S., Bolanos, J. P., Clark, J. B., Moncada, S., & Heales, S. J. (2003). Differential effect of nitric oxide on glutathione metabolism and mitochondrial function in astrocytes and neurones: implications for neuroprotection/neurodegeneration? *J Neurochem, 86*(1), 228-237. doi:10.1046/j.1471-4159.2003.01821.x

Giese, K. P., Fedorov, N. B., Filipkowski, R. K., & Silva, A. J. (1998). Autophosphorylation at Thr286 of the alpha calcium-calmodulin kinase II in LTP and learning. *Science, 279*(5352), 870-873. doi:10.1126/science.279.5352.870

Glazewski, S., Bejar, R., Mayford, M., & Fox, K. (2001). The effect of autonomous alpha-CaMKII expression on sensory responses and experience-dependent plasticity in mouse barrel cortex. *Neuropharmacology, 41*(6), 771-778. doi:10.1016/s0028-3908(01)00097-1

Gould, N., Doulias, P. T., Tenopoulou, M., Raju, K., & Ischiropoulos, H. (2013). Regulation of protein function and signaling by reversible cysteine S-nitrosylation. *J Biol Chem, 288*(37), 26473-26479. doi:10.1074/jbc.R113.460261

Gustin, R. M., Shonesy, B. C., Robinson, S. L., Rentz, T. J., Baucum, A. J., 2nd, Jalan-Sakrikar, N., . . . Colbran, R. J. (2011). Loss of Thr286 phosphorylation disrupts synaptic CaMKIIalpha targeting, NMDAR activity and behavior in pre-adolescent mice. *Mol Cell Neurosci, 47*(4), 286-292. doi:10.1016/j.mcn.2011.05.006

Harda, Z., Dzik, J. M., Nalberczak-Skora, M., Meyza, K., Lukasiewicz, K., Leski, S., & Radwanska, K. (2018). Autophosphorylation of alphaCaMKII affects social interactions in mice. *Genes Brain Behav, 17*(5), e12457. doi:10.1111/gbb.12457

Hardt, S., Heidler, J., Albuquerque, B., Valek, L., Altmann, C., Wilken-Schmitz, A., . . . Tegeder, I. (2017). Loss of synaptic zinc transport in progranulin deficient mice may contribute to progranulin-associated psychopathology and chronic pain. *Biochim Biophys Acta Mol Basis Dis, 1863*(11), 2727-2745. doi:10.1016/j.bbadis.2017.07.014

Hardt, S., Valek, L., Zeng-Brouwers, J., Wilken-Schmitz, A., Schaefer, L., & Tegeder, I. (2018). Progranulin Deficient Mice Develop Nephrogenic Diabetes Insipidus. *Aging Dis, 9*(5), 817-830. doi:10.14336/AD.2017.1127

Hayashi, T., Funato, Y., Terabayashi, T., Morinaka, A., Sakamoto, R., Ichise, H., . . . Miki, H. (2010). Nucleoredoxin negatively regulates Toll-like receptor 4 signaling via recruitment of flightless-I to myeloid differentiation primary response gene (88). *J Biol Chem, 285*(24), 18586-18593. doi:10.1074/jbc.M110.106468

Hill, T. C., & Zito, K. (2013). LTP-induced long-term stabilization of individual nascent dendritic spines. *J Neurosci, 33*(2), 678-686. doi:10.1523/JNEUROSCI.1404-12.2013

Hirota, K., Matsui, M., Murata, M., Takashima, Y., Cheng, F. S., Itoh, T., . . . Yodoi, J. (2000). Nucleoredoxin, glutaredoxin, and thioredoxin differentially regulate NF-kappaB, AP-1, and CREB activation in HEK293 cells. *Biochem Biophys Res Commun, 274*(1), 177-182. doi:10.1006/bbrc.2000.3106

Hirrlinger, J., Schulz, J. B., & Dringen, R. (2002). Glutathione release from cultured brain cells: multidrug resistance protein 1 mediates the release of GSH from rat astroglial cells. *J Neurosci Res, 69*(3), 318-326. doi:10.1002/jnr.10308

Holmgren, A. (2000). Antioxidant function of thioredoxin and glutaredoxin systems. *Antioxid Redox Signal, 2*(4), 811-820. doi:10.1089/ars.2000.2.4-811

Hongpaisan, J., Winters, C. A., & Andrews, S. B. (2004). Strong calcium entry activates mitochondrial superoxide generation, upregulating kinase signaling in hippocampal neurons. *J Neurosci, 24*(48), 10878-10887. doi:10.1523/JNEUROSCI.3278-04.2004

Huang, E. P. (1997). Synaptic plasticity: A role for nitric oxide in LTP. *Current Biology, 7*(3), R141-R143. doi:10.1016/S0960-9822(97)70073-3

Huganir, R. L., & Nicoll, R. A. (2013). AMPARs and synaptic plasticity: the last 25 years. *Neuron, 80*(3), 704-717. doi:10.1016/j.neuron.2013.10.025

Hyder, F., Rothman, D. L., & Bennett, M. R. (2013). Cortical energy demands of signaling and nonsignaling components in brain are conserved across mammalian species and activity levels. *Proc Natl Acad Sci U S A, 110*(9), 3549-3554. doi:10.1073/pnas.1214912110

Inglis, I. R., Langton, S., Forkman, B., & Lazarus, J. (2001). An information primacy model of exploratory and foraging behaviour. *Animal Behaviour, 62*(3), 543-557. doi:https://doi.org/10.1006/anbe.2001.1780

Jackson, P. A., Kesner, R. P., & Amann, K. (1998). Memory for duration: role of hippocampus and medial prefrontal cortex. *Neurobiol Learn Mem, 70*(3), 328-348. doi:10.1006/nlme.1998.3859

Janssen-Heininger, Y. M., Mossman, B. T., Heintz, N. H., Forman, H. J., Kalyanaraman, B., Finkel, T., . . . van der Vliet, A. (2008). Redox-based regulation of signal transduction: principles, pitfalls, and promises. *Free Radic Biol Med, 45*(1), 1-17. doi:10.1016/j.freeradbiomed.2008.03.011

Kaidanovich-Beilin, O., Lipina, T., Vukobradovic, I., Roder, J., & Woodgett, J. R. (2011). Assessment of social interaction behaviors. *J Vis Exp*(48). doi:10.3791/2473

Kamsler, A., & Segal, M. (2004). Hydrogen peroxide as a diffusible signal molecule in synaptic plasticity. *Mol Neurobiol, 29*(2), 167-178. doi:10.1385/MN:29:2:167

Kandlur, A., Satyamoorthy, K., & Gangadharan, G. (2020). Oxidative Stress in Cognitive and Epigenetic Aging: A Retrospective Glance. *Front Mol Neurosci, 13*, 41. doi:10.3389/fnmol.2020.00041

Kang, S. J., & Kaang, B. K. (2016). Metabotropic glutamate receptor dependent long-term depression in the cortex. *Korean J Physiol Pharmacol, 20*(6), 557-564. doi:10.4196/kjpp.2016.20.6.557

Kannan, R., Chakrabarti, R., Tang, D., Kim, K. J., & Kaplowitz, N. (2000). GSH transport in human cerebrovascular endothelial cells and human astrocytes: evidence for luminal localization of Na+-dependent GSH transport in HCEC. *Brain Res, 852*(2), 374-382. doi:10.1016/s0006-8993(99)02184-8

Keck, T., Scheuss, V., Jacobsen, R. I., Wierenga, C. J., Eysel, U. T., Bonhoeffer, T., & Hubener, M. (2011). Loss of sensory input causes rapid structural changes of inhibitory neurons in adult mouse visual cortex. *Neuron, 71*(5), 869-882. doi:10.1016/j.neuron.2011.06.034

Keller, A. (2002). Use-dependent inhibition of dendritic spines. *Trends Neurosci, 25*(11), 541-543; discussion 543-544. doi:10.1016/s0166-2236(02)02260-9

Kim, H. H., Park, J. M., Lee, S. H., & Ho, W. K. (2019). Association of mGluR-Dependent LTD of Excitatory Synapses with Endocannabinoid-Dependent LTD of Inhibitory Synapses Leads to EPSP to Spike Potentiation in CA1 Pyramidal Neurons. *J Neurosci, 39*(2), 224-237. doi:10.1523/JNEUROSCI.2935-17.2018

Klappa, P., Ruddock, L. W., Darby, N. J., & Freedman, R. B. (1998). The b' domain provides the principal peptide-binding site of protein disulfide isomerase but all domains contribute to binding of misfolded proteins. *EMBO J, 17*(4), 927-935. doi:10.1093/emboj/17.4.927

Klomsiri, C., Karplus, P. A., & Poole, L. B. (2011). Cysteine-based redox switches in enzymes. *Antioxid Redox Signal, 14*(6), 1065-1077. doi:10.1089/ars.2010.3376

Krackow, S., Vannoni, E., Codita, A., Mohammed, A. H., Cirulli, F., Branchi, I., . . . Lipp, H. P. (2010). Consistent behavioral phenotype differences between inbred mouse strains in the IntelliCage. *Genes Brain Behav, 9*(7), 722-731. doi:10.1111/j.1601-183X.2010.00606.x

Kramer, P. A., Duan, J., Qian, W. J., & Marcinek, D. J. (2015). The Measurement of Reversible Redox Dependent Post-translational Modifications and Their Regulation of Mitochondrial and Skeletal Muscle Function. *Front Physiol, 6*, 347. doi:10.3389/fphys.2015.00347

Kudin, A. P., Malinska, D., & Kunz, W. S. (2008). Sites of generation of reactive oxygen species in homogenates of brain tissue determined with the use of respiratory substrates and inhibitors. *Biochim Biophys Acta, 1777*(7-8), 689-695. doi:10.1016/j.bbabio.2008.05.010

Kulik, Y. D., Watson, D. J., Cao, G., Kuwajima, M., & Harris, K. M. (2019). Structural plasticity of dendritic secretory compartments during LTP-induced synaptogenesis. *Elife, 8*. doi:10.7554/eLife.46356

Kurooka, H., Kato, K., Minoguchi, S., Takahashi, Y., Ikeda, J., Habu, S., . . . Honjo, T. (1997). Cloning and characterization of the nucleoredoxin gene that encodes a novel nuclear protein related to thioredoxin. *Genomics, 39*(3), 331-339. doi:10.1006/geno.1996.4493

Lamsa, K., Irvine, E. E., Giese, K. P., & Kullmann, D. M. (2007). NMDA receptor-dependent long-term potentiation in mouse hippocampal interneurons shows

a unique dependence on Ca(2+)/calmodulin-dependent kinases. *J Physiol, 584*(Pt 3), 885-894. doi:10.1113/jphysiol.2007.137380

Lechward, K., Sugajska, E., de Baere, I., Goris, J., Hemmings, B. A., & Zolnierowicz, S. (2006). Interaction of nucleoredoxin with protein phosphatase 2A. *FEBS Lett, 580*(15), 3631-3637. doi:10.1016/j.febslet.2006.04.101

Lee, K. H., Cha, M., & Lee, B. H. (2020). Neuroprotective Effect of Antioxidants in the Brain. *Int J Mol Sci, 21*(19). doi:10.3390/ijms21197152

LeGates, T. A., Kvarta, M. D., Tooley, J. R., Francis, T. C., Lobo, M. K., Creed, M. C., & Thompson, S. M. (2018). Reward behaviour is regulated by the strength of hippocampus-nucleus accumbens synapses. *Nature, 564*(7735), 258-262. doi:10.1038/s41586-018-0740-8

Lemieux, M., Labrecque, S., Tardif, C., Labrie-Dion, E., Lebel, E., & De Koninck, P. (2012). Translocation of CaMKII to dendritic microtubules supports the plasticity of local synapses. *J Cell Biol, 198*(6), 1055-1073. doi:10.1083/jcb.201202058

Lisman, J., Schulman, H., & Cline, H. (2002). The molecular basis of CaMKII function in synaptic and behavioural memory. *Nat Rev Neurosci, 3*(3), 175-190. doi:10.1038/nrn753

Lledo, P. M., Hjelmstad, G. O., Mukherji, S., Soderling, T. R., Malenka, R. C., & Nicoll, R. A. (1995). Calcium/calmodulin-dependent kinase II and long-term potentiation enhance synaptic transmission by the same mechanism. *Proc Natl Acad Sci U S A, 92*(24), 11175-11179. doi:10.1073/pnas.92.24.11175

Lu, J., Chew, E. H., & Holmgren, A. (2007). Targeting thioredoxin reductase is a basis for cancer therapy by arsenic trioxide. *Proc Natl Acad Sci U S A, 104*(30), 12288-12293. doi:10.1073/pnas.0701549104

Luo, A. H., Tahsili-Fahadan, P., Wise, R. A., Lupica, C. R., & Aston-Jones, G. (2011). Linking context with reward: a functional circuit from hippocampal CA3 to ventral tegmental area. *Science, 333*(6040), 353-357. doi:10.1126/science.1204622

Luscher, C., & Malenka, R. C. (2012). NMDA receptor-dependent long-term potentiation and long-term depression (LTP/LTD). *Cold Spring Harb Perspect Biol, 4*(6). doi:10.1101/cshperspect.a005710

Magi, S., Piccirillo, S., & Amoroso, S. (2019). The dual face of glutamate: from a neurotoxin to a potential survival factor-metabolic implications in health and disease. *Cell Mol Life Sci, 76*(8), 1473-1488. doi:10.1007/s00018-018-3002-x

Magistretti, P. J., & Allaman, I. (2018). Lactate in the brain: from metabolic end-product to signalling molecule. *Nat Rev Neurosci, 19*(4), 235-249. doi:10.1038/nrn.2018.19

Mammucari, C., Raffaello, A., Vecellio Reane, D., Gherardi, G., De Mario, A., & Rizzuto, R. (2018). Mitochondrial calcium uptake in organ physiology: from molecular mechanism to animal models. *Pflugers Arch, 470*(8), 1165-1179. doi:10.1007/s00424-018-2123-2

Margineanu, M. B., Mahmood, H., Fiumelli, H., & Magistretti, P. J. (2018). L-Lactate Regulates the Expression of Synaptic Plasticity and Neuroprotection Genes

in Cortical Neurons: A Transcriptome Analysis. *Front Mol Neurosci, 11*, 375. doi:10.3389/fnmol.2018.00375

Matson, J. L., & Williams, L. W. (2014). Depression and mood disorders among persons with autism spectrum disorders. *Res Dev Disabil, 35*(9), 2003-2007. doi:10.1016/j.ridd.2014.04.020

Matsuzaki, M., Honkura, N., Ellis-Davies, G. C., & Kasai, H. (2004). Structural basis of long-term potentiation in single dendritic spines. *Nature, 429*(6993), 761-766. doi:10.1038/nature02617

Matsuzaki, M., Honkura, N., Ellis-Davies, G. C. R., & Kasai, H. (2004). Structural basis of long-term potentiation in single dendritic spines. *Nature, 429*(6993), 761-766. doi:10.1038/nature02617

Maus, A., & Peters, G. J. (2017). Glutamate and alpha-ketoglutarate: key players in glioma metabolism. *Amino Acids, 49*(1), 21-32. doi:10.1007/s00726-016-2342-9

McLeod, F., Bossio, A., Marzo, A., Ciani, L., Sibilla, S., Hannan, S., . . . Salinas, P. C. (2018). Wnt Signaling Mediates LTP-Dependent Spine Plasticity and AMPAR Localization through Frizzled-7 Receptors. *Cell Rep, 23*(4), 1060-1071. doi:10.1016/j.celrep.2018.03.119

McLeod, F., & Salinas, P. C. (2018). Wnt proteins as modulators of synaptic plasticity. *Curr Opin Neurobiol, 53*, 90-95. doi:10.1016/j.conb.2018.06.003

McQuate, A., Latorre-Esteves, E., & Barria, A. (2017). A Wnt/Calcium Signaling Cascade Regulates Neuronal Excitability and Trafficking of NMDARs. *Cell Rep, 21*(1), 60-69. doi:10.1016/j.celrep.2017.09.023

Mechan, A. O., Wyss, A., Rieger, H., & Mohajeri, M. H. (2009). A comparison of learning and memory characteristics of young and middle-aged wild-type mice in the IntelliCage. *J Neurosci Methods, 180*(1), 43-51. doi:10.1016/j.jneumeth.2009.02.018

Medina, M. A., Andrade, V. M., Caracci, M. O., Avila, M. E., Verdugo, D. A., Vargas, M. F., . . . De Ferrari, G. V. (2018). Wnt/beta-catenin signaling stimulates the expression and synaptic clustering of the autism-associated Neuroligin 3 gene. *Transl Psychiatry, 8*(1), 45. doi:10.1038/s41398-018-0093-y

Merrill, M. A., Chen, Y., Strack, S., & Hell, J. W. (2005). Activity-driven postsynaptic translocation of CaMKII. *Trends Pharmacol Sci, 26*(12), 645-653. doi:10.1016/j.tips.2005.10.003

Meyer, T., Hanson, P. I., Stryer, L., & Schulman, H. (1992). Calmodulin trapping by calcium-calmodulin-dependent protein kinase. *Science, 256*(5060), 1199-1202. doi:10.1126/science.256.5060.1199

Mijakowska, Z., Lukasiewicz, K., Ziolkowska, M., Lipinski, M., Trabczynska, A., Matuszek, Z., . . . Radwanska, K. (2017). Autophosphorylation of alpha isoform of calcium/calmodulin-dependent kinase II regulates alcohol addiction-related behaviors. *Addict Biol, 22*(2), 331-341. doi:10.1111/adb.12327

Mischley, L. K., Standish, L. J., Weiss, N. S., Padowski, J. M., Kavanagh, T. J., White, C. C., & Rosenfeld, M. E. (2016). Glutathione as a Biomarker in

Parkinson's Disease: Associations with Aging and Disease Severity. *Oxid Med Cell Longev, 2016*, 9409363. doi:10.1155/2016/9409363

Moutin, E., Hemonnot, A. L., Seube, V., Linck, N., Rassendren, F., Perroy, J., & Compan, V. (2020). Procedures for Culturing and Genetically Manipulating Murine Hippocampal Postnatal Neurons. *Front Synaptic Neurosci, 12*, 19. doi:10.3389/fnsyn.2020.00019

Moy, S. S., Nadler, J. J., Young, N. B., Nonneman, R. J., Segall, S. K., Andrade, G. M., . . . Magnuson, T. R. (2008). Social approach and repetitive behavior in eleven inbred mouse strains. *Behav Brain Res, 191*(1), 118-129. doi:10.1016/j.bbr.2008.03.015

Nematullah, M., Hoda, M. N., & Khan, F. (2018). Protein Phosphatase 2A: a Double-Faced Phosphatase of Cellular System and Its Role in Neurodegenerative Disorders. *Mol Neurobiol, 55*(2), 1750-1761. doi:10.1007/s12035-017-0444-3

Nicole, O., & Pacary, E. (2020). CaMKIIbeta in Neuronal Development and Plasticity: An Emerging Candidate in Brain Diseases. *Int J Mol Sci, 21*(19). doi:10.3390/ijms21197272

Ninan, I., & Arancio, O. (2004). Presynaptic CaMKII is necessary for synaptic plasticity in cultured hippocampal neurons. *Neuron, 42*(1), 129-141. doi:10.1016/s0896-6273(04)00143-6

Norat, P., Soldozy, S., Sokolowski, J. D., Gorick, C. M., Kumar, J. S., Chae, Y., . . . Kalani, M. Y. S. (2020). Mitochondrial dysfunction in neurological disorders: Exploring mitochondrial transplantation. *NPJ Regen Med, 5*(1), 22. doi:10.1038/s41536-020-00107-x

Okamoto, K., Bosch, M., & Hayashi, Y. (2009). The roles of CaMKII and F-actin in the structural plasticity of dendritic spines: a potential molecular identity of a synaptic tag? *Physiology (Bethesda), 24*, 357-366. doi:10.1152/physiol.00029.2009

Oliet, S. H., Malenka, R. C., & Nicoll, R. A. (1997). Two distinct forms of long-term depression coexist in CA1 hippocampal pyramidal cells. *Neuron, 18*(6), 969-982. doi:10.1016/s0896-6273(00)80336-0

Opazo, P., & Choquet, D. (2011). A three-step model for the synaptic recruitment of AMPA receptors. *Mol Cell Neurosci, 46*(1), 1-8. doi:10.1016/j.mcn.2010.08.014

Oswald, M. C. W., Garnham, N., Sweeney, S. T., & Landgraf, M. (2018). Regulation of neuronal development and function by ROS. *FEBS Lett, 592*(5), 679-691. doi:10.1002/1873-3468.12972

Pathania, M., Davenport, E. C., Muir, J., Sheehan, D. F., Lopez-Domenech, G., & Kittler, J. T. (2014). The autism and schizophrenia associated gene CYFIP1 is critical for the maintenance of dendritic complexity and the stabilization of mature spines. *Transl Psychiatry, 4*, e374. doi:10.1038/tp.2014.16

Pchitskaya, E., & Bezprozvanny, I. (2020). Dendritic Spines Shape Analysis-Classification or Clusterization? Perspective. *Front Synaptic Neurosci, 12*, 31. doi:10.3389/fnsyn.2020.00031

Perals, D., Griffin, A. S., Bartomeus, I., & Sol, D. (2017). Revisiting the open-field test: what does it really tell us about animal personality? *Animal Behaviour, 123*, 69-79. doi:https://doi.org/10.1016/j.anbehav.2016.10.006

Peters, A., Schweiger, U., Pellerin, L., Hubold, C., Oltmanns, K. M., Conrad, M., . . . Fehm, H. L. (2004). The selfish brain: competition for energy resources. *Neurosci Biobehav Rev, 28*(2), 143-180. doi:10.1016/j.neubiorev.2004.03.002

Poncer, J. C., Esteban, J. A., & Malinow, R. (2002). Multiple mechanisms for the potentiation of AMPA receptor-mediated transmission by alpha-Ca2+/calmodulin-dependent protein kinase II. *J Neurosci, 22*(11), 4406-4411. doi:20026449

Rabinowitz, J. D., & Enerback, S. (2020). Lactate: the ugly duckling of energy metabolism. *Nat Metab, 2*(7), 566-571. doi:10.1038/s42255-020-0243-4

Ray, P. D., Huang, B. W., & Tsuji, Y. (2012). Reactive oxygen species (ROS) homeostasis and redox regulation in cellular signaling. *Cell Signal, 24*(5), 981-990. doi:10.1016/j.cellsig.2012.01.008

Ren, X., Zou, L., Zhang, X., Branco, V., Wang, J., Carvalho, C., . . . Lu, J. (2017). Redox Signaling Mediated by Thioredoxin and Glutathione Systems in the Central Nervous System. *Antioxid Redox Signal, 27*(13), 989-1010. doi:10.1089/ars.2016.6925

Rice, M. E., & Russo-Menna, I. (1998). Differential compartmentalization of brain ascorbate and glutathione between neurons and glia. *Neuroscience, 82*(4), 1213-1223. doi:10.1016/s0306-4522(97)00347-3

Risold, P. Y., & Swanson, L. W. (1997). Connections of the rat lateral septal complex1. *Brain Research Reviews, 24*(2), 115-195. doi:10.1016/s0165-0173(97)00009-x

Rivera, D. S., Lindsay, C. B., Oliva, C. A., Codocedo, J. F., Bozinovic, F., & Inestrosa, N. C. (2020). Effects of long-lasting social isolation and re-socialization on cognitive performance and brain activity: a longitudinal study in Octodon degus. *Sci Rep, 10*(1), 18315. doi:10.1038/s41598-020-75026-4

Roberts, E. L. (2007). 2.1 The Support of Energy Metabolism in the Central Nervous System with Substrates Other than Glucose. In A. Lajtha, G. E. Gibson, & G. A. Dienel (Eds.), *Handbook of Neurochemistry and Molecular Neurobiology: Brain Energetics. Integration of Molecular and Cellular Processes* (pp. 137-179). Boston, MA: Springer US.

Robinson, M. J., Warlow, S. M., & Berridge, K. C. (2014). Optogenetic excitation of central amygdala amplifies and narrows incentive motivation to pursue one reward above another. *J Neurosci, 34*(50), 16567-16580. doi:10.1523/JNEUROSCI.2013-14.2014

Robinson, R. R., Dietz, A. K., Maroof, A. M., Asmis, R., & Forsthuber, T. G. (2019). The role of glial-neuronal metabolic cooperation in modulating progression of multiple sclerosis and neuropathic pain. *Immunotherapy, 11*(2), 129-147. doi:10.2217/imt-2018-0153

Robison, A. J. (2014). Emerging role of CaMKII in neuropsychiatric disease. *Trends Neurosci, 37*(11), 653-662. doi:10.1016/j.tins.2014.07.001

Roifman, M., Brunner, H., Lohr, J., Mazzeu, J., & Chitayat, D. (2019). Autosomal Dominant Robinow Syndrome. In M. P. Adam, H. H. Ardinger, R. A. Pagon, S. E. Wallace, L. J. H. Bean, G. Mirzaa, & A. Amemiya (Eds.), *GeneReviews((R))*. Seattle (WA).

Rose, S., Melnyk, S., Pavliv, O., Bai, S., Nick, T. G., Frye, R. E., & James, S. J. (2012). Evidence of oxidative damage and inflammation associated with low glutathione redox status in the autism brain. *Transl Psychiatry, 2*, e134. doi:10.1038/tp.2012.61

Rossi, R., Dalle-Donne, I., Milzani, A., & Giustarini, D. (2006). Oxidized forms of glutathione in peripheral blood as biomarkers of oxidative stress. *Clin Chem, 52*(7), 1406-1414. doi:10.1373/clinchem.2006.067793

Salinas, P. C. (2007). Modulation of the microtubule cytoskeleton: a role for a divergent canonical Wnt pathway. *Trends Cell Biol, 17*(7), 333-342. doi:10.1016/j.tcb.2007.07.003

Salling, M. C., Faccidomo, S. P., Li, C., Psilos, K., Galunas, C., Spanos, M., . . . Hodge, C. W. (2016). Moderate Alcohol Drinking and the Amygdala Proteome: Identification and Validation of Calcium/Calmodulin Dependent Kinase II and AMPA Receptor Activity as Novel Molecular Mechanisms of the Positive Reinforcing Effects of Alcohol. *Biol Psychiatry, 79*(6), 430-442. doi:10.1016/j.biopsych.2014.10.020

Scelfo, B., Sacchetti, B., & Strata, P. (2008). Learning-related long-term potentiation of inhibitory synapses in the cerebellar cortex. *Proc Natl Acad Sci U S A, 105*(2), 769-774. doi:10.1073/pnas.0706342105

Scheving, R., Wittig, I., Heide, H., Albuquerque, B., Steger, M., Brandt, U., & Tegeder, I. (2012). Protein S-nitrosylation and denitrosylation in the mouse spinal cord upon injury of the sciatic nerve. *J Proteomics, 75*(13), 3987-4004. doi:10.1016/j.jprot.2012.05.006

Shannon, B. J., Vaishnavi, S. N., Vlassenko, A. G., Shimony, J. S., Rutlin, J., & Raichle, M. E. (2016). Brain aerobic glycolysis and motor adaptation learning. *Proc Natl Acad Sci U S A, 113*(26), E3782-3791. doi:10.1073/pnas.1604977113

Sharma, M., Castro-Piedras, I., Simmons, G. E., Jr., & Pruitt, K. (2018). Dishevelled: A masterful conductor of complex Wnt signals. *Cell Signal, 47*, 52-64. doi:10.1016/j.cellsig.2018.03.004

Shen, H., Zhu, H., Panja, D., Gu, Q., & Li, Z. (2020). Autophagy controls the induction and developmental decline of NMDAR-LTD through endocytic recycling. *Nat Commun, 11*(1), 2979. doi:10.1038/s41467-020-16794-5

Shetty, P. K., Huang, F. L., & Huang, K. P. (2008). Ischemia-elicited oxidative modulation of Ca2+/calmodulin-dependent protein kinase II. *J Biol Chem, 283*(9), 5389-5401. doi:10.1074/jbc.M708479200

Sies, H., & Jones, D. P. (2020). Reactive oxygen species (ROS) as pleiotropic physiological signalling agents. *Nat Rev Mol Cell Biol, 21*(7), 363-383. doi:10.1038/s41580-020-0230-3

Sims, N. R., & Anderson, M. F. (2008). Isolation of mitochondria from rat brain using Percoll density gradient centrifugation. *Nat Protoc, 3*(7), 1228-1239. doi:10.1038/nprot.2008.105

Singh, E., & Devasahayam, G. (2020). Neurodegeneration by oxidative stress: a review on prospective use of small molecules for neuroprotection. *Mol Biol Rep, 47*(4), 3133-3140. doi:10.1007/s11033-020-05354-1

Smith, B. C., & Marletta, M. A. (2012). Mechanisms of S-nitrosothiol formation and selectivity in nitric oxide signaling. *Curr Opin Chem Biol, 16*(5-6), 498-506. doi:10.1016/j.cbpa.2012.10.016

Soltani, M. H., Pichardo, R., Song, Z., Sangha, N., Camacho, F., Satyamoorthy, K., . . . Setaluri, V. (2005). Microtubule-associated protein 2, a marker of neuronal differentiation, induces mitotic defects, inhibits growth of melanoma cells, and predicts metastatic potential of cutaneous melanoma. *Am J Pathol, 166*(6), 1841-1850. doi:10.1016/S0002-9440(10)62493-5

Spangenberg, E. M. F., & Wichman, A. (2018). Methods for Investigating the Motivation of Mice to Explore and Access Food Rewards. *J Am Assoc Lab Anim Sci, 57*(3), 244-252. doi:10.30802/AALAS-JAALAS-17-000080

Steinbrenner, H., & Sies, H. (2013). Selenium homeostasis and antioxidant selenoproteins in brain: implications for disorders in the central nervous system. *Arch Biochem Biophys, 536*(2), 152-157. doi:10.1016/j.abb.2013.02.021

Stephenson, J. R., Wang, X., Perfitt, T. L., Parrish, W. P., Shonesy, B. C., Marks, C. R., . . . Colbran, R. J. (2017). A Novel Human CAMK2A Mutation Disrupts Dendritic Morphology and Synaptic Transmission, and Causes ASD-Related Behaviors. *J Neurosci, 37*(8), 2216-2233. doi:10.1523/JNEUROSCI.2068-16.2017

Sun, J., Steenbergen, C., & Murphy, E. (2006). S-nitrosylation: NO-related redox signaling to protect against oxidative stress. *Antioxid Redox Signal, 8*(9-10), 1693-1705. doi:10.1089/ars.2006.8.1693

Sun, X., Shih, A. Y., Johannssen, H. C., Erb, H., Li, P., & Murphy, T. H. (2006). Two-photon imaging of glutathione levels in intact brain indicates enhanced redox buffering in developing neurons and cells at the cerebrospinal fluid and blood-brain interface. *J Biol Chem, 281*(25), 17420-17431. doi:10.1074/jbc.M601567200

Suzuki, A., Stern, S. A., Bozdagi, O., Huntley, G. W., Walker, R. H., Magistretti, P. J., & Alberini, C. M. (2011). Astrocyte-neuron lactate transport is required for long-term memory formation. *Cell, 144*(5), 810-823. doi:10.1016/j.cell.2011.02.018

Tegeder, I., Scheving, R., Wittig, I., & Geisslinger, G. (2011). SNO-ing at the nociceptive synapse? *Pharmacol Rev, 63*(2), 366-389. doi:10.1124/pr.110.004200

Thiagarajan, T. C., Piedras-Renteria, E. S., & Tsien, R. W. (2002). alpha- and betaCaMKII. Inverse regulation by neuronal activity and opposing effects on synaptic strength. *Neuron, 36*(6), 1103-1114. doi:10.1016/s0896-6273(02)01049-8

Tobimatsu, T., & Fujisawa, H. (1989). Tissue-specific expression of four types of rat calmodulin-dependent protein kinase II mRNAs. *J Biol Chem, 264*(30), 17907-17912.

Toledo, J. H. d. S. d., Fraga-Silva, T. F. d. C., Borim, P. A., de Oliveira, L. R. C., Oliveira, E. d. S., Périco, L. L., . . . Zorzella-Pezavento, S. F. G. (2020). Organic Selenium Reaches the Central Nervous System and Downmodulates Local Inflammation: A Complementary Therapy for Multiple Sclerosis? *Frontiers in Immunology, 11*(2810). doi:10.3389/fimmu.2020.571844

Tran, B. N., Valek, L., Wilken-Schmitz, A., Fuhrmann, D. C., Namgaladze, D., Wittig, I., & Tegeder, I. (2021). Reduced exploratory behavior in neuronal nucleoredoxin knockout mice. *Redox Biol, 45*, 102054. doi:10.1016/j.redox.2021.102054

Tricoire, L., & Vitalis, T. (2012). Neuronal nitric oxide synthase expressing neurons: a journey from birth to neuronal circuits. *Front Neural Circuits, 6*, 82. doi:10.3389/fncir.2012.00082

Urbainsky, C., Nolker, R., Imber, M., Lubken, A., Mostertz, J., Hochgrafe, F., . . . Lillig, C. H. (2018). Nucleoredoxin-Dependent Targets and Processes in Neuronal Cells. *Oxid Med Cell Longev, 2018*, 4829872. doi:10.1155/2018/4829872

Valek, L., Heidler, J., Scheving, R., Wittig, I., & Tegeder, I. (2019). Nitric oxide contributes to protein homeostasis by S-nitrosylations of the chaperone HSPA8 and the ubiquitin ligase UBE2D. *Redox Biol, 20*, 217-235. doi:10.1016/j.redox.2018.10.002

Ventura, R., Morrone, C., & Puglisi-Allegra, S. (2007). Prefrontal/accumbal catecholamine system determines motivational salience attribution to both reward- and aversion-related stimuli. *Proc Natl Acad Sci U S A, 104*(12), 5181-5186. doi:10.1073/pnas.0610178104

Viale, B., Song, L., Petrenko, V., Wenger Combremont, A. L., Contestabile, A., Bocchi, R., . . . Kiss, J. Z. (2019). Transient Deregulation of Canonical Wnt Signaling in Developing Pyramidal Neurons Leads to Dendritic Defects and Impaired Behavior. *Cell Rep, 27*(5), 1487-1502 e1486. doi:10.1016/j.celrep.2019.04.026

Vila-Ballo, A., Mas-Herrero, E., Ripolles, P., Simo, M., Miro, J., Cucurell, D., . . . Rodriguez-Fornells, A. (2017). Unraveling the Role of the Hippocampus in Reversal Learning. *J Neurosci, 37*(28), 6686-6697. doi:10.1523/JNEUROSCI.3212-16.2017

Vogel, A., Wilken-Schmitz, A., Hummel, R., Lang, M., Gurke, R., Schreiber, Y., . . . Tegeder, I. (2020). Low brain endocannabinoids associated with persistent non-goal directed nighttime hyperactivity after traumatic brain injury in mice. *Sci Rep, 10*(1), 14929. doi:10.1038/s41598-020-71879-x

Voikar, V., Colacicco, G., Gruber, O., Vannoni, E., Lipp, H. P., & Wolfer, D. P. (2010). Conditioned response suppression in the IntelliCage: assessment of mouse strain differences and effects of hippocampal and striatal lesions on acquisition and retention of memory. *Behav Brain Res, 213*(2), 304-312. doi:10.1016/j.bbr.2010.05.019

Voikar, V., Krackow, S., Lipp, H. P., Rau, A., Colacicco, G., & Wolfer, D. P. (2018). Automated dissection of permanent effects of hippocampal or prefrontal lesions on performance at spatial, working memory and circadian timing

tasks of C57BL/6 mice in IntelliCage. *Behav Brain Res, 352*, 8-22. doi:10.1016/j.bbr.2017.08.048

Walf, A. A., & Frye, C. A. (2007). The use of the elevated plus maze as an assay of anxiety-related behavior in rodents. *Nat Protoc, 2*(2), 322-328. doi:10.1038/nprot.2007.44

Wang, H., Ardiles, A. O., Yang, S., Tran, T., Posada-Duque, R., Valdivia, G., . . . Kirkwood, A. (2016). Metabotropic Glutamate Receptors Induce a Form of LTP Controlled by Translation and Arc Signaling in the Hippocampus. *J Neurosci, 36*(5), 1723-1729. doi:10.1523/JNEUROSCI.0878-15.2016

Wang, J., Xie, R., Kou, X., Liu, Y., Qi, C., Liu, R., . . . Gao, X. (2019). A protein phosphatase 2A deficit in the hippocampal CA1 area impairs memory extinction. *Mol Brain, 12*(1), 51. doi:10.1186/s13041-019-0469-9

Watson, D. J., Loiseau, F., Ingallinesi, M., Millan, M. J., Marsden, C. A., & Fone, K. C. (2012). Selective blockade of dopamine D3 receptors enhances while D2 receptor antagonism impairs social novelty discrimination and novel object recognition in rats: a key role for the prefrontal cortex. *Neuropsychopharmacology, 37*(3), 770-786. doi:10.1038/npp.2011.254

Watson, S., Mercier, S., Bye, C., Wilkinson, J., Cunningham, A. L., & Harman, A. N. (2007). Determination of suitable housekeeping genes for normalisation of quantitative real time PCR analysis of cells infected with human immunodeficiency virus and herpes viruses. *Virol J, 4*, 130. doi:10.1186/1743-422X-4-130

Wefelmeyer, W., Puhl, C. J., & Burrone, J. (2016). Homeostatic Plasticity of Subcellular Neuronal Structures: From Inputs to Outputs. *Trends Neurosci, 39*(10), 656-667. doi:10.1016/j.tins.2016.08.004

White, J. J., Mazzeu, J. F., Coban-Akdemir, Z., Bayram, Y., Bahrambeigi, V., Hoischen, A., . . . Carvalho, C. M. B. (2018). WNT Signaling Perturbations Underlie the Genetic Heterogeneity of Robinow Syndrome. *Am J Hum Genet, 102*(1), 27-43. doi:10.1016/j.ajhg.2017.10.002

White, S. L., Schmidt, H. D., Vassoler, F. M., & Pierce, R. C. (2013). Acute cocaine increases phosphorylation of CaMKII and GluA1 in the dorsolateral striatum of drug naive rats, but not cocaine-experienced rats. *Neurosci Lett, 537*, 71-76. doi:10.1016/j.neulet.2013.01.017

Wilson, C., Munoz-Palma, E., & Gonzalez-Billault, C. (2018). From birth to death: A role for reactive oxygen species in neuronal development. *Semin Cell Dev Biol, 80*, 43-49. doi:10.1016/j.semcdb.2017.09.012

Winiarska-Mieczan, A., Baranowska-Wojcik, E., Kwiecien, M., Grela, E. R., Szwajgier, D., Kwiatkowska, K., & Kiczorowska, B. (2020). The Role of Dietary Antioxidants in the Pathogenesis of Neurodegenerative Diseases and Their Impact on Cerebral Oxidoreductive Balance. *Nutrients, 12*(2). doi:10.3390/nu12020435

Winterbourn, C. C., & Metodiewa, D. (1999). Reactivity of biologically important thiol compounds with superoxide and hydrogen peroxide. *Free Radical Biology and Medicine, 27*(3), 322-328. doi:10.1016/s0891-5849(99)00051-9

Xiong, C. H., Liu, M. G., Zhao, L. X., Chen, M. W., Tang, L., Yan, Y. H., . . . Qiu, Y. (2019). M1 muscarinic receptors facilitate hippocampus-dependent cognitive

flexibility via modulating GluA2 subunit of AMPA receptors. *Neuropharmacology, 146*, 242-251. doi:10.1016/j.neuropharm.2018.12.005

Yamagata, Y., Kobayashi, S., Umeda, T., Inoue, A., Sakagami, H., Fukaya, M., . . . Okabe, S. (2009). Kinase-dead knock-in mouse reveals an essential role of kinase activity of Ca2+/calmodulin-dependent protein kinase IIalpha in dendritic spine enlargement, long-term potentiation, and learning. *J Neurosci, 29*(23), 7607-7618. doi:10.1523/JNEUROSCI.0707-09.2009

Yang, J., Ruchti, E., Petit, J. M., Jourdain, P., Grenningloh, G., Allaman, I., & Magistretti, P. J. (2014). Lactate promotes plasticity gene expression by potentiating NMDA signaling in neurons. *Proc Natl Acad Sci U S A, 111*(33), 12228-12233. doi:10.1073/pnas.1322912111

Yang, K., Wang, X., Zhang, H., Wang, Z., Nan, G., Li, Y., . . . He, T. C. (2016). The evolving roles of canonical WNT signaling in stem cells and tumorigenesis: implications in targeted cancer therapies. *Lab Invest, 96*(2), 116-136. doi:10.1038/labinvest.2015.144

Zalcman, G., Federman, N., & Romano, A. (2018). CaMKII Isoforms in Learning and Memory: Localization and Function. *Frontiers in Molecular Neuroscience, 11*. doi:10.3389/fnmol.2018.00445

Zalcman, G., Federman, N., & Romano, A. (2018). CaMKII Isoforms in Learning and Memory: Localization and Function. *Front Mol Neurosci, 11*, 445. doi:10.3389/fnmol.2018.00445

Zhang, X., Connelly, J., Levitan, E. S., Sun, D., & Wang, J. Q. (2021). Calcium/Calmodulin-Dependent Protein Kinase II in Cerebrovascular Diseases. *Transl Stroke Res*. doi:10.1007/s12975-021-00901-9

Zhou, Q., Homma, K. J., & Poo, M. M. (2004). Shrinkage of dendritic spines associated with long-term depression of hippocampal synapses. *Neuron, 44*(5), 749-757. doi:10.1016/j.neuron.2004.11.011

Zucker, R. S., & Regehr, W. G. (2002). Short-term synaptic plasticity. *Annu Rev Physiol, 64*, 355-405. doi:10.1146/annurev.physiol.64.092501.114547

9. Appendix

9.1 List of abbreviations

A

AA *Antimycin A*

ADP *adenosine diphosphate*

APC *Adenomatous polyposis coli*

Ara-C *Cytosine arabinoside*

ARRIVE *Animal Research: Reporting of in Vivo Experiments*

ATP *Adenosine 5'-triphosphate*

B

BBB *Blood brain barrier*

BCA assay *Bicinchoninic acid assay*

BSA *Albumin fraction V*

C

CA *cornu ammonis*

Ca^{2+} *Calcium ion*

CaM *Calmodulin*

Camk2 *Calcium-calmodulin-dependent protein kinase 2*, *Calcium-calmodulin-dependent protein kinase 2*

CAT *Catalases*

CNS *Central nervous system*

CO_2 *Carbon dioxide*

CREB *cAMP response element-binding protein*

D

DM *Dissociation medium*

DVL *Dishevelled protein*

E

EAAT *Excitatory amino acid transporters*

EPM *Elevated plus maze*

ETC *Electron transport chain*

F

FADH2 *Flavin adenine dinucleotide*

FCCP *Carbonyl cyanide-p-trifluormethoxyphenylhydrazone*

Flp *flippase recombinase*

FRT *Flippase recognition target*

Fzd *Transmembrane Frizzled*

G

GABA *γ-aminobutyric acid*

GLRX *Glutaredoxin*

GPX *Glutathione peroxidase*

GSH *Glutathione*, *Glutathione*

GSH/GPX *Glutathione/ Glutathione peroxidase*

GSK3β *Glycogen synthase kinase 3β*

GV-SOLAS *Society of Laboratory Animal Science*

H

H_2O_2 *Hydrogen peroxide*

HRP *Horseradish peroxidase*

L

LPS *Lipopolysaccharide*

LS *Lateral septum nuclei*

LTD *Long term depression*

LTP *Long-term potentiation*

M

MAP2 *Microtubule-associated protein 2*

MAS *Mitochondrial assay solution*

mGlut *Metabotropic glutamate receptors*

MyD88 *Myeloid differentiation primary response gene*

N

NaCl *Sodium chloride*

NADH *Nicotinamide adenine dinucleotide*

NADPH *Nicotinamide adenine dinucleotide phosphate*

NF-κB *Nuclear factor kappa-light-chain-enhancer of activated B cells*

NMDAR *N methyl D aspartate receptor*

nNOS *neuronal nitric oxide synthase*

NO *Nitric oxide*

NOS *Nitric oxide synthase*

NOX *NADPH oxidase*

NRF2 *Nuclear factor erythroid 2–related factor 2*

NTB *Nitrotetrazolium blue chloride*

NXN *Nucleoredoxin*

O

$O2^{-\bullet}$ *Superoxide anion radicals*

OCR *Oxygen consumption ratio*

OFT *Open field test*

OXPHOS *oxidative phosphorylation*

P

PBSTx *0.1 %Triton X-100*

PCP *WNT/planar cell polarity*

PDI *protein disulfide protein isomerase*

PFA *Paraformaldehyde*

PLA *Proximity ligation assay*

PMS *Phenazine methosulfate*

PP1A *Peptidylprolyl isomerase A*

PP2A *Protein phosphatase 2A*

PPARγ *Peroxisome proliferator-activated receptors γ*

PPP *Pentose phosphate pathway*

PRDX 1 *Peroxiredoxin 1*

R

RAC3 *Ras-related C3 botulinum toxin substrate 3*

RFID *Radio-frequency identification*

RNS *Reactive nitric species*

ROS *Reactive oxygen species*

RRS2 *Robinow syndrome-2*

RSS *Reactive sulfur species*

S

SNO *S- nitrolysation*

SOD *Superoxide dismutase*

-SOH *Sulfenic acid*

T

TCA cycle *Tricarboxylic acid cycle*

TCF/LEF *T-cell factor/lymphocyte enhancer factor*

TLR4 *Toll- like- 4 receptors*

TXN *Thioredoxin*

TXN/PRDX *Thioredoxin/Peroxiredoxin*

V

VWR *Voluntary wheel running*

X

X-Gal *5-Bromo-4-chloro-3-indolyl-β-D-galactopyranoside*

B

β -Gal *β-Galactosidase expression, β-Galactosidase*

9.2 List of tables

TAB. 3.1 SIMPLIFIED OVERVIEW OF ANTIOXIDANTS IN THE BRAIN (LEE ET AL., 2020). ..... - 12 -

TAB. 4.1 DNA EXTRACTION (EACH SAMPLE) ..... - 27 -

TAB. 4.2 PCR MASTER MIX (20 µL REACTION) ..... - 27 -

TAB. 4.3 LIST OF PRIMER SEQUENCES FOR GENOTYPING. ..... - 28 -

TAB. 4.4 LIST OF ANTIBODIES USED FOR IMMUNOFLUORESCENCE STAININGS. PAB (POLYCLONAL ANTIBODY), MAB (MONOCLONAL ANTIBODY) ..... - 30 -

TAB. 4.5 COMPOSITION OF CELL CULTURE MEDIA OF PRIMARY GLIAL CELLS, CORTICAL AND HIPPOCAMPAL NEURONS. ..... - 32 -

TAB. 4.6 COMPOSITION OF NON-DENATURING LYSIS BUFFER ..... - 33 -

TAB. 4.7 COMPOSITION OF CA2+/CAM CONTAINING ASSAY BUFFER AND CA2+/CAM NEGATIVE ASSAY BUFFER. ..... - 34 -

TAB. 4.8 SAMPLE PREPARATION FOR EACH SAMPLE WELL ..... - 35 -

TAB. 4.9 COMPONENTS OF THE ISOLATION BUFFER FOR TISSUE HOMOGENIZATION. ..... - 35 -

TAB. 4.10 COMPOSITION OF 1X MITOCHONDRIAL ASSAY SOLUTION (MAS BUFFER). ..... - 36 -

TAB. 4.11 CONCENTRATIONS OF SUBSTRATES AND INHIBITORS OF MITOCHONDRIAL RESPIRATION LOADED TO THE DEFINED PORTS. - 37 -

TAB. 4.12 AGENT INJECTION SCHEME OF SUBSTRATES AND INHIBITORS FOR SEAHORSE ASSAY (HH:MM:SS) ..... - 38 -

TAB. 4.13 VERSO MASTER MIX (20µL REACTION) SHOWN FOR ONE RNA SAMPLE. ..... - 38 -

TAB. 4.14 REVERSE TRANSCRIPTION CYCLING PROGRAM ..... - 38 -

TAB. 4.15 PRIMER SEQUENCES OF PP1A AND MURINE NXN (MNXN) ..... - 39 -

TAB. 4.16 RT-QPCR CYCLING PROGRAM DEFINED FOR EXPERIMENT IN THE QUANTSTUDIO™ 5 SYSTEM ..... - 39 -

TAB. 4.17 CHRONOLOGIC DESCRIPTION OF INTELLICAGE TASKS. ..... - 42 -

9.3 List of figures

FIG 3.1 LACTATE SHUTTLE FROM ASTROCYTES TO NEURONS. ....- 9 -

FIG 3.2 GLUTAMATE-GLUTAMINE CYCLE BETWEEN ASTROCYTES AND NEURONS. ....- 11 -

FIG 3.3 CONNECTION BETWEEN THE CELLULAR DISULFIDE REDUCTASE SYSTEMS OF THIOREDOXIN AND GLUTATHIONE (AOYAMA & NAKAKI, 2015). ....- 13 -

FIG 3.4 MECHANISMS OF SYNAPTIC PLASTICITY AT DENDRITIC SPINES THROUGH LONG TERM POTENTIATION (LTP). ....- 18 -

FIG 3.5 LINKAGE BETWEEN WNT7A INITIATING THE CANONICAL WNT PATHWAY AND CAMK2A MEDIATED NEURONAL PLASTICITY.- 25 -

FIG 4.1 GENE CONSTRUCT OF THE CONDITIONED KNOCKOUT OF NXN. ....- 27 -

FIG 4.2 GENERATION OF THE DENSITY GRADIENT. ....- 35 -

FIG 5.1 IHC ANALYZES VISUALIZE EXPRESSION OF NXN IN LACZ REPORTER MICE (CONDUCTED BY VALEK; TRAN ET AL, 2021) AND IMMUNOFLUORESCENCE STAINGS (IF) OF NXN (GREEN) AND CAMK2A (RED) IN ADULT MURINE BRAIN TISSUE. ....- 47 -

FIG 5.2 ANALYSIS OF NXN EXPRESSION IN LATERAL SEPTUM NUCLEI WHICH IS THE BRAIN REGION INVOLVED CIRCUITS FOR EXPLORATIONAL GOAL-DIRECTED BEHAVIOR (LUO ET AL., 2011). ....- 48 -

FIG 5.3 BODY WEIGHT OF FEMALE NESNXN$^{-/-}$ YOUNG MICE IS REDUCED BUT NORMALIZES BY AGEING. ....- 49 -

FIG 5.4 NXN PRESERVES CAMK2A ACTIVITY IN THE PRESENCE OF H_2O_2. ....- 50 -

FIG 5.5 MORE PLA SIGNALS IN PRIMARY CORTICAL NEURONS OF NXN-FLFL MICE THAN IN NEURONS OF NESNXN$^{-/-}$ MICE. ...- 51 -

FIG 5.6 CAMK2A-POSITIVE NEURONS IN PRIMARY CORTICAL CULTURES. ....- 52 -

FIG 5.7 NXN IS LOCALIZED IN NEURONAL FIBERS OF DIFFERENT BRAIN REGIONS. ....- 54 -

FIG 5.8 NXN IS EXPRESSED IN DENDRITIC SPINES. ....- 54 -

FIG 5.9 RESPIRATORY ACTIVITY IN NESNXN$^{-/-}$ MICE IS REDUCED IN BRAIN TISSUE. ....- 55 -

FIG 5.10 TIME COURSE OF NOSEPOKE RATIO FROM NOSEPOKE PER VISIT IN INTELLICAGES. ....- 56 -

FIG 5.11 EXPLORATORY AND GOAL DIRECTED ACTIVITY OF NESNXN$^{-/-}$ VERSUS NXN-FLFL MICE IN INTELLICAGES. ....- 57 -

FIG 5.12 THE NUMBER OF LICKS PER VISIT REVEALS REWARD COLLECTION FOR SUCCESSFUL GOAL-DIRECTED LVISITS. ....- 58 -

FIG 5.13 INTELLICAGE BEHAVIOR OF NESNXN$^{-/-}$ VERSUS NXN-FLFL MICE AVERAGED OVER DIFFERENT TASKS. ....- 59 -

FIG 5.14NSPATIAL LEARNING BEHAVIOR DURING PPL AND PPL REVERSAL TASKS IN IC. ....- 61 -

FIG 5.15 LEARNING PROBABILITY CURVES SHOW THE PROPORTION OF CORRECT CORNER VISITS. ....- 62 -

FIG 5.16 TIME COURSES OF THE PROPORTION OF CORRECT VISITS AND CORRECT NOSEPOKES DURING PLACE AVOIDANCE ACQUISITION (PAA) AND PLACE AVOIDANCE EXTINCTION (PAEX). ....- 63 -

FIG 5.17 PHENOMASTER SHOWS SAME FOOD AND DRINK INTAKE BUT REDUCED VOLUNTARY WHEEL RUNNING OF NESNXN$^{-/-}$ COMPARED TO NXN-FLFL. ..... - 63 -

FIG 5.18 NESNXN$^{-/-}$ SHOW LOWER EXPLORATIVE BEHAVIOR IN OPEN FIELD TEST (OFT) AND NO ABNORMAL ANXIETY BEHAVIOR IN THE ELEVATED PLUS MAZE (EPM) COMPARED TO NXN-FLFL. ..... - 64 -

FIG 5.19 SOCIABILITY AND SOCIAL NOVELTY/MEMORY OF NXN-FLFL AND NESNXN$^{-/-}$ MICE WERE CONDUCTED IN A 3-CHAMBER MAZE TEST WITH TWO SOCIAL COMPARTMENTS. ..... - 65 -

9.4 Curriculum Vitae

PERSONAL DATA

Name:	Bao-Ngoc Tran
Birth date:	May 10, 1992
Place of birth:	Halle/Saale
Nationality:	German
Email address:	baongoc.tran@outlook.de
Address:	Bergweg 38a 61440 Oberursel Germany

EDUCATION

09/2017 – exp. 2022	**Ph.D. Pharmacy** Institute of Clinical Pharmacology Johann-Wolfgang-Goethe-Universität, Frankfurt/Main Graduate Program of collaborative research center 815: Redox regulation
05/2017	**3rd state examination in pharmacy** Frankfurt/Main
09/2015 – 11/2015	**2nd state examination in pharmacy** Johann-Wolfgang-Goethe-Universität, Frankfurt/Main
04/2011 – 04/2015	**University of Pharmacy** Johann-Wolfgang-Goethe-Universität, Frankfurt/Main
08/2005 – 06/2010	**Johann-Gottfried-Herder grammar school** Halle/Saale

PRACTICAL EXPERIENCE

12/2016 – 05/2017	Infectopharm – Medical affairs Internship for final year of graduation
05/2016 – 11/2016	University Florida – College of Pharmacy Orlando Internship for final year of graduation
12/2015 – 05/2016	Apotheke am Magistralen Carré - Halle Internship for final year of graduation

05/2015 – 07/2015	Apotheke Pharmacie Raphael - Frankfurt Student assistant
09/2011 – 10/2011	Carl - von- Basedow - Klinikum – Weißenfels Traineeship
07/2011 – 08/2011	Würde Apotheke - Teutschenthal Traineeship

PUBLICATIONS

Tran, B. N., Valek, L., Wilken-Schmitz, A., Fuhrmann, D. C., Namgaladze, D., Wittig, I., & Tegeder, I. (2021). Reduced exploratory behavior in neuronal nucleoredoxin knockout mice. *Redox biology*, *45*, 102054. https://doi.org/10.1016/j.redox.2021.102054

Ande, A., Vaidya, T. R., **Tran, B. N.**, Vicchiarelli, M., Brown, A. N., & Ait-Oudhia, S. (2018). Utility of a Novel Three-Dimensional and Dynamic (3DD) Cell Culture System for PK/PD Studies: Evaluation of a Triple Combination Therapy at Overcoming Anti-HER2 Treatment Resistance in Breast Cancer. *Frontiers in pharmacology*, *9*, 403. https://doi.org/10.3389/fphar.2018.00403

CONFERENCES

10/2020	Poster Presentation at Paris Redox 2020 – 22nd International Conference Antioxidants: *Interaction of Nucleoredoxin with Camk2α – impact of neuronal redox- regulation on behavioral paradigms in mice*
06/2018	Biennial Meeting of the Rhine Main neuroscience network (rmn^2) in Oberwesel, Germany
10/2016	Poster Presentation at Lake Nona Medical City Research Day, Orlando: *Effects of paclitaxel on HER2-refractory breast cancer cell line – Implications for combination therapy*

9.5 Acknowledgement

First and foremost, I want to thank my first supervisor and working group leader, Irmgard Tegeder, for giving me the opportunity to learn and develop through her professional advice.

I also wish to thank my colleagues Annett Wilken-Schmitz, Lucie Valek, Caroline Fischer, Alexandra Vogel and Vanessa Kraft for the great support during lab work and also for our intense discussions and brain storming.

Additionally, I want to thank Riad Haceni from the institute of pharmacology and toxicology of the University hospital Frankfurt for providing technical advice and patiently helping several times.

Special thanks also go to the member of the Redox-Regulation SFB815 graduate school. I had a great time during summer school learning a lot about poster presentations and other helpful workshops. I would like to thank Prof. Dr. Brandes and Prof. Dr. Brüne for their inspiring feedback during that time.

I also want to thank the director of the Institute for Clinical Pharmacology of the University hospital Frankfurt, Prof. Dr. Dr. Gerd Geisslinger.

9.6 Declaration

Except where stated otherwise by reference or acknowledgment, the work presented was generated by myself under the supervision of my advisors during my doctoral studies. Whenever a figure, table or text is identical to a previous publication, it is stated explicitly in the thesis that copyright permission and/or co-author agreement has been obtained.

The following parts of the thesis have been previously published in (Tran et al., 2021): Figure(s) 5.3 to 5.5, 5.7, 5.9, to 5.19. Intellicage data (Figures 5.10 to 5.16) were analyzed by Irmgard Tegeder and experiments were performed by me.

The material listed below was obtained in the context of collaborative research published in (Tran et al., 2021):

Fig. 5.1: Lucie Valek (clinical pharmacology university hospital frankfurt, working group of Irmgard Tegeder), her contribution: LacZ staining, my own contribution: Immunofluorescence staining.